

NORTHWESTERN UNIVERSITY

Cancer-Associated Isocitrate Dehydrogenase 1 Promotes Growth and Resistance to Targeted
Therapies in the Absence of Mutation

A DISSERTATION

SUBMITTED TO THE GRADUATE SCHOOL
IN PARTIAL FULFILLMENT OF THE REQUIREMENTS

for the degree

DOCTOR OF PHILOSOPHY

Field of Driskill Graduate Training Program in Life Sciences

By

Andrea E. Calvert

EVANSTON, ILLINOIS

September 2017

ABSTRACT

Cancer-Associated Isocitrate Dehydrogenase 1 Promotes Growth and Resistance to Targeted Therapies in the Absence of Mutation

Andrea E. Calvert

Metabolic abnormalities of cancers provide opportunities for novel tumor-specific therapies. Isocitrate dehydrogenases (IDHs) catalyze the oxidative decarboxylation of isocitrate to α -ketoglutarate (α KG) and the reduction of NAD(P)⁺ to NAD(P)H. Oncogenic mutations in two *IDH*-encoding genes (*IDH1* and *IDH2*) have been identified in acute myelogenous leukemia, low-grade glioma, and secondary glioblastoma (GBM), however it has been demonstrated that primary GBM patients with wild-type *IDH1* have a shorter overall survival compared to those patients with mutated *IDH1*. We therefore decided to determine if wild-type IDH1 might have a role in the pathogenesis of GBM. We employed *in silico* analysis of The Cancer Genome Atlas (TCGA) data with wet-bench analysis of tumor extracts and discovered that non-mutated IDH1 mRNA and protein are commonly overexpressed in primary GBM. We show that genetic inactivation of IDH1 decreases GBM cell growth and prolongs survival of animal subjects bearing patient-derived xenografts (PDXs). On molecular levels, diminished IDH1 activity results in reduced α KG and NADPH production, which is paralleled by deficient metabolic flux from glucose or acetate into lipids. Loss of IDH1 expression also promotes a more differentiated tumor cell state, as seen by enhanced histone methylation and differentiation marker expression, and leads to increased levels of Reactive Oxygen Species (ROS) and exhaustion of reduced glutathione. While targeted therapies, including receptor tyrosine kinase inhibitors (RTKi) have been developed for GBM, their potential has yet to be realized in the clinic. IDH1 protein and

mRNA levels are increased in response to RTKi treatment through a FoxO6-mediated mechanism, and IDH1 loss increases apoptosis in response to these targeted therapies, pointing to IDH1 as a resistance mechanism for RTKi therapeutics. We furthermore use a pharmacologic inhibitor of IDH1, which reduces NADPH levels, increases RTKi-induced apoptosis, and prolongs the survival of GBM xenograft bearing mice. Our findings suggest that IDH1 upregulation represents a common mechanism of metabolic adaptation of GBM to support macromolecular synthesis, aggressive growth, and therapy resistance, and point to IDH1 inhibition as a promising therapeutic strategy, especially in combination with RTKi, for GBM.

ACKNOWLEDGEMENTS

First and foremost, I would like to thank my advisor, Dr. Alexander Stegh. I would not be where I am today if it wasn't for the dedication and commitment Alex had in helping me with all aspects of this project along the way. Alex was always available for discussion about the project as well as helping come up with great ideas for how to make this project as successful as it was. He's made my graduate school experience very enjoyable and taught me so much. I am very fortunate to have had such a wonderful advisor.

This work could also not have been completed without the help of many different people, including all my lab members over the years. Everyone in the lab was responsible for making the environment of the lab a truly great place to work. Sam Jensen was a true mentor to me early on and really taught me how to think and work within this lab environment. I missed his insights on my project as well as his friendship outside the lab when he graduated. Timothy Sita is a wonderful, kind, and smart person who really helped make the lab a better place. Jasmine May helped with my project during her rotation within the lab and helped push the LSS and IDH1 part of the project forward. Her bubbly personality brought so much to the lab when she joined us. Fotini Kouri and Alexandra Chalastanis were both so helpful and always willing to help with anything as well as lend an ear to anything going on in or outside of the lab. These post docs were true blessings in helping me get here today. I know I would not be here today without their constant support and help when things did not seem to be going right. Yongfei Wu was integral in this project by helping to get it started as well as taking on the original part of the IDH1 inhibitor screen. All of his help while he was in the lab was also very helpful and necessary for

my project. Lisa Hurley is a remarkable lab manager and things would definitely not go as smooth if she wasn't around. Her constant help with my animal experiments was always so much appreciated. Serena Ghelfi, the newest member of our lab has been a great friend and coworker from her start. It's been wonderful to sit by her, have her support, and have someone to rant to.

All of our collaborators on my project were integral in my work. I would very much like to thank Yingtao Bi and Ramana Davuluri as well as Youjia Hua and Marcus Peter for their constant help regarding bioinformatics of microarray and RNA-Sequencing data and analysis of the TCGA dataset; Maureen Kachman and Charles Burant from the University of Michigan for their help on designing the metabolomics experiments and running GC-MS for the ¹³C experiments; Andrea Piunti, Elizabeth Bartom, and Ali Shilatifard for their help and support for the CHIP-Sequencing; Rama Mishra, Oleksii (Alex) Dubrovskiy, Gary Schiltz, and Andrew Mazar for their chemistry expertise and help with our IDH1 inhibitor screen and characterization of inhibitors; David James for his expertise in GBM PDX models and input of the project along the way; Hongwu Zheng for isolating the NSCs and helping with this aspect of the project; Navdeep Chandel for his expertise in metabolism, specifically cancer metabolism and helping me design experiments to further my project; and Craig Horbinski who not only gave us more samples from the University of Kentucky, but also was able to use his expertise as a pathologist to stain and grade our human samples for IDH1.

I would also like to thank all the core facilities that without them I would not have been able to complete all of the experiments in my thesis. I would especially like to thank Jeff, Paul, Carolina,

and Suchitra from the Flow Cytometry Core; Lin from the Mouse Histology and Phenotyping Core; and Wilson from the Cell Imaging Core.

My committee was also integral in my project and I always appreciated all their feedback along the way, starting with my qualifying exam in which they believed that my project could be more streamlined and better, as well as everything they had to say during all of my committee meetings to make my thesis the best and strongest that it could be. Thank you Chonghui, Jonathan, and Marcus.

My family and friends are incredibly supportive of me, not only during my PhD, but also every moment of my life leading up until this point. My parents are the most selfless and caring people I know and I truly appreciate all that they have done for me, believing in me, and pushing me to be the best that I can be. I love you Mom and Dad. My siblings, grandparents, extended family and all of my friends, both near and far, you are all amazing and supportive people. Thank you.

And last, but certainly not least, I would like to thank my husband, Will. You have been nothing but the most supportive person in my life. From pushing me from the first day I met you to apply for grad school, to all the times that I've had to miss dinners or plans because I was working late, and even pushing back our honeymoon indefinitely, you have never complained. You are my rock and have gotten me through so much in the last 8 years. Thank you for all your selflessness in pushing me to complete my dreams. I will never be able to thank you enough. I love you.

TABLE OF CONTENTS

ACKNOWLEDGEMENTS	4
TABLE OF CONTENTS	7
LIST OF FIGURES	11
CHAPTER 1: INTRODUCTION	14
1.1 Opening	15
1.2 Glioblastoma (GBM)	15
1.2.1 Overview and Standard of Care	15
1.2.2 Genomic Subtypes	17
1.2.3 RTK Signaling and Targeted Therapies	20
1.2.4 GBM Cancer Stem Cells	23
1.2.5 Metabolic Adaptations in GBM	25
1.3 Isocitrate Dehydrogenase 1 (IDH1)	31
1.3.1 Function of wild-type IDH1	31
1.3.2 IDH1 and α KG-dependent dioxygenases	32
1.3.3 IDH1 and Metabolism	33
1.3.4 IDH1 and Redox Homeostasis	35
1.3.5 Mutated IDH1 in Cancer	38
1.4 Conclusions	43
CHAPTER 2: MATERIALS AND METHODS	45
2.1 <i>In Silico</i> Genomic and Genetic Analysis	46
2.1.1 Preprocessing of TCGA GBM exon-array data and subtyping	46

2.1.2 Analysis of TCGA GBM, low grade glioma, lung adenocarcinoma, and squamous cell carcinoma RNA-Seq data	46
2.1.3 TCGA GBM mutation data	47
2.2 RT-qPCR	47
2.3 R132H Mutation Status	49
2.4 Immunohistochemistry	49
2.5 Cell Lines	50
2.6 Cell Culture and Reagents	51
2.7 Mutagenesis and Cloning of IDH1	51
2.8 Lentiviral Production and Cell Infection	52
2.9 Retroviral Production and Cell Infection	53
2.10 Transfection	54
2.11 Western Blot Analysis	54
2.12 Cell Proliferation Assay	55
2.13 <i>In Vivo</i> Xenograft Studies	55
2.14 <i>In Vivo</i> Bioluminescence Imaging	56
2.15 α-Ketoglutarate Quantification	57
2.16 NADPH Quantification	57
2.17 ¹³Carbon-Glucose and -Acetate Studies	58
2.17.1 ¹³ Carbon Sample Preparation	58
2.17.2 GC-MS	58
2.17.3 GC-MS Data Analysis	59

	9
2.18 Extreme Limiting Dilution Assay	59
2.19 Differentiation Experiment	59
2.20 Chromatin Immunoprecipitation-Sequencing	60
2.21 Copy Number Alterations	61
2.22 Quantification of Apoptosis	61
2.23 ROS Quantification	62
2.24 GSH Quantification	62
2.25 RTK Profile Array	62
2.26 Chromatin Immunoprecipitation	63
2.27 MicroArray	64
2.28 MTT Assay	65
2.29 Statistical Analysis	65
CHAPTER 3: RESULTS	66
3.1 Wild-type IDH1 is overexpressed in GBM	67
3.2 IDH1 expression modulates GBM progression <i>in vivo</i>	72
3.3 Suppression of IDH1 reduces αKG and NADPH levels, and diminishes lipid biosynthesis	77
3.4 IDH1 regulates histone methylation and GIC differentiation	79
3.5 IDH1 ablation increases RTKi-induced apoptosis through decreased lipid biosynthesis and increased ROS in GBM	86
3.6 IDH1 protects cancer cells derived from non-glioma tumors from apoptosis	92

	10
3.7 FoxO6 transcriptionally induces IDH1 expression in response to RTK inhibition	94
3.8 Pharmacological inhibition of IDH1 reduces growth, augments RTKi susceptibility, reduces stem cell frequency, and decreases GBM progression	98
CHAPTER 4: DISCUSSION	103
4.1 Discussion	104
4.2 Summary and Future Directions	119
REFERENCES	123
CURRICULUM VITAE	152

LIST OF FIGURES

Figure 1. GBM Genomic Subtypes	19
Figure 2. Altered GBM Metabolism	30
Figure 3. IDH1 wild-type and mutated functions	37
Figure 4. Wild-type IDH1 is overexpressed in GBM	67
Figure 5. TCA cycle enzyme mRNA expression in normal brain vs. GBM	68
Figure 6. IDH1 mRNA is increased in high-grade gliomas, in wild-type tumors, and the Classical subtype	69
Figure 7. Wild-type IDH1 protein is overexpressed in GBM	70
Figure 8. Elevated levels of IDH1 are not associated with copy number gains, amplification, or promoter methylation	71
Figure 9. On target effect of shIDH1	73
Figure 10. IDH1 promotes GBM cell growth	74
Figure 11. IDH1 promotes GBM progression <i>in vivo</i>	75
Figure 12. Knockdown of IDH1 results in increased apoptosis and decreased cell proliferation while overexpression of IDH1 results in decreased apoptosis and increased cell proliferation <i>in vivo</i>	76
Figure 13. Knockdown of IDH1 decreases α KG and NADPH levels	78
Figure 14. Knockdown of IDH1 reduces carbon flux from glucose or acetate into fatty acids	79
Figure 15. Knockdown of IDH1 increases histone methylation	80
Figure 16. Decreased IDH1 expression is associated with diminished stem cell frequency	80

	12
Figure 17. IDH1 knockdown induces a more differentiated GIC state	81
Figure 18. Increased H3K4me3 binding at promoter regions of tumor suppressor genes	83
Figure 19. Increased binding of H3K4me3 leads to increased transcript levels of <i>GNG4</i> , <i>NDUFS1</i> , and <i>TNFAIP1</i>	84
Figure 20. Increased binding of H3K4me3 leads to unchanged transcript levels of <i>ETV6</i> and <i>TUSC2</i>	85
Figure 21. Knockdown of IDH1 sensitizes cells toward Erlotinib-induced apoptosis	87
Figure 22. Knockdown of IDH1 sensitizes cells toward Erlotinib-induced apoptosis by decreasing lipid production	88
Figure 23. Knockdown of IDH1 sensitizes cells toward Erlotinib-induced apoptosis by increasing ROS production	89
Figure 24. Knockdown of IDH1 sensitizes transformed glioma cells harboring co- activation of multiple RTKs toward RTKi	91
Figure 25. IDH1 protects cancer cells derived from non-glioma tumors from apoptosis	93
Figure 26. RTKi induce IDH1 expression through FoxO6	95
Figure 27. Transcriptomic survey of RTKi-treated and untreated LN382 cells point to lipid biosynthesis as a major roadblock to RTKi-treatment	96
Figure 28. Knockdown of IDH1 or LSS increases RTKi-induced apoptosis	98
Figure 29. GSK864, an inhibitor of mutant IDH1, has activity against wild-type IDH1	100
Figure 30. GSK864 inhibits GBM cell growth and increases RTKi-induced apoptosis <i>in</i> <i>vitro</i>	101
Figure 31. GSK864 decreases tumor burden and prolongs subject survival <i>in vivo</i>	102

Figure 32. IDH1 promotes tumor progression

CHAPTER 1: INTRODUCTION

1.1 Opening

Since the discovery of specific point mutations in *IDH1* in 2008 in GBM, IDH1 biology has become a major field of study for GBM, and other cancers. However, this has been mainly in respect to IDH1 mutation biology and not wild-type IDH1 biology. GBM can be classified as either primary or secondary. Secondary GBM develop from lower grade tumors, many of which harbor IDH1 mutations, whereas primary or *de novo* GBM occur as a Grade IV tumor without a preceding lower grade malignancy (Ohgaki and Kleihues, 2005). As primary GBM accounts for the majority of GBM cases, which contain few IDH1 mutations, and patients with mutated IDH1 have a significantly prolonged survival compared to patients with wild-type IDH1 (Ohgaki and Kleihues, 2005), we wanted to determine if wild-type IDH1 impacted *de novo* GBM pathogenesis. We discovered that wild-type IDH1 is overexpressed in primary GBM, protects cells from targeted therapy induced apoptosis through increasing metabolic flux to lipids, maintaining a more dedifferentiated state, and inhibiting ROS. Furthermore, IDH1 levels are increased further by receptor tyrosine kinase inhibitor (RTKi) treatment and inhibition of IDH1 increases the efficacy of RTKi therapies. We have extended the view of IDH1 biology by functionally characterizing the upregulation of non-mutated IDH1 in primary GBM as a novel oncogenic mechanism to be exploited to augment the efficacy of targeted therapies.

1.2 Glioblastoma (GBM)

1.2.1 Overview and Standard of Care

Glioblastoma (GBM; World Health Organization Grade IV glioma) is the most prevalent and fatal form of primary brain tumors. Survival for GBM patients is just 14-16 months after initial

diagnosis (Cloughesy et al., 2014; Dunn et al., 2012). Malignant diffuse gliomas consist of astrocytic, oligodendroglial, and mixed oligoastrocytic cell populations based on their histological appearance. Astrocytomas are defined by a large amount of cytoplasm and expression of glial fibrillary acidic protein (GFAP) while oligodendrocytomas are characterized by small, round nuclei, little cytoplasm, and no expression of GFAP (Holland, 2001). A Grade III neoplasm is characterized by nuclear atypia and mitotic activity while Grade IV GBM are necrotic and have microvascular proliferation (Dunn et al., 2012).

There are two main types of GBM, primary and secondary. Primary or '*de novo*' GBM account for more than 90% of malignant glioma, while secondary GBM, which arise from lower-grade gliomas in younger patients represent less than 10% of clinical cases (Ohgaki and Kleihues, 2005). While primary and secondary GBM are histopathologically identical, they represent two distinct diseases that arise through deregulation of different genetic pathways. *EGFR* mutations and amplifications, and *PTEN* mutations are more frequent in primary GBM, whereas *TP53* mutations are more frequent in secondary GBM. Secondary GBM patients have a median survival of 7.8 months, whereas primary GBM patients only have a median survival of 4.7 months (Ohgaki and Kleihues, 2005).

Current standard of care for patients is surgical resection followed by co-treatment of radiotherapy and the chemotherapeutic agent, temozolomide (TMZ). Because of these tumors location and highly infiltrative behavior, it is very difficult to achieve a complete surgical resection, always leading to tumor recurrence. In fact most tumor recurrence occurs within 2-3 cm from the original tumor (Jue and McDonald, 2016). Recurrent tumors can also differ in genetic profile from the original tumor, especially if the tumor is harboring *TP53* mutations.

These tumors have increased complexity when they recur, while wild-type *TP53* tumor recurrences are more similar to the debulked tumor (Jue and McDonald, 2016). While most chemotherapeutics have shown little to no effect in GBM patient survival, TMZ has been the most successful advancement in the treatment of GBM patients in recent history. TMZ acts as an alkylating agent, which leads to DNA damage through depletion of the DNA repair enzyme O⁶-methylguanine-DNA methyltransferase (MGMT), and subsequent cell death (Li et al., 2016). In a phase III clinical trial of newly diagnosed GBM patients, when TMZ was added to radiotherapy overall survival was significantly increased compared to the radiotherapy alone group after 28-month median follow-up. The 2-year survival was also significantly increased in the TMZ group compared to the radiotherapy-alone group. This study provided the current standard of care of adding TMZ to tumor debulking and radiotherapy as a first line of defense in GBM patients (Stupp et al., 2005). However, all patients still succumb to the disease.

1.2.2 Genomic Subtypes

GBM was the first cancer subtype studied by The Cancer Genome Atlas (TCGA) project and their initial study was published in 2008. The TCGA looked at over 200 GBM tumors and found that there are three main pathways altered in GBM; Receptor Tyrosine Kinase pathway, p53 pathway, and Retinoblastoma pathway. 74% of tumors had alterations in all three of these pathways, suggesting that a core requirement for GBM is deregulation of all three pathways (TCGA, 2008). *PTEN* is mutated, epigenetically inactivated, or lost in 40-50% of gliomas and as it directly antagonizes PI3K signaling, PI3K signaling is maintained at high levels in gliomas (Dunn et al., 2012). GBM patients with activated PI3K/Akt/mTOR pathway have a poorer

overall survival compared to patients without alterations in this pathway (Li et al., 2016). *NF1*, a tumor suppressor that is known to inhibit Ras, is found to be mutated or deleted in 10% of GBM (Brennan et al., 2013). *NF1* loss can increase glioma cell growth *in vitro* and *in vivo*, but does not have the ability to induce gliomagenesis alone (Dunn et al., 2012).

Furthermore, Verhaak et al., took the information from the TCGA database as well as several other independent studies to segregate GBM tumors into subtypes based on their genomic characteristics. The four subtypes are Classical, Mesenchymal, Proneural, and Neural. The Classical, Mesenchymal, and Proneural subtypes are not only found in patient tumors, but are also maintained in xenografts. The Classical subtype is defined by chromosome 7 amplification (*EGFR* locus) and chromosome 10 loss (*PTEN* locus). While *EGFR* amplification is observed in other subtypes, it is much more highly expressed in the Classical subtype. Other defining characteristics of the Classical subtype include lack of *TP53* mutations, 9p21.3 homozygous deletion (targeting *CDKN2A*), neural precursor and stem cell marker expression (*NES*, *NOTCH3*, *JAG1*, *LFNG*), and high expression of sonic hedgehog genes (*SMO*, *GAS1*, *GLI2*). The Mesenchymal subtype consists of tumors with deletion of 17q11.2 (*NF1* gene), resulting in lower *NF1* expression levels, *PTEN* loss, mesenchymal (*CHI3LI*, *MET*) and astrocytic (*CD44*, *MERTK*) marker expression, high expression of TNF and NF- κ B (*TRADD*, *RELB*, *TNFRSF1A*) genes, and higher overall necrosis and inflammation. The Proneural subtype is defined by alteration in *PDGFRA* and *IDH1* mutations, however most *IDH1* mutant tumors do not have *PDGFRA* alterations. It was also found that this subtype contains many *TP53* mutations and loss-of-heterozygosity (LOH), high expression of oligodendrocytic genes (*PDGFRA*, *NKX2-2*, *OLIG2*), and proneural developmental genes (*SOX*, *DCX*, *DLL3*, *ASCL1*, *TCF4*). The Neural

subtype is the least well defined, as these tumors contain many of the abnormalities seen in the other subtypes, but also contain expression of neuron markers (*NEFL*, *GABRA1*, *SYT1*, *SLC12A5*). (Verhaak et al., 2010) These characteristics are summarized in Figure 1.

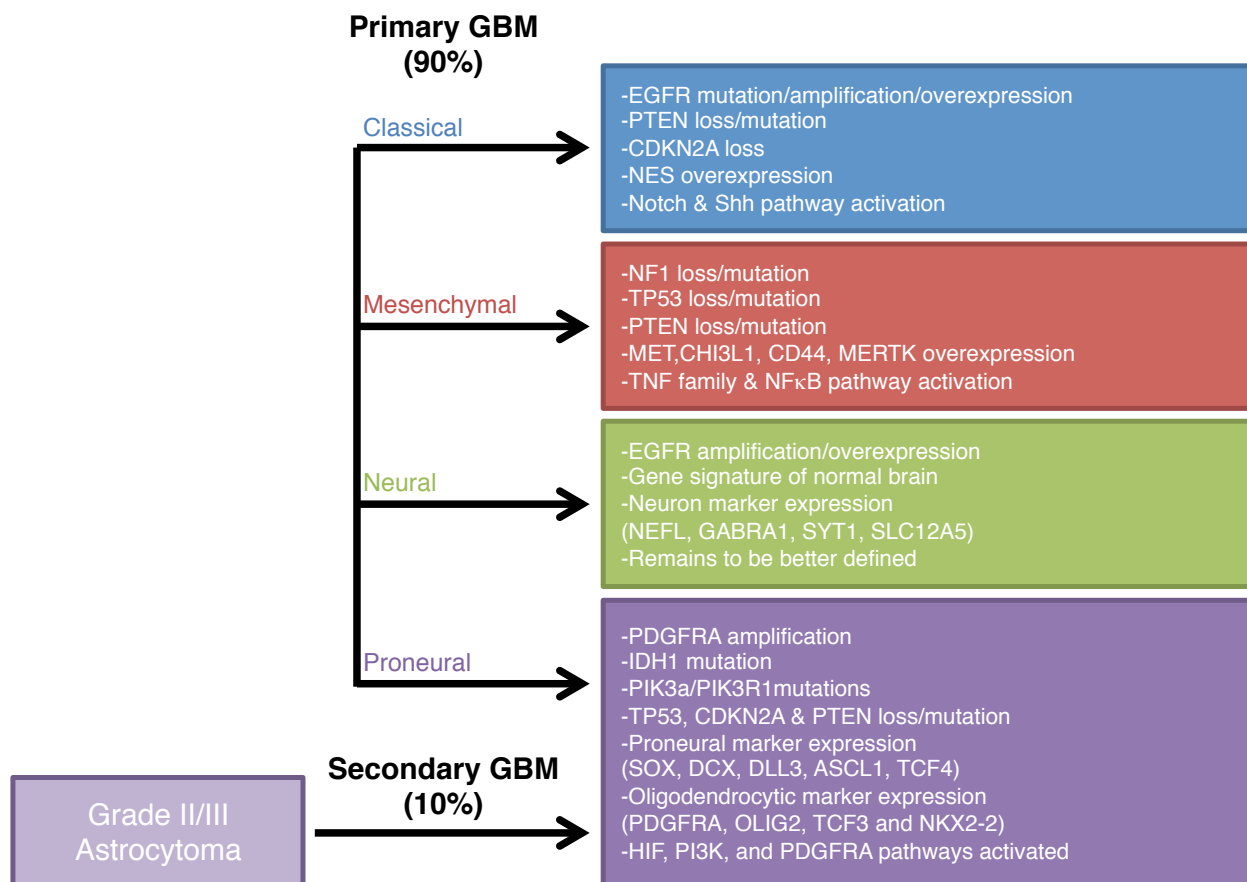


Figure 1. GBM Genomic Subtypes

GBM can be categorized into 4 subtypes based on their genetic profiles. (Adapted from Van Meir et al., 2010.)

Each of these subtypes have similarities to different neural cell types, indicating that these subtypes may arise from different cells of origin. The Proneural subtype are enriched with an oligodendrocytic signature, the Classical subtype are enriched with a murine astrocytic signature,

the Neural subtype are enriched with oligodendrocytic and astrocytic differentiation signature and neurons, and the Mesenchymal subtype are enriched for a cultured astroglial signature (Verhaak et al., 2010). These subtypes also give us insight into survival and treatment outcomes. Patients with Proneural tumors have a trend to increased overall survival, which may be due to the younger age of patients with this subtype as well as most secondary GBMs being included in this subtype, or because mutant *IDH1* tumors are found in the Proneural subtype. If the Proneural subtype is split into those with and those without *IDH1* mutations, only those with *IDH1* mutations have a survival advantage (Jue and McDonald, 2016). When looking at the effect of aggressive treatment on the various subgroups, combined chemotherapy and radiation or at least three rounds of chemotherapy did have a significant benefit to survival in patients with Classical and Mesenchymal tumors and a trend towards significance in Neural tumors, but did not affect tumors with a Proneural signature (Verhaak et al., 2010). This suggests that our treatment regimens can and should be based on the genomic analysis of each patient's tumor.

1.2.3 RTK Signaling and Targeted Therapies

Most GBMs harbor RTK amplifications and mutations and are driver mutations in many of these tumors. Alterations in RTKs usually occur in the context of other PI3K-pathway alterations and *CDKN2A* loss (Furnari et al., 2015). *EGFR* amplifications and mutations are the prevailing RTK alteration in GBM (57%; Brennan et al., 2013). The major mutation in *EGFR* is *EGFR* variant III (*EGFRvIII*), which consists of the loss of exons 2 through 7 in the extracellular domain, resulting in the constitutive activation of *EGFR*. While *EGFR* is amplified or mutated in most GBM tumors and *EGFR* targeted therapies, including Erlotinib and Gefitinib, are approved for use in

non-small cell lung cancer (NSCLC) (Mahipal et al., 2014), these drugs have shown little to no efficacy in GBM patients in clinical trials, even in combination with other targeted therapies, including mTOR and VEGF inhibitors (Reardon et al., 2010; Raizer et al., 2015). Some of the reasons that EGFR-targeted therapies have not worked in GBM will be discussed below.

Erlotinib and Gefitinib are kinase domain competitive inhibitors that work in patients with *EGFR* mutations in NSCLC, the most common of which are L858R and del746-750, both occurring in the kinase domain. Mutations in GBM are found almost exclusively in the extracellular domain (Lee et al., 2006b; Vivanco et al., 2012). These reversible kinase domain inhibitors do not effectively bind with the same affinity to EGFR in GBM as they do in NSCLC (Barkovich et al., 2012; Vivanco et al., 2012). To correct for this, newer classes of drugs have been made, including Lapatinib which is dual inhibitor of both EGFR and HER2 and inhibits EGFR by binding to the ATP binding pocket, but this drug has also shown little efficacy in GBM patients. This is thought to be due to the inability of Lapatinib to reach significant levels in the brain (Vivanco et al., 2012). It is also not certain that these drugs easily cross the blood brain barrier (BBB). While Erlotinib and Gefitinib do enter the brain, and decrease phosphorylated EGFR (pEGFR) activity, it might not be to the extent necessary to decrease downstream signaling. The BBB is an extensive network of capillaries formed by neurovascular and endothelial cells, as well as astrocytes and pericytes. This barrier limits what can access the brain from the blood stream (Jue and McDonald, 2016). While this protective function is typically advantageous as it prevents entry of potentially harmful molecules such as neurotoxins into the brain and helps regulate concentrations of essential molecules within the brain, in the case of delivering drugs to the brain, it becomes another obstacle that needs to be overcome in the treatment of gliomas.

Not only do the mutations in *EGFR* differ between GBM and NSCLC, but ways in which the tumors become resistant to targeted therapies also vary between these two cancer types. While Erlotinib and Gefitinib have shown to reduce levels of pEGFR in GBM patient tumors, downstream signaling is maintained, leading to no survival benefit in response to these inhibitors (Li et al., 2016). Several studies have pointed to co-activation of multiple RTKs as a resistance mechanism to EGFR-targeted therapies. While most GBMs harbor activation of numerous RTKs that activate the same downstream pathways, co-extinction strategies must be employed to decrease downstream signaling and viability (Stommel et al., 2007). EGFRvIII can phosphorylate and activate cMET and combined inhibition of cMET and EGFR led to increased apoptosis compared to inhibition of EGFR alone (Huang et al., 2007). Furthermore, in a genetic mouse model of GBM with inactivation of *Pten* and *Ink4a/Arf*, with inducible expression of *EGFRvIII*, treatment with either Erlotinib or Gefitinib did not significantly reduce tumor formation as genetic ablation of *EGFRvIII* did even though pEGFR expression was significantly reduced in the tumors. Further analysis of these tumors found that inhibition of cMET, which is increased as a resistance mechanism, did not prolong survival of mice in combination with EGFR inhibition, but downstream inhibition of PI3K/mTOR did prolong survival in combination with EGFR inhibition (Klinger et al., 2015), demonstrating inhibition of multiple targets in the same pathway has more effect than targeting several parallel pathways.

Intriguingly, RTK expression is heterogenous. Co-amplification of both *EGFR*, *PDGFRA*, and/or *cMET* can occur in the same tumor. However, they are rarely found in the same cells, but in distinct subpopulations within the tumor (Snuderl et al., 2011; Szerlip et al., 2012). Furthermore, *EGFRvIII* DNA can be located in double minute DNA fragments outside of chromosomes,

which are then passed to cells in an unequal manner resulting in differing levels of *EGFRvIII* in different cells throughout the tumor (Nathanson et al., 2014). These diverse, heterogenetic alterations lead to the pro-proliferative characteristic of tumors and protection against targeted therapies.

1.2.4 GBM Cancer Stem Cells

Stem cells are defined by the ability to self-renew and have multi-potent differentiation capacity. Neural stem cells (NSCs), which give rise to all neurons and macroglial cells in the brain, are located in a hypoxic niche, which helps maintain an undifferentiated state (Ito and Suda, 2014). There are two types of macroglial cells, astrocytes and oligodendrocytes, both of which can become GBMs. Astrocytes are the major type of glial cell, help form the BBB, and a subpopulation of astrocytes function as adult neural stem cells, while oligodendrocytes form the myelin sheath (Gotz and Huttner, 2005). It is unclear if NSCs, astrocytes, or oligodendrocytes are the cell of origin for GBM, or if all could be, but neural stem cells, astrocytes, and differentiated neurons can all become gliomas through lentiviral transduction (Friedmann-Morvinski et al., 2012). The order of molecular events leading to primary GBM is hard to delineate as the tumors are already very malignant when first diagnosed (Furnari et al., 2015). Cancer stem cells (CSCs), while similar to normal stem cells, are not necessarily the cell of origin of tumors. Understanding the biology of GBM CSCs is important as they are resistant to conventional therapies. In a mouse model of GBM, lineage tracing experiments found that CSCs are resistant to TMZ treatment and can repopulate the tumor after treatment (Lathia et al., 2015).

If we are able to define the GBM CSCs, we will be better able to specifically target these cells to potentially halt tumor recurrence.

CSCs may have slightly different features than normal stem cells (Lathia et al., 2015). CSCs self-renew and are able to differentiate into various progeny, have the same transcription factor signatures (*SOX2*, *NANOG*, *OLIG2*, *MYC*, *MUSASHI*, *BMI1*, *NESTIN*, *ID1*) as NSCs, and have several surface markers that differentiate CSCs from non-stem tumor cells (CD133, CD15, integrin $\alpha 6$, CD44, LICAM, A2B5) (Lathia et al., 2015). CD133 is the most widely used marker for glioma stem cells. It is a cell surface glycoprotein that is encoded by the *Prominin-1* gene. It is enriched in cells that have higher rates of self-renewal and proliferation, as well as decreased as cells undergo differentiation. However, mRNA expression of *Prominin-1* is not correlated with stemness (Lathia et al., 2015).

To determine if cells are in fact actually stem cells, the most important experiment to perform is to transplant potential CSCs in a limiting dilution fashion orthotopically into mice, and determine if the tumors formed are similar to the parental tumor that the CSCs came from. There are four transcription factors that can reprogram glioma cells into glioma CSCs: *POU3F2*, *SOX2*, *SALL2*, and *OLIG2* (Suva et al., 2014). When these induced tumor propagating cells (iTPCs) are orthotopically injected into mice, they form high-grade glioma tumors with typical features, including necrosis, atypical cytonuclear features, high mitotic index, and high levels of CD133. As few as 50 iTPCs were able to produce tumors in 50% of the mice, while 500 cells were able to produce tumors in 100% of the mice (Suva et al., 2014). These experiments show that transcription factors important for normal stem cells are also necessary for CSCs.

Metabolic changes in stem cells and their niches also provide maintenance of these cells. GBM CSCs reside in hypoxic niches which limits oxygen and glucose availability. Therefore, GBM CSCs do not depend on oxidative phosphorylation for ATP generation, but are mostly supported by anaerobic glycolysis (Lathia et al., 2015). These cells also have increased glucose uptake compared to NSCs as CSCs have increased GLUT3 transporter protein (Lathia et al., 2015) and NSCs require Fatty Acid Synthase (FASN) to maintain lipogenesis to promote proliferation and maintain neurogenesis in mice (Ito and Suda, 2014; Yasumoto et al., 2016). Reactive oxygen species (ROS) play an important role in NSCs, which are sensitive to increases in ROS. Increases in ROS in normoxic conditions cause NSCs to be forced out of their hypoxic state of quiescence and into a more proliferative cell state (Ito and Suda, 2014). Furthermore, there are many similarities between pluripotent stem cells and cancer cells, for example, both cell types exhibit elevated levels of TCA intermediates to increase anaplerosis and rapid cell proliferation (Zhang et al., 2012).

1.2.5 Metabolic Adaptations in GBM

Alterations in cancer cell metabolism have been described since the 1920s. Otto Warburg observed that cancer cells undergo glycolysis even in the presence of abundant oxygen (aerobic glycolysis) (Warburg et al., 1927). The ‘Warburg Effect’ has been confirmed in many cancer types and the enhanced glucose uptake necessary for this process has been exploited for tumor imaging. Positron emission tomography (PET)-based imaging of ^{18}F -fluorodeoxyglucose has been used for tumor diagnosis, staging, and treatment response in patients (Pavlova and Thompson, 2016). While Warburg initially described this phenomenon necessary for tumor cell

growth because of dysfunctional mitochondria in these cells, this was later reputed as most tumors maintain mitochondrial function for oxidative phosphorylation. Why do tumors then have increased glycolytic flux? Increased glycolysis leads to increased ATP production necessary for the high energy demands of proliferating cells. It has also been proposed that this process occurs as an adaptation during early tumorigenesis under hypoxic conditions when tumor cells do not have enough oxygen supplied to them because of the avascular nature of the tumor, and/or it occurs to provide carbon and reducing equivalents for macromolecular biosynthesis necessary for rapid proliferation through offshoots of glycolysis, including the pentose phosphate pathway (PPP) (Cairns et al., 2011).

In GBM particularly, glycolysis is enhanced three-fold compared to normal brain (Wolf et al., 2010). Various genetic alterations have been shown to increase glucose uptake in tumor cells, including Ras, c-MYC, and PI3K/Akt pathway activation. Ras can increase glucose consumption of tumors as well as increase glucose transporter GLUT1 (Pavlova and Thompson, 2016). c-MYC is a master transcription factor of energy metabolism and while it is mutated in many types of cancer, it is rarely mutated in GBM, however, EGFRvIII can co-opt c-MYC to reprogram GBM metabolism (Masui et al., 2016). PI3K/Akt is a master regulator of glucose uptake. It activates the glucose transporter GLUT1 and its translocation to the membrane, as well as activates the glycolytic enzymes hexokinase (HK) and phosphofructokinase (PFK) (Pavlova and Thompson, 2016). HK2 and transketolase (TKTL1) are increased glycolytic enzymes in GBM (Wolf et al., 2010). TKTL1 is an enzyme in the non-oxidative branch of the PPP responsible for converting ribulose-5-phosphate to fructose-6-phosphate. TKTL1 expression and activity are increased in GBM and other cancers and its expression is positively correlated with tumor

growth (Volker et al., 2008; Langbein et al., 2006). HK2 is the first step in glycolysis converting glucose to glucose-6-phosphate. HK2 is overexpressed in GBM, whereas other isoforms (HK1 and HK3) are not. HK2 expression is correlated with poorer overall survival in GBM patients and xenograft mouse models with decreased HK2 expression have decreased proliferation and angiogenesis (Wolf et al., 2011), pointing to HK2 as a potential therapeutic target in GBM. Vartanian et al. made an inducible knockdown of HK2 intracranial xenograft model and found that the knockdown of HK2 sensitized these tumors to radiation and TMZ (Vartanian et al., 2016). Furthermore, the knockdown of 7 different glycolytic genes (*PFK1*, *PDK1*, *PGAM1*, *ENO1*, *HK2*, *ALDOA*, and *ENO2*) each had survival benefits of intracranial xenograft GBM mouse models (Sanzey et al., 2015).

However, increased glycolysis cannot account for all the metabolic changes required for enhanced tumor cell growth. GBM tumors also have increased glutamine uptake and glutaminolysis to provide cells with carbon precursors for anaplerosis (Wolf et al., 2010). While it was once thought that glutamine was the main carbon source for anaplerosis, it has now been shown that while GBM tumors have an increased uptake in glutamine, it is not deaminated to glutamate and then reductively carboxylated to α KG (Marin-Valencia et al., 2012). Furthermore, it has been demonstrated that it is glucose and acetate that are oxidized in GBM patient tumors implanted directly into mouse brains (Marin-Valencia et al, 2012; Mashimo et al., 2014). While these tumors have enhanced glucose oxidation through the TCA cycle, they also maintain high levels of glycolysis. In addition, these PDX (patient-derived xenograft) tumors came from patients with various genetic backgrounds, yet they all displayed similar metabolic abnormalities.

Another metabolic abnormality that was originally published over 60 years ago described tumor tissues as having increased *de novo* fatty acid synthesis (Medes et al., 1953). While this phenotype was not extensively studied at the time, it has now gained more attention in the last twenty years. On molecular levels, expression of enzymes implicated in *de novo* fatty acid synthesis (ACLY, ACC, FASN) is increased in many cancers including GBM. ACLY (ATP citrate lyase) converts citrate to acetyl-CoA, a necessary substrate for fatty acid synthesis. ACC (acetyl-CoA carboxylase) then converts acetyl-CoA to malonyl-CoA, which is then used by FASN (fatty acid synthase) to produce palmitate, a saturated fatty acid. Palmitate can then further be converted into mono- or poly-unsaturated fatty acids (Guo et al., 2013). This increased fatty acid synthesis in GBM results in accumulation of various lipids, including unsaturated fatty acids, cholesterol esters, phosphatidyl choline, and cholesterol uptake within the tumor (Guo et al., 2013). This accumulation of fatty acids is necessary for cancer cells as substrates of cellular membranes and energy metabolism (Menendez and Lupu, 2007). ACLY, ACC, and FASN are upregulated by the transcription factor sterol regulatory element binding protein 1 (SREBP1), which is activated by the RTK/PI3K/Akt/mTOR pathway (Wolf et al., 2010). In GBM cells that have persistent EGFR signaling, activation of AMPK or inhibition of FASN inhibits tumor growth through inhibition of lipogenesis (Guo et al., 2009a; Guo et al., 2009b). AMPK (AMP-activated protein kinase) opposes the function of Akt and is a known integrator of metabolic energy status and growth factor receptor signaling (Guo et al., 2009a). Akt also activates *de novo* lipogenesis through phosphorylation and direct activation of ACLY (Cantor and Sabatini, 2012). In addition to the above, mutations in IDH1/2 have been identified and will be further described below. Alterations in GBM metabolism are many and contribute to the increased proliferation of

these tumor cells. The hallmarks described above, i.e., enhanced glycolysis, TCA cycle, and *de novo* lipogenesis are summarized in Figure 2 and point to altered GBM metabolism as pathways that can potentially be therapeutically exploited.

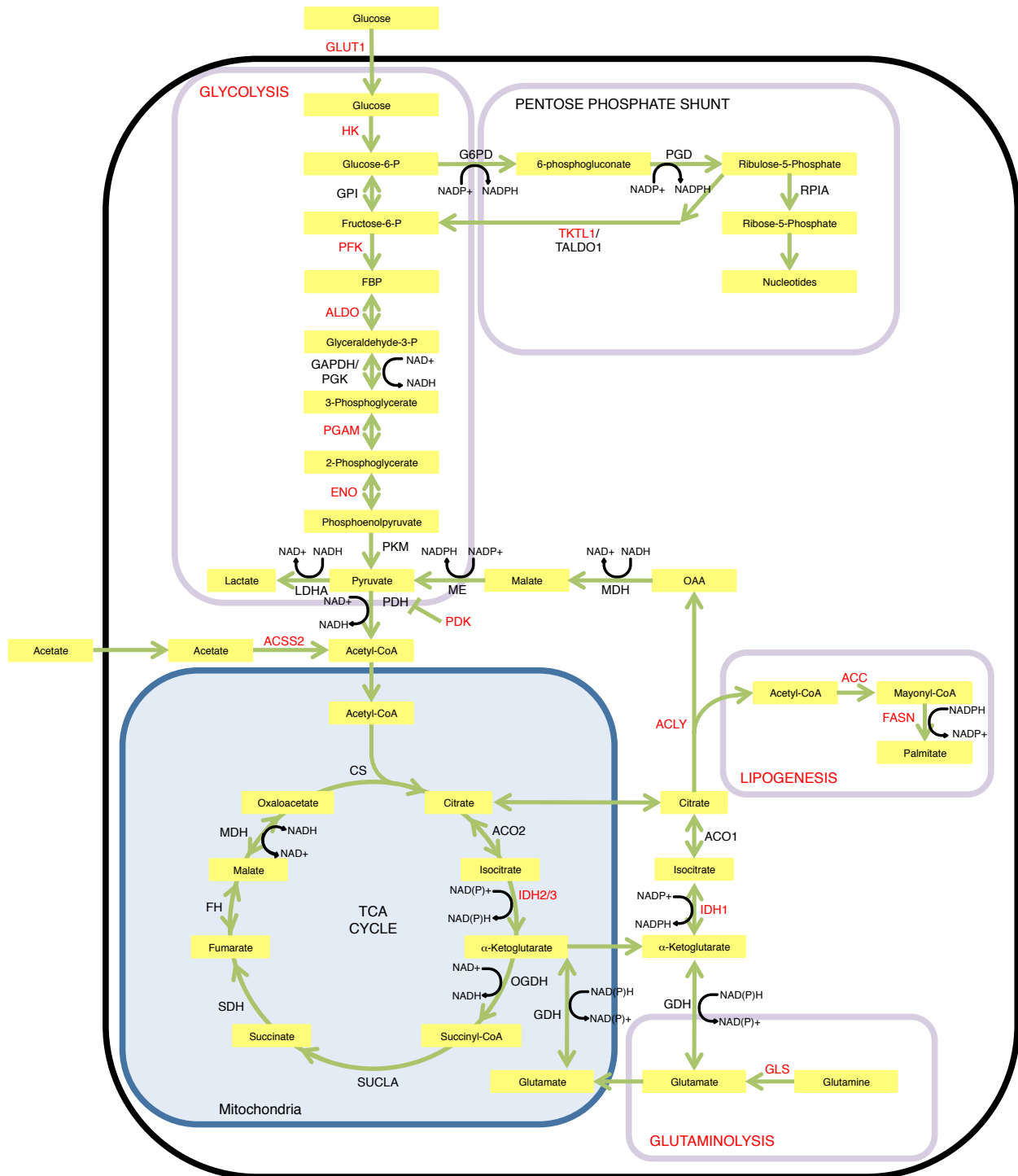


Figure 2. Altered GBM Metabolism

This schematic shows enzymes and pathways which play a role in the pathogenesis of GBM through altered metabolism (in red). GLUT1, solute carrier family member 1; HK, hexokinase; GPI, glucose-6-phosphate isomerase; PFK, phosphofructokinase; ALDO, aldolase; GAPDH, glyceraldehyde-3-phosphate dehydrogenase; PGK, phosphoglycerate kinase; PGAM, phosphoglycerate mutase; ENO, enolase; PKM, pyruvate kinase; LDHA, lactate dehydrogenase A; PDH, pyruvate dehydrogenase; PDK, pyruvate dehydrogenase kinase; ACSS2, acyl-CoA synthetase; CS, citrate synthase; ACO2, aconitase 2; IDH2/3, isocitrate dehydrogenase 2/3; OGDH, α -ketoglutarate dehydrogenase; SUCLA2, succinyl-CoA synthetase; SDH, succinate dehydrogenase; FH, fumarase; MDH, malate dehydrogenase; GLS, glutaminase; GDH, glutamate dehydrogenase; IDH1, isocitrate dehydrogenase 1; ACO1, aconitase 1; ACLY, ATP citrate lyase; ME, malic enzyme; ACC, acetyl-CoA carboxylase, FASN, fatty acid synthase; G6PD, glucose-6-phosphate dehydrogenase; PGD, phosphogluconate dehydrogenase; RPIA, ribose-5-phosphate isomerase A; TKTL1, transketolase; TALDO1, transaldolase.

1.3 Isocitrate Dehydrogenase 1 (IDH1)

1.3.1 Function of wild-type IDH1

Isocitrate dehydrogenase (IDH) is responsible for the oxidative decarboxylation of isocitrate to α -ketoglutarate (α KG). There are three isoforms of IDH in eukaryotic cells (Dalziel, 1980). IDH1 and IDH2 are homodimeric NADP⁺-dependent enzymes that are reversible reactions, while IDH3 is a structurally distinct heterotetrameric enzyme that utilizes NAD⁺ as a co-factor and is irreversible. The different IDH isoforms have overlapping, but non-redundant roles in cellular metabolism (Mailloux et al., 2007; Reitman and Yan, 2010). IDH3 is responsible for the rate-limiting step within the tricarboxylic acid (TCA) cycle. IDH2 is also located in the mitochondria and is involved in regulation of the TCA cycle and oxidative phosphorylation. IDH2 is highly expressed in the heart, muscle and activated lymphocytes and modestly elsewhere. Whereas IDH1 is highly expressed in the liver with modest expression in other tissues, including the brain. IDH1 expression is also decreased overtime in aging mice (Reitman

and Yan, 2010). Cytoplasmic and peroxisomal IDH1 produces non-mitochondrial α KG and NADPH, to activate various α KG-dependent dioxygenases (Hausinger, 2004), and to provide reducing equivalents to support lipid biosynthesis and redox homeostasis (Jo et al., 2002; Lee et al., 2002; Kim et al., 2007), (Figure 3A).

1.3.2 IDH1 and α KG-dependent dioxygenases

Epigenetics has gained increased interest in cancer research as it plays a major role in the regulation of many different developmental and transcriptional programs. α KG is a cofactor for many enzymes involved in the regulation of epigenetics, including Jumonji (JmjC) family of histone demethylases and the TET (ten-eleven translocation) family of DNA hydroxylases. As IDH1 is a contributor to cellular α KG pools, IDH levels can play a role in epigenetic regulation. Similarly, mutations in D2HGDH (D-2-hydroxyglutarate dehydrogenase) in diffuse large B cell lymphoma (DLBCL) leads to decreased α KG accumulation, causing increased histone methylation, decreased 5hmC, decreased NADPH/NADP⁺, and increased ROS (Lin et al., 2015).

Histone methylation while once thought to be a static process has been determined to be very dynamic and regulated by various histone demethylases. Histone methylation can occur at lysine and arginine residues on histone tails. Methylation at these residues does not change the charge of the DNA, like histone acetylation does, and has no direct effect on DNA and histone interaction. Histone methylation acts as a recognition motif for other various activating or repressing proteins depending on the specific mark. For example, methylation on H3K4 and H3K36 are activating marks while methylation on H3K9 and H3K27 are repressing marks. One

of the largest classes of histone demethylases are the JmjC family. The JmjC family consists of 30 different histone demethylases which require α KG as a cofactor. The JmJC histone demethylases bind to Fe^{2+} to form a complex that can then bind to the cofactor α KG, then its substrate and oxygen. This allows α KG to be oxidatively decarboxylated to form succinate, carbon dioxide, and ferryl. Ferryl is able to oxidize the carbon-nitrogen bond in lysine and methyl groups, allowing that bond to break, and release a methyl group (Cloos et al., 2008). In addition to the α KG-dependent JmjC demethylases, the TET family of DNA hydroxylases require α KG (Kaelin and McKnight, 2013). The TET family hydroxylate 5-methylcytosine (5mC) to 5-hydroxymethylcytosine (5hmC) leading to decreased DNA methylation and actively transcribed genes. As both JmjC and TET proteins require α KG, a product of IDH1, IDH1 may regulate epigenetics.

1.3.3 IDH1 and Metabolism

IDH1 has been implicated in *de novo* lipogenesis, as it produces NADPH. A transgenic mouse model that overexpresses IDH1 in the liver and adipose tissue has fatty livers, hyperlipidemia, and increased body weight as well as decreased acetyl-CoA and malonyl-CoA levels. (Koh et al., 2004). Acetyl-CoA and malonyl-CoA are necessary carbon sources for fatty acid synthesis. As these levels are decreased in transgenic IDH1 overexpressing mice, it is thought that they are being used up more rapidly to produce more fatty acids and leading to the obese mouse phenotype. Ablation of IDH1 in another mouse model through overexpression of IDH1-targeting miR-181a led to decreased size and lower body weight (Chu et al., 2015). Another group transduced mice with an shRNA targeted to IDH1 and found that these mice with decreased

IDH1 expression in the liver, had significantly less weight gain, and blood triglyceride levels than control mice when on a high fat diet (Nam et al., 2012).

Under hypoxic conditions or in tumor cells with defective mitochondria, IDH1 works in the reverse reaction as it reductively carboxylates glutamine derived α KG to isocitrate to citrate (Wise et al., 2011; Metallo et al., 2012; Mullen et al., 2012). Citrate can then be converted into cytosolic acetyl-CoA for lipogenesis. This was an important finding showing that IDH1 plays another role in lipid metabolism through maintenance of citrate production necessary for fatty acid biosynthesis.

NADPH is a necessary cofactor in lipid biosynthesis, the synthesis of one molecule of palmitate requires 14 molecules of NADPH and cholesterol requires 26 molecules of NADPH. NADPH specifically from IDH1 has been more recently implicated in lipogenesis. As SREBPs are the master regulatory transcription factors of cholesterol and fatty acid biosynthesis and IDH1 is upregulated in response to SREBP activation, it is possible that NADPH from IDH1 is necessary for this biosynthesis (Shecter et al., 2003) whereas other cytosolic NADPH-producing enzymes have not specifically been implicated in lipogenesis. Furthermore, NADPH from IDH1 is 16- and 18- fold higher than from glucose 6-phosphate dehydrogenase (G6PD) and malic enzyme respectively, in rat liver (Veech et al., 1969) and increased fatty acid biosynthesis in high IDH1 expressing adipocytes is likely due to the ability of IDH1 to produce cytosolic NADPH (Koh et al., 2004). These studies all point to IDH1 as playing a major role in *de novo* lipogenesis.

1.3.4 IDH1 and Redox Homeostasis

NADPH is an important reducing equivalent and is necessary for maintaining reduced glutathione (GSH) levels. GSH is the major antioxidant in the cell necessary to neutralize reactive oxygen species (ROS). During oxidative stress, ROS (superoxide, H₂O₂, hydroxyl radical), reactive nitrogen species (RNS; NO, ONOO⁻), reactive sulfur species (RSS), and reactive chloride species (RCS) are produced. These reactive species can oxidize DNA to generate 8-hydroxy-2-deoxyguanosine, leading to DNA mutations as well as interact with DNA, RNA, protein, and lipids to induce DNA alterations, cellular damage, and ultimately cell death (Salazar-Ramiro et al., 2016).

While it has long been thought that glucose G6PD is the major cytosolic enzyme producing NADPH, more recent studies have shown a major role for IDH1 to produce cytosolic NADPH. When cells are treated with oxidative stressors, the amount of IDH1 present determines if the cells are sensitive or not. Overexpression of IDH1 makes cells more resistant to UVB radiation, H₂O₂, and menadione, while knockdown of IDH1 makes cells more sensitive (Jo et al., 2002; Lee et al., 2002; Kim et al., 2007), demonstrating that NADPH from IDH1 has a protective role against oxidative damage. Furthermore, α KG can play a role in scavenging H₂O₂. Non-enzymatic decarboxylation of α KG to succinate and H₂O will also detoxify ROS (Chakrabarti et al., 2015). To demonstrate the importance of IDH1 in redox homeostasis *in vivo*, a global IDH1 knockout (KO) mouse was developed. This group had previously used these IDH1^{LSL/WT} mice on a C57BL/6 background crossed with LysMCre or NestinCre mice to generate mice with the IDH1-R132H mutation in either hematopoietic or neuronal cells, respectively (Sasaki et al., 2012a; Sasaki et al., 2012b). In the absence of Cre recombinase, the IDH1^{LSL/LSL} mice are null

for IDH1 in all tissues. While this mouse developed and reproduced normally, it was more sensitive to oxidative damage induced by LPS treatment. LPS treated IDH1 KO mice had more oxidative damage, increased oxidative stress-induced genes, and increased mortality compared to wild-type LPS treated mice (Itsumi et al., 2015). Since the IDH1 KO mice do not have as much NADPH to counteract the increased oxidative stress brought on by LPS treatment, they become more susceptible to LPS treatment. These studies demonstrate that cytoplasmic NADPH from IDH1 is necessary to help maintain a balanced cellular redox state.

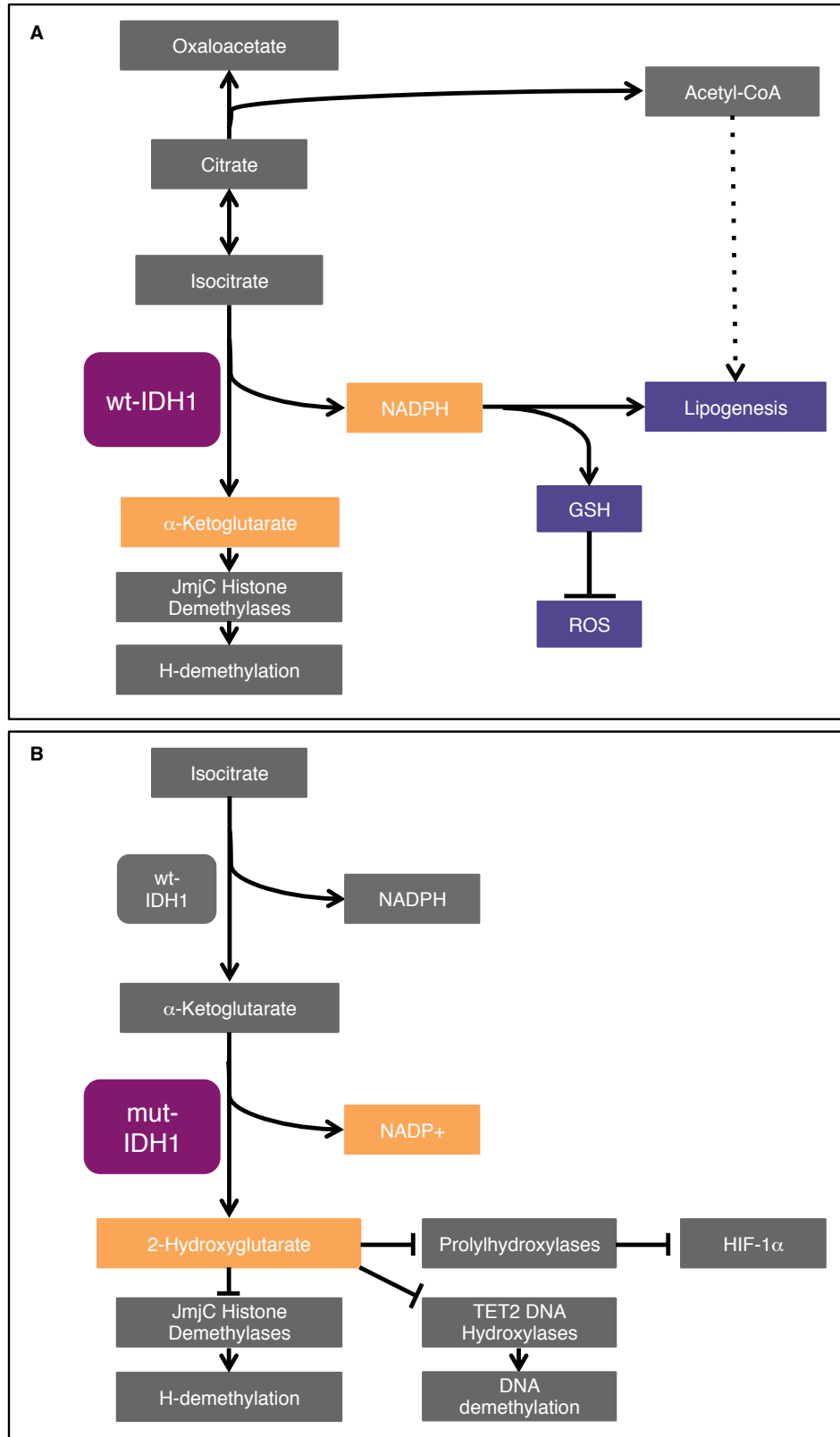


Figure 3. IDH1 wild-type and mutated functions

(A) Wild-type IDH1 produces NADPH and α -ketoglutarate necessary for redox homeostasis and lipogenesis, and histone demethylation, respectively. (B) Mutant IDH1 produces the oncometabolite 2-hydroxyglutarate which inhibits α KG-dependent histone demethylases and DNA hydroxylases and prolylhydroxylases, necessary for epigenetic modifications and HIF-1 α degradation, respectively.

1.3.5 Mutated IDH1 in cancer

IDH1 mutations were discovered in GBM in 2008 in a genomic analysis done by Parsons et al. They found that there were recurrent mutations in the active site of IDH1 in 12% of GBM patients and this mutation was associated with increased patient survival. Point mutations were found at the Arginine-132 position, part of the active site of IDH1 where it interacts with the α -carboxylate of isocitrate. *IDH1* mutations were found mostly in younger patients (mean: 33 years vs. 53 years for wild-type) and these patients had a significantly prolonged survival (3.8 years vs. 1.1 years). Furthermore, it was determined that almost all patients with secondary GBM had mutations in *IDH1* (Parsons et al., 2008). *IDH1* and *IDH2* mutations are also found in acute myeloid leukemia (AML) in 12 to 17% of cases (Mardis et al., 2009; Paschka et al., 2010; Graubert and Mardis, 2011), central and periosteal cartilaginous tumors in 56% of tumors (Amary et al., 2011), and in cholangiocarcinomas in 23% of cases (Borger et al., 2012).

Wild-type and mutant IDH1 GBMs are clearly two separate diseases. While histopathologically similar, there are differences; mutant IDH1 tumors are initially larger, have less contrast enhancement, less peritumoral edema, and are more likely found in the frontal lobe than wild-type IDH1 tumors (Dunn et al., 2012). In the TCGA follow-up study on GBM in 2013, *IDH1* was found to be mutated in only ~7% of the over 400 tumors that they looked at, most of these (28 out of 423) had the *R132H* mutation, one tumor had an *R132G* mutation, and there were no

mutations found in *IDH2* (Brennan et al., 2013). When the mutated IDH1 tumors were looked at more closely, it was found that most also had *TP53* mutations (12 of 13) and that these mutations occurred most often in tumors without RTK alterations, consistent with these tumors being secondary GBM tumors (Brennan et al., 2013). There is a vast difference when comparing *IDH1* mutation status between primary and secondary GBM. Primary GBM tumors have mutations in *IDH1* in less than 5% of cases, while mutations in *IDH1* occur in greater than 70% of Grade II, III, or secondary GBM (Cloughesy et al., 2014).

When comparing expression profiles of GBM mutant and wild-type IDH1 containing tumors, mutant IDH1 tumors look more like lineage-committed neural precursors while wild-type IDH1 tumors more closely resemble neural stem cells (Dunn et al., 2012). This is consistent with other studies looking at the evolution of IDH1 mutant tumors which describe the cell of origin for these tumors to be either neural stem cells or their progeny that has been differentiated (Lai et al., 2011). Furthermore, it is believed that the evolution of IDH1 mutant tumors is initiated by mutant IDH1 protein, followed by mutations in *TP53*, and copy number alterations in *PTEN* and *EGFR* (Lai et al., 2011).

The function of IDH mutations has been widely studied since they were discovered (Figure 3B). The first study that came out about the functionality of IDH1 mutations was by Zhao et al. They found that *IDH1-R132* mutations impaired the interaction between isocitrate and IDH1 both sterically and electrostatically while NADP⁺ binding was not altered, leading to a reduction in activity of IDH1. They further went on to look at prolylhydroxylases (PHDs), which require α KG to hydroxylate and degrade hypoxia inducible factor 1 α (HIF-1 α). During hypoxic conditions, HIF-1 α is not degraded and acts as a transcription factor that is important for the

regulation of genes involved in glucose metabolism, angiogenesis, and other important pathways involved in tumor cell growth. This group concluded that IDH1 acts as a tumor suppressor through its involvement in the activation of HIF-1 α (Zhao et al., 2009). However, while loss of α KG may play a part in tumorigenesis of IDH1 mutant tumors, further studies found that *IDH1* mutations lead to the production of the oncometabolite D-2HG. D-2HG is very similar structurally to α KG except that a hydroxyl group replaces an oxygen atom at C2 in α KG (Xu et al., 2011), formed from the reduction, but not carboxylation of α KG. Accumulation of D-2HG is enhanced in IDH1 mutant cells by forming a heterodimer with a wild-type allele, whereas D-2HG levels are higher in IDH2 mutant tumors, independent of IDH2 wild-type allele which they do not form heterodimers with (Losman and Kaelin, 2013). D-2HG is a competitive inhibitor of α KG-dependent dioxygenases, including histone demethylases and the TET family of 5mC hydroxylases, leading to increased histone methylation and reduced 5hmC, causing global changes in epigenetics and contributing to tumorigenesis (Xu et al., 2011). Furthermore, expression of mutant IDH1 in cortical astrocytes was sufficient to cause G-CIMP (Glioma CpG island methylator phenotype), demonstrating the important role mutant IDH1 plays in epigenetic changes (Turcan et al., 2012). Another group went on to show that changes in histone methylation caused by D-2HG production prevent progenitor cells from differentiating, further confirming a role of histone methylation in stem cell maintenance, differentiation, and tumorigenesis (Lu et al., 2012).

While cells normally produce D-2HG, it is at very low levels, the IDH mutation is responsible for an increase of 10- to 100-times higher than wild-type cells at levels between 10 and 30 mM (Horbinski, 2013). 2-hydroxyglutaric aciduria is a rare metabolic disease resulting in production

of either D-2HG or L-2HG. Patients producing L-2HG, have onset of the disease in early childhood, progress slowly, have leukodystrophy, psychomotor retardation, cerebellar ataxia, seizures, and an increase in tumor formation. Those patients with D-2HG have severe encephalopathy with cardiomyopathy and dysmorphisms, or they have a milder form with developmental delay and hypotonia (Horbinski, 2013).

As IDH1 is an important molecule in metabolism within the cell and mutations in IDH1 have similar functions to other abnormalities in metabolic enzymes (succinate dehydrogenase and fumarase), the role of IDH1 mutations on the cellular metabolome has been extensively studied. When IDH1 is mutated, these tumors have increased free amino acids and lipid precursors and decreased TCA cycle intermediates (Reitman et al., 2011). This group also compared IDH1-R132H expressing cells with those that had knockdown of IDH1 and found few similarities in changes in metabolites, concluding that mutations in IDH1 do not affect the cellular metabolome through dominant negative effect or inhibition of wild-type IDH1, but rather through its neomorphic activity of producing D-2HG. IDH1-R132H knock-in mice were created to determine the effect *in vivo*. Sasaki et al. created two different glioma knock-in mice by crossing IDH1^{LSL/WT} mice with either Nestin-Cre or GFAP-Cre mice, both models had increased expression of D-2HG in the brain. Mice that expressed IDH1-R132H in Nestin positive cells were born in the expected ratio, but died shortly after birth from massive hemorrhage in the cerebral hemispheres and cerebellum (Sasaki et al., 2012b). Mice that expressed IDH1-R132H in GFAP cells had about 8% survival to adulthood with the rest dying of hemorrhage similar to the Nestin mice. GFAP-Cre is known to be a leaky model, most likely accounting for the reason that

some of these mice survived. The GFAP-driven IDH1 -knockin mice that survived had shorter lifespan than wild-type mice and did not show any glioma formation (Sasaki et al., 2012b).

Inhibitors of mutant IDH1 have become a growing field to treat patients, as many are currently under clinical trials, but they also are an invaluable tool to help further determine the mechanism of IDH1 mutations. Rohle et al. published on an Agios-made specific IDH1-R132 mutation inhibitor (AGI-5198) in glioma cells derived from an anaplastic oligodendroglioma (Grade III) patient. In an *in vivo*, subcutaneous glioma model, AGI-5198 decreased tumor size, and promoted a differentiation gene-expression profile towards astrocytes and oligodendrocytes without changing DNA methylation patterns (Rohle et al., 2013). These results point to mutant IDH1 promoting tumor progression and proliferation through epigenetic pathways.

While IDH1 mutations clearly are important for LGG initiation, it is possible that they are not involved in further tumor progression. When IDH1-R132H mutations are overexpressed in cell lines, there is actually a decrease in proliferation *in vitro* and *in vivo* (Bralten et al., 2011). The mutation of IDH1 in and of itself may not lead to tumorigenesis, but might be more important in slowing down differentiation so that more oncogenic mutations have a chance to occur in undifferentiated cells (Horbinski, 2013). IDH1 mutated glioma cells are also more sensitive to radiotherapy, as IDH mutations lead to decreased NADPH levels (from reaction using α KG and NADPH to produce D-2HG) necessary for reduced GSH and subsequent oxidative stress. R132H glioma cells treated with IR have increased ROS, DNA double-strand breaks, and cell death. These outcomes are reversed by treatment with the mutant IDH1 inhibitor, AGI-5198 (Molenaar et al., 2015). These inhibitors must be used with caution as using them concomitantly with radiation may prove to be unfavorable in the clinic. Furthermore, when accounting for grade,

patients with mutations in IDH1 have less aggressive tumors, leading to prolonged survival of these patients (Horbinski, 2013).

1.4 Conclusions

IDH1 mutations are important in the pathogenesis of LGG and secondary GBM, however they rarely occur in primary GBM. Remarkably, patients with wild-type GBM tumors have a mean survival of 15 months compared to 31 months for patients with mutant IDH1. GBM tumors and ectopic expression studies point to tumor suppressive effects of mutant IDH1. Expression of Arg132 point-mutated IDH1 in established IDH1-wild-type glioma cell lines reduced proliferation *in vitro* and extended the survival of mice bearing derived orthotopic xenografts (Bralten et al., 2011). Similarly, RCAS-driven expression of mutant IDH1 in NSCs derived from *p53*-deficient Nestin-*tv-a* mice reduces progenitor cell growth *in vitro* and glioma formation *in vivo* despite elevated D-2HG production in IDH1 mutant compared to wild-type cells. This growth-inhibitory effect of mutant IDH1 is associated with diversion of α KG from wild-type IDH1 and reduced carbon flux from glucose or glutamine into lipids (Chen et al., 2014). Murine NSCs lack glutamate dehydrogenase 2 (GLUD2) and expression of GLUD2 or administration of glutamate, a neocortical neurotransmitter and substrate for GLUD2, compensates for growth and flux deficiencies elicited by mutant IDH1 by replenishing α KG via increased glutaminolysis. These observations suggest that IDH1 mutant tumors require a specialized metabolic niche characterized by elevated glutamate flux for growth and expansion. Recent studies suggest that IDH1 mutant gliomas arise from a neural precursor population that is spatially and temporally restricted in the brain, possibly coinciding with remodeling of the prefrontal cortex (Lai et al., 2011). Primary GBM, on the other hand, inefficiently metabolize glutamine and most likely are

unable to sustain high glutamine flux to support α KG and lipid biogenesis. To support anaplerosis, in particular lipid biogenesis flux via enhanced α KG and NADPH, we investigated whether wild-type IDH1 activity is regulated in primary GBM, and whether such regulation, by impacting macromolecular synthesis activities, redox homeostasis and gene expression, affects the tumor biologic properties of GBM.

CHAPTER 2: MATERIALS AND METHODS

2.1 *In Silico* Genomic and Genetic Analysis

2.1.1 Preprocessing of TCGA GBM exon-array data and subtyping

The unprocessed Affymetrix exon-array datasets for 419 GBM samples and 10 normal brain samples (control samples) were downloaded from the TCGA data portal (<https://tcga-data.nci.nih.gov/tcga>). We followed the data preprocessing procedure described in our recent study (Pal et al., 2014). Samples underwent subtyping into one of four molecular classes of GBM (Classical, Mesenchymal, Proneural, and Neural) (Verhaak et al., 2010). We used an isoform-based classifier to obtain the patient subtype information (Pal et al., 2014).

2.1.2 Analysis of TCGA GBM, low grade glioma, lung adenocarcinoma, and lung squamous cell carcinoma RNA-Seq data

RNASeqV2 level 3 released gene level expression data for RNA-Seq were downloaded for glioblastoma (GBM), low grade glioma (LGG), lung adenocarcinoma (LUAD) and lung squamous cell carcinoma (LUSC) from TCGA, and transcript levels in lymphoma from GSE12195 (Compagno et al., 2009) and GSE6338-60 (Piccaluga et al., 2007) for the analysis of *IDH1*, *IDH2*, *IDH3A*, *IDH3B*, *IDH3G*, *OGDH*, *SUCLA2*, *SDH*, *FH*, *MDH*, *CS*, *ACO1*, *ACO2*, *GNG4*, *NDUFS1*, and *TNFAIP1*. The TCGA data processing and quality control were done by the Broad Institute's TCGA workgroup. The reference gene transcript set was based on the HG19 UCSC gene standard track. MapSplice (Wang et al., 2010) was used to do the alignment, and RSEM (Li and Dewey, 2011) to perform the quantitation. Student's *t*-test was used to determine whether *IDH1*, *IDH2*, *IDH3A*, *IDH3B*, *IDH3G*, *OGDH*, *SUCLA2*, *SDH*, *FH*, *MDH*, *CS*, *ACO1*, *ACO2*, *GNG4*, *NDUFS1*, or *TNFAIP1* was differentially expressed between tumor and

corresponding normal tissue. The upper quartile normalized RSEM count estimates were base-10 log transformed before the *t*-test.

2.1.3 TCGA GBM mutation data

We obtained level 2 GBM somatic mutation data from the TCGA web site (<http://tcga-data.nci.nih.gov/tcga/>). All non-silent *IDH1* mutations were used. There were a total of 147 samples for which both expression and mutation data were available.

2.2 RT-qPCR

Total RNA from tumors or cell lines was extracted using RNeasy kit (Qiagen) according to manufacturer's protocol. cDNA was reversed transcribed (500 ng of total RNA as template) using M-MLV Reverse Transcriptase reactions (Promega), according to the manufacturer's protocol. To analyze *IDH1* expression levels in glioma tumor samples, RT-qPCR was performed using cDNA isolated from GBM tumor samples. Samples were acquired from patients having undergone surgery at Northwestern Memorial Hospital (NMH) in compliance with the NMH Institutional Review Board. Expression of *IDH1* in glioma tumors was compared with a normal brain reference pool consisting of 23 individual brain samples (FirstChoice Human Brain Reference, catalog no. AM6050; Life Technologies). cDNA of matched CD133+ and CD133- patient samples was obtained from Dr. Jeremy Rich (Cleveland Clinic). qPCR was performed using SYBR Green technology (Life Technologies). The following primers were used to amplify *IDH1*, *GNG4*, *NDUFS1*, *TNFAIP1*, *ETV6*, *TUSC2*, *IDH1*, *LSS*, and *SREBP1* respectively: *IDH1* (forward primer: GGCGAGCAGCACAGAGAC and reverse primer:

TCACCCCAGATACCATCAGA); *GNG4* (forward primer: GAGGGCATGTCTAATAACAGCAC and reverse primer: AGACCTTGACCCTGTCCATAC); *NDUFS1* (forward primer: TTAGCAAATCACCCATTGGACTG and reverse primer: CCCCTCTAAAAATCGGCTCCTA); *TNFAIP1* (forward primer: ACCTCCGAGATGACACCATCA and reverse primer: GGC ACTCTGGCACATATTCAC); *ETV6* (forward primer: GCTCAGTGTAGCATTAAGCAGG and reverse primer: CGAGGAAGCGTAACTCGGC); *TUSC2* (forward primer: GGAGACAATCGTCACCAAGAAC and reverse primer: TCACACCTCATAGAGGATCACAG); *ID11* (forward primer: GGCGAGCAGCACAGAGAC and reverse primer: TCACCCCAGATACCATCAGA); *LSS* (forward primer: CTGAACGGGATGACATTTTACG and reverse primer: GGAAAAGTGGGCCACCATAA); *SREBP1* (forward primer: CCCTGTAACGACCACTGTGA and reverse primer: ACAGTGGCTCCGTCTGTCTT); *HPRT* was used as a house keeping control gene (forward primer: AAGGACCCCACGAAGTGTTG and reverse primer: GCTTTGTATTTGCTTTTCCA). qPCR using Taqman Universal PCR Master Mix (Life Technologies) was used for *GFAP* and *Nestin* mRNA expression using the following Taqman probes: *GAPDH* (Hs02758991_g1), *GFAP* (Hs00909233_m1), and *Nestin* (Hs04187831_g1). All reactions were performed on a 7900HT Fast Real-Time PCR System (Applied Biosystems). Results were analyzed and mRNA expression quantified using the $\Delta\Delta C_t$ method.

2.3 R132H Mutation Status

To determine if GBM patient tumor samples, GBM transformed cell lines, and glioma initiating cells (GICs) have the common R132H mutation in IDH1, cDNA was reverse transcribed (500 ng of total RNA as template) using M-MLV Reverse Transcriptase reactions (Promega), according to the manufacturer's protocol. PCR amplification was performed using PrimeSTAR Taq (Clontech) according to the manufacturer's protocol using the following primers: forward primer (AAAAATCAGTGGCGGTTCTG) and reverse primer (GACAGAGCCATTTGGAATGA). The PCR products underwent standard Sanger sequencing using the above primers and mutations at position 396 was evaluated for wild-type (G) or mutation (typically A). This mutation is the most common IDH1 mutation of Histadine replacing Arginine at position 132.

2.4 Immunohistochemistry

Deidentified tissue microarrays (TMAs) were purchased (US Biomax; GL806d), or constructed from gliomas after obtaining University of Kentucky (UK) Institutional Review Board Approval (UK-TMA). UK-TMA contained three 2- μ m diameter cores per tumor, with each core embedded in a separate TMA block. A total of 104 cases comprised the UK-TMA, including 9 non-neoplastic controls (cortical dysplasias) and 47 Grade IV GBMs. Paraffin-embedded mouse brains isolated from PDX mouse models were deparaffinized, and incubated with 3% hydrogen peroxide (to block endogenous peroxidases), avidin (to block endogenous biotin), and 5% normal donkey serum (to reduce unspecific antibody binding). PDX tumor slides were incubated with primary antibodies [1:1000 Ki67 (Abcam ab16667); and 1:500 Caspase-3 (Cell Signaling 9661)]. After primary antibody incubation, slides were incubated with secondary biotinylated

antibodies (Vectastain ABC kit-Vector Laboratories), and finally with Biotinyl Tyramide Working solution, Streptavidin-HRP, and DAB. TMA slides were processed as described above, but antigen retrieval was done at 80° C for 1 hour (10mM sodium citrate, 0.1% Tween 20, pH 6). TMA slides were incubated with an anti-IDH1 antibody (1:100; HistoBioTec DIA-W09) for 1 hour. Each TMA core was quantified by laser scanning cytometry (LSC) or visually semiquantified via light microscopy. The TissueGnostics LSC system was used to take representative photographs and the US Biomax TMA analyzed using HistoQuest software. Light microscopy of UK-TMA by pathologist Dr. Craig Horbinski rated IDH1 expression on a relative scale from 0 to 3, with 0 = negative and 3 = strongest. Results from all 3 cores were averaged together to produce a final score for a tumor. Results were plotted, and differences were calculated via one-way ANOVA with post-hoc Tukey's test.

2.5 Cell Lines

Transformed glioma cell lines (LN382, U87, and LNZ308) were from Dr. Webster Cavenee (University of California, San Diego) and normal human astrocytes (NHA) were from Dr. Russ Pieper (University of California, San Francisco). GIC-20 was a gift from Dr. Kenneth Aldape (University of M.D. Anderson Cancer Center). GIC-387 was a gift from Dr. Jeremy Rich (Cleveland Clinic). NSC-2201 was a gift from Dr. Hongwu Zheng (Cold Spring Harbor Laboratory). SUDHL4 diffuse large B-cell lymphoma cell line was a gift from Dr. Shad Thaxton. Primary human astrocytes were from ScienCell (#1800).

2.6 Cell Culture and Reagents

Transformed glioma cell lines and NHA were grown in DMEM 1X with 4.5 g/L glucose, L-glutamine and sodium pyruvate (Corning), and supplemented with 10% fetal bovine serum (Life Technologies) and 1% PenStrep (Life Technologies). GICs were grown as neurospheres in DMEM/F12 50:50 with L-glutamine (Corning), supplemented with 1% PenStrep, B27 (Invitrogen), N2 (Invitrogen), human-Epidermal Growth Factor (hEGF; Shenandoah Biotech), Fibroblast Growth Factor (FGF; Shenandoah Biotech), Leukemia Inhibitory Factor (LIF; Shenandoah Biotech), and GlutaMAX (Life Technologies). SUDHL4 cells were grown in RPMI 1640 supplemented with 10% FBS and 1% PenStrep. Primary human astrocytes were grown in astrocyte media (ScienCell) supplemented with 1% astrocyte growth supplement (ScienCell) and 2% FBS (ScienCell). Cells were routinely tested for mycoplasma contamination using Plasmotest (InvivoGen) according to the manufacturer's protocol. Cells grown under hypoxic conditions were grown in a 1.5% O₂ incubator. Cells were treated with the following drugs: 5 μM Erlotinib (Sigma), 5 μM SU11274 (Sigma), 5 μM Imatinib (Selleck Chemicals), 5 or 10 mM dimethyl α-ketoglutarate (Sigma), 0.5 mM *N*-Acetyl-L-Cysteine, 25 μM EUK-134 (Sigma), 1 μM Sodium Palmitate (Sigma), 100 μM Mevalonic Acid Lithium Salt (Sigma), 7.5 μM Ibrutinib (ChemieTek), or 5, 10, 20, 25, 50, or 100 μM GSK864 (Sigma).

2.7 Mutagenesis and Cloning of IDH1

IDH1 wild-type cDNA (Origene) was mutated to be resistant to shIDH1-89 sequence using the following mutagenesis primers: forward primer (TGGGAGTTAATCAAAGAGAACTCATTTTTCC) and reverse primer

(GATAATCCGTGTCATTTTCATCTCCTTGCATC) and digested with DpnI (IDH1^{siR}). IDH1 wild-type cDNA and IDH1^{siR} cDNA were cloned into CSII-CMV-MCS-IRES2-Venus vector using unique NheI and AgeI restriction sites. RT-PCR was done on cDNA prepared from cells as described previously using PrimeStar Taq (Promega) according to the manufacturer's protocol and HPRT and IDH1 primers from RT-qPCR above and specific IDH1^{siR} primers: forward primer (ACGGATTATCTGGGAGTTAATCA) and reverse primer (AAGGCCAACCCCTTAGACAGA).

2.8 Lentiviral Production and Cell Infection

GIC, NSC, transformed glioma cells, and lymphoma cells were lentivirally transduced with pLKO.1-puro-CMV-tGFP, pLKO.1-puro-CMV-tGFP-SHC016 (shScramble), pLKO.1-CMV-tGFP-shIDH1 (TRCN000027249, TNCN000027253, TRCN000027284, TRCN000027289, TRCN000027298; Sigma-Aldrich), pGIPZ-puro, pGIPZ-puro-shIDI1 (V2LHS_48970, V2LHS_67394, V2LHS_67395, V2LHS_67396), pGIPZ-puro-shLSS (V2LHS_134081, V2LHS_134083), CSII-CMV-MCS-IRES2-Venus, CSII-CMV-MCS-IRES2-Venus IDH1, CSII-CMV-MCS-IRES2-Venus IDH1^{siR}, or pLV-Tomato-IRES-Luciferase (Northwestern University SDRC DNA/RNA Delivery Core). 293T cells were plated in T-175 flasks (75% confluence). Cells were then transfected using lipofectamine 2000 (Life Technologies) with 20 µg of lentiviral construct, 15 µg of psPAX2 (HIV-Gag-Pol-Rev), and 10 µg of pMD2.G (envelope). After 48-72 hours, virus-containing media was harvested, filtered through 45 µm low protein binding filter (Millipore), and concentrated at 25,000 rpm for 2 hours (Beckman Coulter). The resulting viral pellet was resuspended in 30 µL of serum free media. For lentiviral transduction,

transformed cells at 75% confluence or GICs, NSCs, and lymphoma cells at 1×10^6 cells per T-25 flask were incubated with 5 μ L of virus for 48 hours. Subsequently, cells were sorted by FACS to enrich for GFP-positive cells (pLKO, shIDH1, CSII, CSII-IDH1, CSII-IDH1^{siR} constructs) or RFP-positive cells (luc), or puromycin-selected (pGIPZ, shIDI1, shLSS constructs).

2.9 Retroviral Production and Cell Infection

Transformed glioma cells overexpressing Bcl-2 were generated by retroviral transduction using pBabe-puro or pBabe-puro-Bcl-2. pBABE-puro was a gift from Harmut Land, Jay Morgenstern, and Bob Weinberg (Addgene plasmid #1764; Morgenstern and Land, 1990). Bcl-2 was cloned into the pBabe-Puro retroviral vector using unique EcoRI restriction site. In a 10 cm dish, 40% confluent 293T cells in OptiMEM were transfected with 4 μ g of retroviral construct, 1 μ g of pVSVG (envelope), and 4 μ g pCL-Ampho (packaging) using lipofectamine 2000 (Life Technologies). The medium was changed to full-DMEM medium 24 hours post-transfection, and cells were incubated at 37° C for an additional 24 hours. Medium was harvested, supplemented with Polybrene (8 μ g/mL; Sigma-Aldrich), and filtered through a 0.45 μ m filter. For retroviral infection, glioma cells at 50% confluence were incubated overnight with 3 mL of virus-containing medium. Cells were selected by changing the medium to puromycin-containing medium (1.5 μ g/mL; Invitrogen).

2.10 Transfection

Subconfluent glioma cells were transfected with a non-targeting siRNA control or with an siRNA pool targeted to IDH1 (50 nM) or FoxO6 (100 nM) (Dharmacon) using Oligofectamine or Lipofectamine 2000 (Invitrogen) according to the manufacturer's protocol. Subconfluent GIC-387 cells were transfected with a pCMV6-XL4-ME1 plasmid (Origene; 2 µg per well in 6 well plate) or mock transfected using RNAiMax (Invitrogen) according to the manufacturer's protocol. Expression analysis for FoxO6, IDH1, ME1, and cleaved effector caspases was performed 48 hours post transfection.

2.11 Western Blot Analysis

For all Western Blot analyses, proteins were separated by 4-12% SDS/PAGE (Life Technologies), transferred to Hybond PVDF membranes (Amersham), blocked with 5% milk in PBS with 0.1% Tween 20 (PBS/Tween) for 1 hour, and incubated with the following antibodies: anti-cleaved caspase-3 (Cell Signaling, 9664), anti-cleaved caspase-7 (Cell Signaling, 9491), anti-Hsp70 (BD Pharmingen, 610607), anti-IDH1 (Cell Signaling, 8137), anti-H3K4me3 (Millipore, CS200580), anti-H3K9me3 (Active Motif, 39161), anti-H3K27me3 (Millipore, CS200603), anti-H3K36me3 (Abcam, ab9050), anti-Histone H3 (Cell Signaling, 4499), anti-ME1 (Abcam, ab97445), anti-FoxO6 (Thermo Scientific PA5-35117), anti-phospho-FoxO6 (Abcam, ab154832), anti-phospho-EGFR (Cell Signaling, 2236S), anti-EGFR (Santa Cruz, sc-373746), anti-phospho-Akt (Cell Signaling, 4060S), and anti-Akt (Cell Signaling, 9272S). The blots were washed with PBS/Tween and subsequently incubated with goat anti-rabbit IgG or goat anti-mouse IgG antibodies (Santa Cruz) in 5% milk in PBS/Tween. After washing with

PBS/Tween, the blots were developed with Supersignal West Dura ECL (Pierce) following manufacturer's protocol. Quantification of blots determined by densitometry using ImageJ software.

2.12 Cell Proliferation Assay

GICs or NSC-2201 cells were plated at 50,000 cells per well in triplicate. After 3 days cells were accutased and counted by trypan blue exclusion on Countess Cell Counter (Invitrogen). All cells were replated, and recounted every three days for twelve days total.

2.13 *In Vivo* Xenograft Studies

All animals were used under an approved protocol of the Institutional Animal Care and Use Committee of Northwestern University. Luciferase-expressing GIC-20, GIC-387, and NSC-2201 cells were injected intracranially into ~7 week old female CB17 SCID mice (Taconic Farms). Briefly, cells were dissociated by accutase (Life Technologies), and suspended in HBSS. Each mouse was anesthetized and placed in a stereotaxic frame, and the surgical area was cleaned with alcohol and Betadine. An incision was made in the scalp, and a 0.7 mm burr hole was created in the skull with a microsurgical drill 2 mm lateral right of the sagittal suture and 0.5 mm posterior of bregma. A Hamilton syringe was loaded with 3×10^5 cells (GIC-20), 2×10^3 (GIC-387), or 4×10^5 (NSC-2201) in 3 μ L and inserted 3.5 mm into the brain. The cells were implanted over a period of 3 minutes, and the needle was left in place for 1 minute before the syringe was withdrawn. After surgery, the skin was closed with sutures. Mice were sacrificed upon observation of neurological impairment. 7-10 animals were used in each group. Mice were

randomized to groups based on body weight. No blinding was possible in these studies. Survival analysis between control and experimental groups was determined by the Kaplan-Meier method, and statistical significance was assessed using the logrank (Mantel-Cox) test. For GSK864 inhibitor treatment, 20 animals were intracranially injected as described above with GIC-20.luc cells. Two weeks after implantation, mice were randomized into two groups based on bioluminescence from the IVIS spectrum. 10 animals received 150 mg/kg GSK864 (Sigma) in propylene glycol, DMSO, PEG-400, and water (16.7:3.3:40:40) or vehicle for 10 days, M-F for 2 weeks. For lymphoma flank model, 2×10^6 cells in 100 μ L of HBSS were combined with 100 μ L of ice cold Matrigel (Fischer Scientific). Mice were anesthetized and 200 μ L of cells in Matrigel were injected into either the left flank (pLKO) or right flank (shIDH1-98) of 5 mice.

2.14 *In Vivo* Bioluminescence Imaging

shIDH1-expressing GIC-20, GIC-387, and SUDHL4 cells, and IDH1 overexpressing NSC-2201 cells were lentivirally transduced with a cDNA encoding firefly luciferase. Upon orthotopic cell implantation, tumor growth was monitored by bioluminescence imaging (IVIS Spectrum, PerkinElmer). Mice were injected with 200 μ L luciferin potassium salt (Perkin Elmer), anesthetized, and imaged using IVIS spectrum. Bioluminescence was analyzed using Living Image (Caliper Life Sciences) software, and bioluminescence was quantified relative to non-tumor bearing mice.

2.15 α -Ketoglutarate Quantification

To quantify α KG, the α KG Assay Kit (BioVision) was used as a readout for IDH1 activity according to manufacturer's protocol. GBM cells and GICs were grown in 6 well plates and treated with drug or vehicle for 24 hours. Cells were collected in 50 μ L of α KG Assay Buffer and incubated on ice for 30 minutes. Samples were then deproteinized using PCA and neutralized with KOH from Deproteinizing Sample Preparation Kit (BioVision). 50 μ L of sample was added to 3 wells each of 96 well plate and 50 μ L of Reaction Mix was added to each sample. The plate was incubated at 37° C for 30 minutes in the dark, and read at Ex/Em 535/587 nm.

2.16 NADPH Quantification

To quantify NADPH, GBM cells and GICs (treated with drug or vehicle for 24 hours), were processed using the NADP⁺/NADPH Quantification Kit (BioVision) according to manufacturer's protocol. Cells were collected on ice and washed with ice cold PBS and lysed with 350 μ L of NADP/NADPH extraction buffer. Samples were then filtered through 10 kDa molecular weight cut off filters (BioVision) to remove enzymes that can rapidly consume NADPH. Half of each extracted sample was heated at 60° C for 30 minutes to decompose NADP⁺ and leave only NADPH. 50 μ L NADPH and NADPH/NADP⁺ samples were transferred to 96 well plate in triplicate and 100 μ L of NADP Cycling Mix was added to each well, followed by 10 μ L of NADPH developer per well. The plate was incubated at room temperature for 1 hour and read at OD450. Results are expressed as NADPH/NADP⁺ ratio.

2.17 ¹³Carbon-Glucose and -Acetate Studies

2.17.1 ¹³Carbon Sample Preparation

GIC-20 cells were grown in medium supplemented with 10 mM glucose or 1 mM acetate until 90% confluence was reached. After 24 hours, media was added, which contained either 10 mM [U-¹³C] Glucose or 1 mM [U-¹³C] Acetate (Cambridge Isotope Laboratories). After 3 hours (acetyl-CoA) or 72 hours (fatty acids), cells were collected and pelleted, washed without disturbing the pellet using 150 mM Ammonium Acetate, and snap frozen in liquid nitrogen. Samples were sent to University of Michigan Metabolomics Core for GC-MS processing. Microtubes containing cell pellets were removed from -80° C storage and maintained on wet ice throughout the processing steps. To initiate protein precipitation, 0.3 mL of a chilled mixture of isopropanol:chloroform (8:2) (EMD) was added to each sample. Extracted metabolites were dried under vacuum at 45° C, and 1 mL of BF₃/Methanol was added to each sample. Samples were incubated at 60° C for 3 hours and cooled. Subsequently, 200 µL LCMS water, and 300 µL of Hexane was added. The samples were vortexed, allowed to sit for 5 minutes, vortexed again and then centrifuged for 3 minutes to separate the layers. The organic layer was transferred to an autosampler vial for GC-MS analysis.

2.17.2 GC-MS

GC-MS analysis was performed on an Agilent 69890N GC-5975 MS detector with the following parameters: a 1 µL sample was injected splitlessly on an HP-5MS 15m column (Agilent Technologies) with an He gas flow rate of 1.4 mL/minute. The GC oven initial temperature was 60° C, and was increased at 10° C per minute to 300° C, and held at 300° C for 5 minutes. The

inlet temperature was 250° C and the MS-source and quad temperatures were 230° C and 150° C respectively.

2.17.3 GC-MS Data Analysis

Metabolites were identified by matching the retention time and mass (+/- 10 ppm) to authentic standards. Isotope peak areas were integrated using MassHunter Quantitative Analysis vB.07.00 (Agilent Technologies). Peak areas were corrected for natural isotope abundance using an in-house written software package based on a method previously described (Fernandez et al., 1996), and the residual isotope signal was reported. Data were normalized to cell protein content prior to analysis of metabolite fluxes for fatty acid metabolites.

2.18 Extreme Limiting Dilution Assay

GIC-20, NSC-2201, or GIC-387 cells were plated at 1, 5, 10, or 20 cells per well in 96 well plates. Spheres were determined by observation using an inverted microscope 6 or 7 days after plating. Data was analyzed by ELDA software (<http://bioinf.wehi.edu.au/software/elda/index.html>) to determine stem cell frequency (Hu and Smyth, 2009).

2.19 Differentiation Experiment

GIC-20 cells were plated at 50,000 cells per mL on poly-D-lysine/laminin-coated coverslips in GIC media with 1 ng/mL EGF and bFGF and no LIF. RNA was collected for RT-qPCR analysis or immunocytochemistry was performed as previously described (Kouri et al., 2015). Cells were fixed in 4% paraformaldehyde in PBS for 20 minutes, washed 3X with PBS and incubated

overnight at 4° C using the following antibodies: rabbit anti-GFAP (1:1000; DakoCytomation Z0334) and mouse anti-MAP2 (1:500; BD Pharmingen 556320). Cells were washed 3X with PBS and incubated with 1:500 of the appropriate secondary antibody for 1 hour at room temperature. Nuclei were counterstained with DAPI, and coverslips mounted. Cells were imaged using a Nikon A1R Spectral confocal microscope, and quantification was performed using TissueGnostics LSC System, and data were analyzed with HistoQuest Software.

2.20 Chromatin Immunoprecipitation-Sequencing

GIC-20 and GIC-387 cells were grown in 4 T75 flasks and infected with either shScramble, shIDH1-89, or shIDH1-98 lentivirus. After 48 hours, media was changed on the cells and they continued to grow. After 48 hours more, 6 million cells per sample were fixed with 1% formaldehyde and ChIP-Seq was performed according to previous studies (Chen et al., 2015a and Chen et al. 2015b) using antibodies against H3K4me3 (Hu et al., 2013), H3K27me3 (Active Motif 39155), and H3K36me3 (Abcam ab9050). ChIP-Seq libraries were prepared with Illumina's TruSeq DNA sample preparation kit. Sequencing reads were aligned to the human genome (University of California at Santa Cruz [UCSC] hg19). Datasets were analyzed using Spatial Clustering for Identification of ChIP-Enriched Regions [SICER; (Xu et al., 2014)], to delineate ChIP-enriched regions, to assess their statistical significance, and to identify regions of differential enrichment in shIDH1 versus control GICs. For each antibody, regions detected by the SICER peak caller as reproducibly bound by the antibodies in at least one ChIP dataset were identified. The number of reads for each sample in each of these regions were then counted, and the R package edgeR (Robinson et al., 2010) was used to identify regions that significantly

differed in H3K4me3, K27me3 and K36me3 binding between both shIDH1 infectants versus the control cultures. A p value of <0.05 was considered significant. Subsequently, Ingenuity Pathway Analysis (IPA; Qiagen) was performed to prioritize genes based upon enrichment in signaling pathways associated with cancer and development. Genes in the top 5 canonical pathways, as well as genes associated with pathways implicated in cellular and organismal development, were ranked based upon most significant differential in H3K4me3 binding between two independent shIDH1 infectants versus shScramble cells (64 genes). Genes with annotated oncogenic or tumor-suppressive function (30 genes) were then analyzed by RT-qPCR.

2.21 Copy Number Alterations

For the analysis of *EGFR* copy number in GICs, genomic DNA was isolated [Blood and Cell Culture DNA Mini Kit (Qiagen)], and 10 ng were analyzed using the TaqMan Copy Number Assay (Applied Biosystems) following the manufacturer's protocol. RNase P TaqMan was used as a reference.

2.22 Quantification of Apoptosis

To quantify apoptosis of GBM cells and GICs, Annexin V positivity was determined by FACS using the Annexin V-Cy5 Apoptosis Kit (BioVision) according to manufacturer's protocol. Cells were treated for 24 hours and cells collected by either accutase (GICs) or trypsin (adherent cells) into single cell suspension. Cells were washed 1X with PBS, and resuspended in 500 μ L of Annexin V Binding Buffer. 5 μ L of Annexin V-Cy5 was added to each samples and incubated in the dark for 5 minutes. Cells were analyzed by FACS (Fortessa; BD Biosciences).

2.23 ROS Quantification

To quantify ROS levels, GBM cells and GICs were treated with vehicle or RTKi for 24 hours, followed by treatment of cells with 5 μ M CellROX Deep Red (Life Technologies). Cells were incubated at 37° C for 4 hours, washed twice with PBS, trypsinized (GBM cells; Life Technologies) or accutased (GICs; Life Technologies) into single cell suspension, resuspended into PBS and analyzed by flow cytometry (Fortessa; BD Biosciences).

2.24 GSH Quantification

To quantify GSH production, GBM cells and GICs (vehicle or RTKi treated for 24 hours), were processed using the Glutathione Assay Kit (BioVision). Cells were homogenized 20 times with loose fitting dounce homogenizer and deproteinized using Perchloric Acid (PCA) and neutralized with KOH. 10 μ L of sample was added in triplicate to 96 well plates, and volume brought to 90 μ L with Glutathione Assay Buffer. 10 μ L of o-phthalaldehyde (OPA) probe was added to each well, incubated at room temperature for 40 minutes and read at Ex/Em 340/420nm on Cytation3 (BioTek).

2.25 RTK Profile Array

RTK activation was determined using Human Phospho-RTK Array Kit (R&D Systems) according the manufacturer's protocol. Briefly, an RTK array was blocked for 1 hour and then incubated with 200 μ g of protein from cell lysates overnight. Arrays were washed and incubated with anti-phospho-tyrosine-HRP antibody for 2 hours, washed again and developed using Supersignal West Dura ECL (Pierce) following manufacturer's protocol.

2.26 Chromatin Immunoprecipitation

Chromatin Immunoprecipitations (ChIP) were performed using EZ-ChIP System (Millipore) according to manufacturer's protocol with slight modifications. LN382 cells were grown to 75% confluence in four 15 cm plates, two plates each treated with 5 μ M SU11274 plus 5 μ M Imatinib, or vehicle. After 48 hours, plates were washed with ice-cold PBS and fixed with 1% formaldehyde in DMEM media for 10 minutes. The plates were washed with PBS and a stop solution was added (1X glycine, 1X PBS, in ddH₂O) for 5 minutes. The plates were washed 2X with PBS and cells scraped on ice in 1 mL PBS + 5 μ L PIC into a 15 mL falcon tube. The cells were centrifuged at 2,500 rpm for 10 minutes at 4° C. The supernatant was removed and the cells were lysed using 600 μ L lysis solution and pipetting up and down. The cell lysis was then incubated on ice for 30 minutes. After 30 minutes, each sample was sonicated five times each for 20 seconds and resting for 40 seconds between each sonication. The sonicated samples were centrifuged at 12,500 rpm for 12 minutes at 4° C. 75 μ L of sonicated lysate was transferred into 904.5 μ L dilution mixture and mixed. 60 μ L of Protein G agarose beads were added to each tube and rotated by end-over-end mixing at 4° C for 1 hour. The samples were centrifuged at 4,000 rpm for 1 minute at 4° C. The supernatants were transferred to new tubes and 10 μ L of supernatant (1%) was saved as Input and stored at -20° C until the elution step. 5 μ g of anti-FoxO6 (Thermo Scientific PA5-35117) or IgG Rabbit (Santa Cruz) was added to the non-input supernatant and mixed by end-over-end mixing overnight at 4° C. The next day 10 μ L of protein G agarose beads were added to each sample to pull down the antibody and mixed by end-over-end mixing for 1 hour. The supernatant was carefully removed and each sample was washed by

adding 1 mL of the following each and mixing by end-over-end mixing; Low Salt Buffer, Hi Salt Buffer, LiCl Complex Buffer, and twice with TE Buffer. The DNA from the beads was eluted twice with 100 μ L of elution buffer (1% SDS, 0.1M NaHCO₃ in ddH₂O) for 15 minutes at room temperature and was centrifuged at 8,000 rpm for 1 minute and the supernatant collected. 8 μ L of NaCl was added to each tube and incubated at 65° C overnight. The next day, 1 μ L of RNase A was added and incubated for 30 minutes at 37° C, followed by the addition of 4 μ L of 0.5 M EDTA, 8 μ L of 1 M Tris-HCl, and 1 μ L of Proteinase K and incubated at 45° C for 1.5 hours. DNA was then purified using the spin columns. qPCR was performed using the following primers for *IDH1* (forward primer: TATACTCCAGCCTGGGCAAC and reverse primer: ACAGCCCCTAGGGTTCTTTG) and confirmed with an independent second set of *IDH1* primers (forward primer: CTGAGATCACGCCACTATACTCCAGC and reverse primer: GCCCTTACCCCATGCATGAAACTTCC).

2.27 MicroArray

LN382 cells were treated with 5 μ M Erlotinib, 5 μ M SU11274, a combination of both drugs, or vehicle for 6 or 24 hours. Total RNA was extracted using RNeasy Kit (Qiagen). The quality of the RNA was evaluated by Bioanalyzer, and subjected to whole genome profiling using the Illumina HumanHT-12 Beadchip expression technology (Illumina). Cutoff conditions for significant gene changes were *fold change (fc)* > 2, *p* < 0.01, and *false discovery rate (FDR)* > 0.05. Results were analyzed using Ingenuity Pathway Analysis (Qiagen).

2.28 MTT Assay

LN382 or GIC-387 cells were plated at 10,000 cells per well in 96 well plates. Cells were treated with Vehicle or 5 μ M RTKi and/or 5, 50, or 100 μ M GSK864 in 100 μ L of media. After 48 hours, MTT assay was performed according to manufacturer's protocol (ATCC). Briefly, 10 μ L of MTT Reagent was added to each well, followed by incubation at 37° C incubator for 3 hours. 100 μ L of Detergent Reagent was added to each well and plates were incubated in the dark at room temperature overnight. Plates were read at OD 570.

2.29 Statistical Analysis

All experimental data are presented as mean \pm Standard Deviation, unless otherwise specified. Control and experimental groups were compared by two-tailed Student's *t*-test. A *p* value of ≤ 0.05 was considered statistically significant. Sample size estimates were not used. Kaplan-Meier survival curves were analyzed by Mantel-Cox and Gehan-Breslow-Wilcoxon tests.

CHAPTER 3: RESULTS

3.1 Wild-type IDH1 is overexpressed in GBM

The motivation for this study was initially provided by an *in silico* analysis of GBM specimens profiled by TCGA (Brennan et al., 2013; TCGA, 2008), which revealed that wild-type *IDH1* had elevated expression in 65% of primary GBM in 419 tumor samples compared to 10 normal brain samples, whereas the *IDH1 R132H* point mutation occurred in only 2% of these tumors (Figure 4A) demonstrating that overexpression of *IDH1* is not associated with the mutation. We confirmed the TCGA data in flash-frozen GBM tumors obtained from Northwestern Memorial Hospital, which also showed elevated *IDH1* mRNA in over 90% of tumors (Figure 4B). Again, this was not associated with mutation as none of these tumors had point mutations in R132.

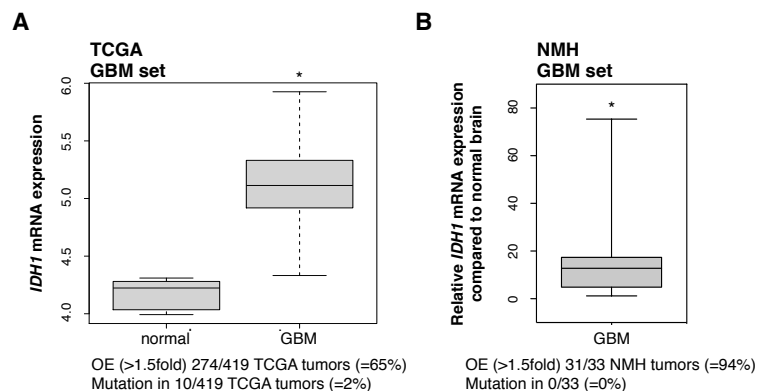


Figure 4. Wild-type IDH1 is overexpressed in GBM

(A) *IDH1* mRNA expression in TCGA GBM tumors (*GBM* $n=419$; *normal* $n=10$). (B) *IDH1* transcript levels in an independent set of primary GBM resected at NMH ($n=33$). * $p<0.0001$. OE, overexpression. TCGA analysis done with help from Yingtao Bi and Youjia Hua.

Increased mRNA in GBM was specific for *IDH1*, as *IDH2* transcript levels were not elevated relative to normal brain, and *IDH3* variants and all other enzymes of the TCA cycle were significantly downregulated in GBM relative to normal brain (Figure 5). Aconitase 1 (*ACO1*)

was the only other enzyme that showed upregulation in GBM, but not to the same extent as *IDH1* (Figure 5).

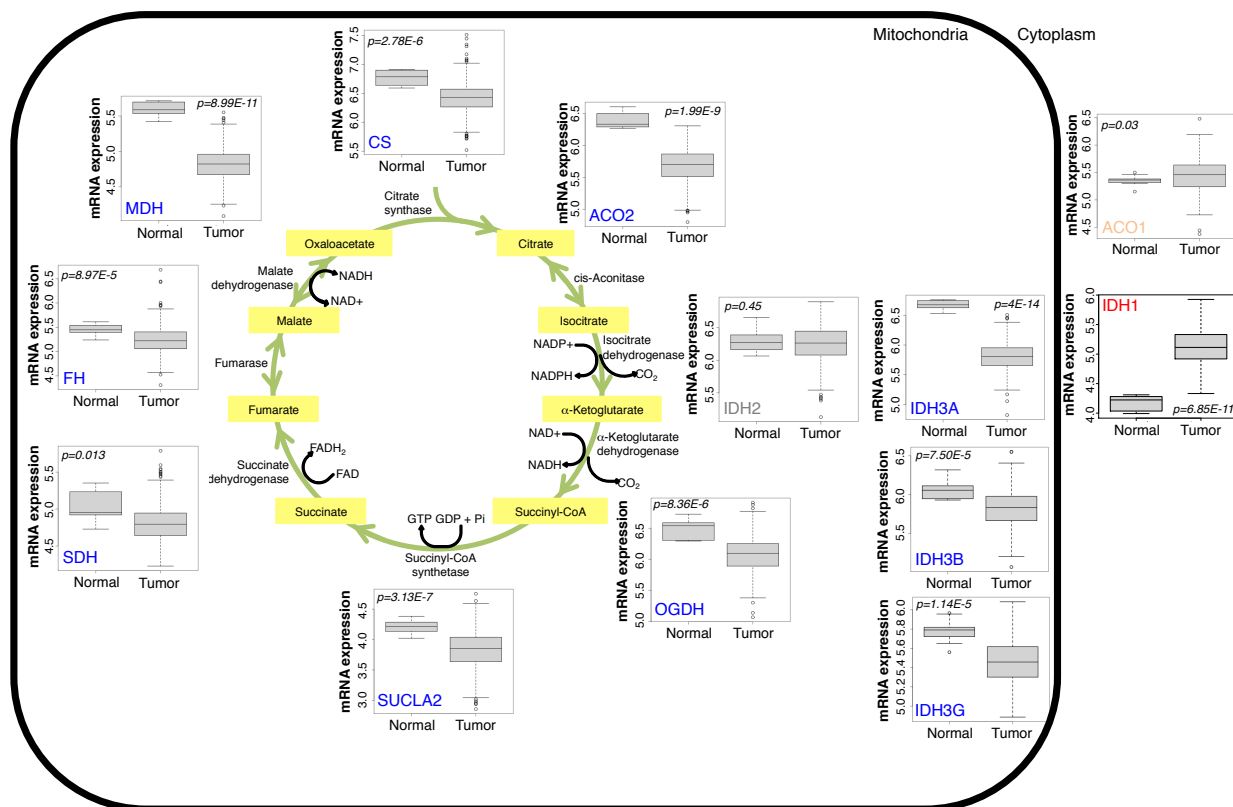


Figure 5. TCA cycle enzyme mRNA expression in normal brain vs. GBM

mRNA expression of *IDH1*, *IDH2*, *IDH3A*, *IDH3B*, *IDH3G*, *OGDH*, *SUCLA2*, *SDH*, *FH*, *MDH*, *CS*, *ACO1*, and *ACO2* in TCGA GBM ($n=420$) versus normal brain ($n=10$). *IDH1*, isocitrate dehydrogenase 1; *IDH2*, isocitrate dehydrogenase 2; *IDH3A*, isocitrate dehydrogenase 3-alpha; *IDH3B*, isocitrate dehydrogenase 3-beta; *IDH3G*, isocitrate dehydrogenase 3-gamma; *OGDH*, α -ketoglutarate dehydrogenase; *SUCLA2*, succinyl-CoA synthetase; *SDH*, succinate dehydrogenase; *FH*, fumarase; *MDH*, malate dehydrogenase; *CS*, citrate synthase; *ACO1*, aconitase 1; *ACO2*, aconitase 2. TCGA analysis done with help from Yingtao Bi.

Levels of *IDH1* mRNA varied with tumor type, grade and subclass, as *IDH1* was expressed at lower levels in TCGA Grade II and III gliomas (The Cancer Genome Atlas Research, 2015) (Figure 6A) compared to GBM, irrespective of tumor subclassification as astrocytoma, oligoastrocytoma and oligodendroglioma (Figure 6B). Expression of *IDH1* transcripts was enriched in *IDH1* WT compared to *IDH1* R132H mutant GBM (Figure 6C), and was highest in GBM tumors of the Classical subtype, with other subtypes exhibiting similar average and range of expression (Figure 6D).

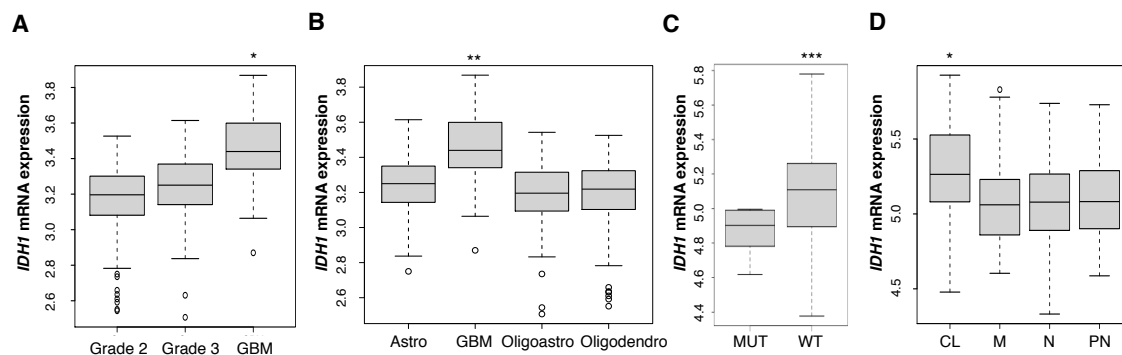


Figure 6. *IDH1* mRNA is increased in high-grade gliomas, in wild-type tumors, and the Classical subtype

(A) *IDH1* mRNA levels in GBM compared to lower grade gliomas (GBM, $n=159$; Grade 2, $n=190$; Grade 3, $n=203$). (B) Levels of *IDH1* mRNA in GBM compared to lower grade subtypes (GBM, $n=159$; astro, $n=140$; oligoastro, $n=104$; oligodendro, $n=149$). (C) mRNA expression of *IDH1* in *IDH1*-R132H mutant ($n=8$) versus *IDH1*^{wt} ($n=139$) GBM tumors. (D) *IDH1* mRNA expression in GBM subtypes. * $p<0.00005$; ** $p<0.0001$; *** $p<0.005$. Astro, astrocytoma; oligoastro, oligoastrocytoma; oligodendro, oligodendroglioma; CL, Classical; M, Mesenchymal; N, Neural; PN, Proneural. TCGA analysis done with help from Yingtao Bi.

Elevated IDH1 expression was also evident through immunohistochemical analysis of protein using two independent tissue microarrays followed by quantitative analysis of staining intensity using laser scanning cytometry (LSC; Figure 7A) or by semi-quantitative evaluation using light microscopy (Figure 7B, 7C). These studies demonstrated diffuse cytoplasmic and speckled staining distribution, which is consistent with well-described functions of IDH1 within the cytosol and peroxisomes (Losman and Kaelin, 2013).

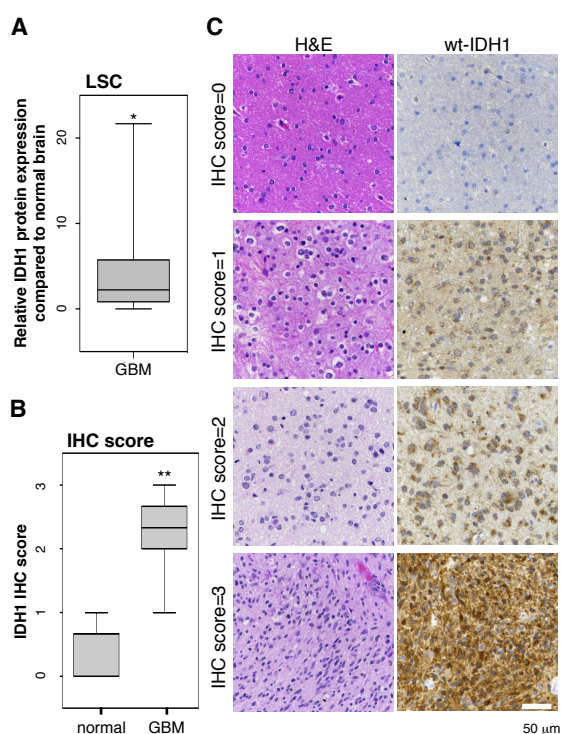


Figure 7. Wild-type IDH1 protein is overexpressed in GBM

(A) Quantification of IDH1 staining intensities in TMA of GBM tumors ($n=33$) relative to normal brain ($n=5$). (B) Quantification of relative IDH1 protein expression on an independent TMA; shown is the IHC score in normal brain ($n=7$) and GBM tumors ($n=35$). (C) Representative IDH1 IHC staining intensities for scores of 0, 1, 2, and 3. Bar, 50 μ m. * $p<0.05$; ** $p<0.001$. LSC, laser scanning cytometry. IHC scoring done by pathologist Craig Horbinski.

Elevated IDH1 mRNA and protein in primary GBM was not due to *IDH1* copy number gains, as the *IDH1*-encoding 2q34 locus was not amplified in GBM, nor was the elevated expression due to changes in *IDH1* promoter methylation (Figure 8B). Together, these observations suggest that in the absence of copy number gains or epigenetic activation through changes in CpG methylation, primary GBM tumors are characterized by elevated IDH1 mRNA and protein expression.

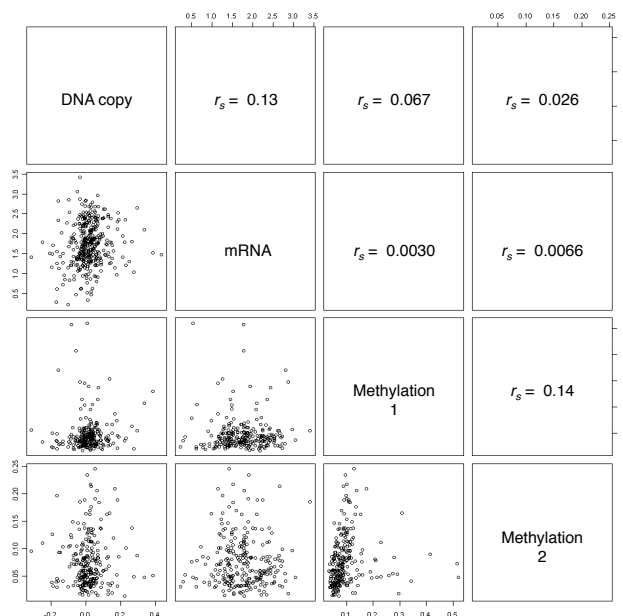


Figure 8. Elevated levels of IDH1 are not associated with copy number gains, amplification, or promoter methylation

TCGA dataset analysis of *IDH1* mRNA, DNA copy number, and promoter methylation ($n=419$). r_s , spearman correlation coefficients. TCGA analysis done by Yingtao Bi.

3.2 IDH1 expression modulates GBM progression *in vivo*

To determine whether altering IDH1 expression affects GBM cell growth *in vitro* and tumor growth *in vivo*, we suppressed IDH1 expression in two independent luciferase-labeled, patient-derived glioma initiating cells (GICs) via lentiviral infection with IDH1-specific shRNA, or overexpressed an *IDH1* cDNA in neural stem cells (NSCs) derived from mice with CNS-specific deletion of *p53* and *PTEN* tumor suppressors [mice develop Grade III anaplastic astrocytoma or GBM with high penetrance; (Zheng et al., 2008)]. GICs are grown in specially formulated media without serum, but containing human Epidermal Growth Factor (EGF), basic Fibroblast Growth Factor (bFGF), and Leukemia Initiating Factor (LIF). This maintains these cells in a more stem-like state as they grow in spheres and do not attach to the plate. These cells have been shown to be more like a human tumor compared to transformed glioma cells as they give rise to tumors in mice that are more infiltrative and maintain the genetic profile of the tumor they are derived from, unlike transformed glioma cells (Lee et al., 2006a). shIDH1 on-target effect was verified by analyzing IDH1 knockdown in glioma cells expressing RNAi-sensitive or RNAi-resistant IDH1 proteins (Figure 9).

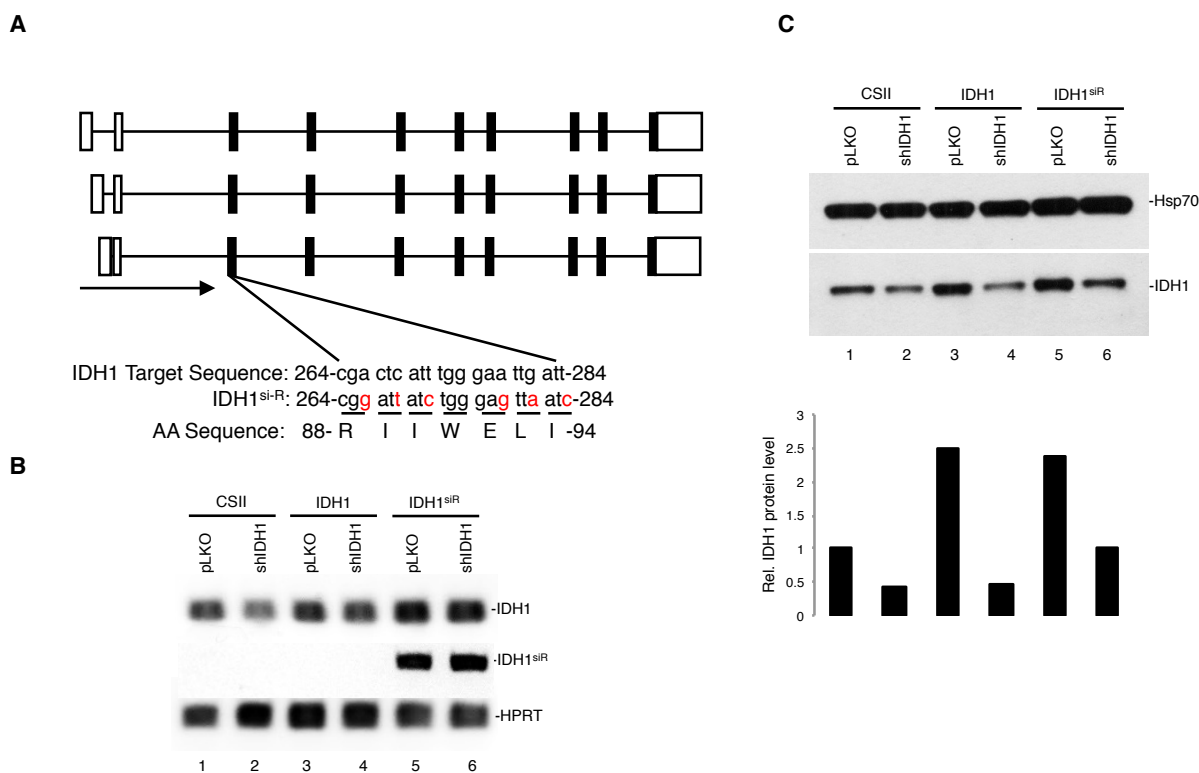


Figure 9. On target effect of shIDH1

(A) shRNA binding site in IDH1 target sequence, and sequence of point-mutated IDH1 (IDH1^{siR}). (B) RT-PCR for *IDH1* and *IDH1*^{siR} in vector control, IDH1, and IDH1^{siR}-expressing glioma cells, co-expressing pLKO or shIDH1. HPRT is shown as a loading control. (C) Corresponding western blot analysis. Hsp70 is shown as a loading control.

Knockdown of IDH1 with two different shRNA constructs reduced GIC proliferation (Figure 10A, 10B), while ectopic expression of IDH1 accelerated NSC growth (Figure 10C).

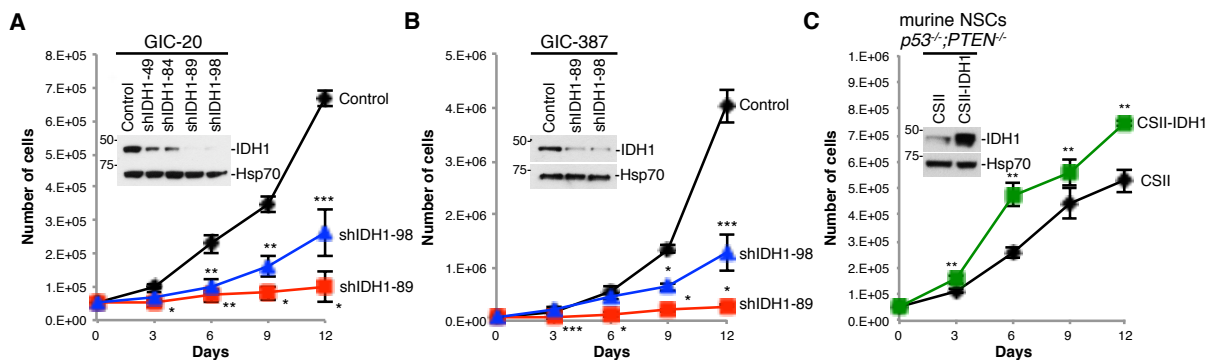


Figure 10. IDH1 promotes GBM cell growth

Cell proliferation in GIC-20 expressing shScramble or shIDH1 (A), GIC-387 with pLKO or shIDH1 (B), and in NSCs with stable overexpression of IDH1 (C) ($n=3$; Mean \pm SD). * $p<0.005$; ** $p<0.05$; *** $p<0.01$.

SCID mice receiving orthotopic implantation of luciferase-labeled GICs modified for reduced IDH1 expression showed diminished tumor growth in comparison to mice implanted with cells infected with empty lentivirus, as indicated by bioluminescence monitoring and survival analysis (Figure 11A-11D). Correspondingly, in a gain-of-function approach, animal subjects engrafted with the luciferase-labeled IDH1-overexpressing NSCs showed accelerated intracranial tumor progression (Figure 11E) and reduced survival when compared to vector controls (Figure 11F).

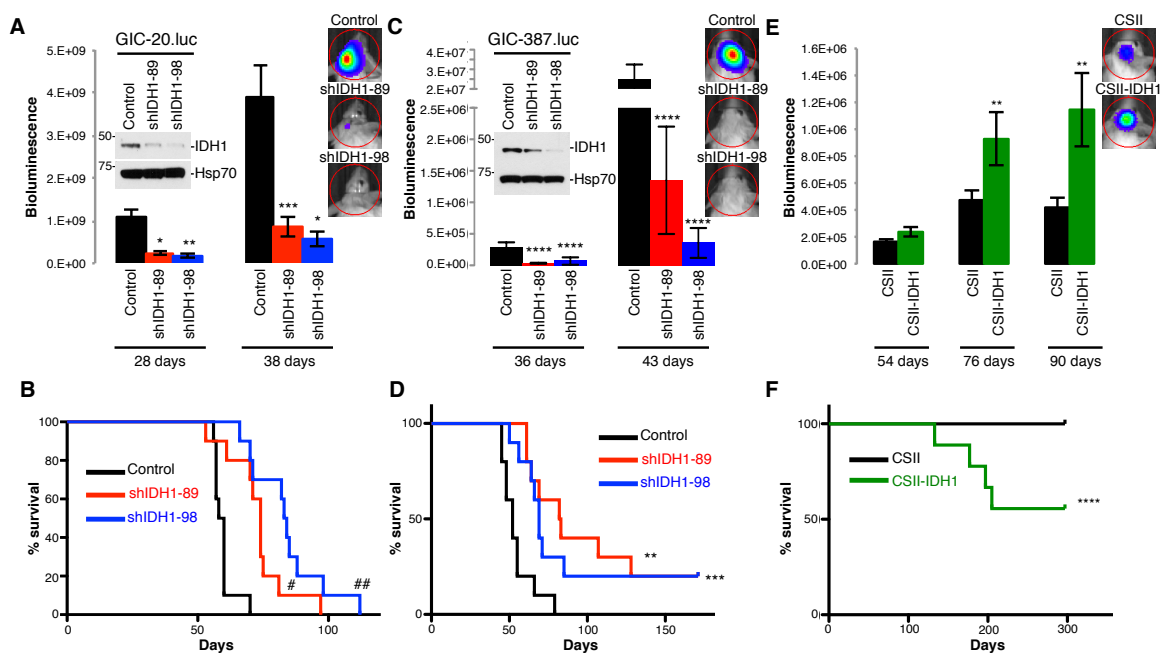


Figure 11. IDH1 promotes GBM progression *in vivo*

Quantification of bioluminescence of intracranial engraftment models, using GIC-20 expressing pLKO and shIDH1 (**A**), GIC-387 with shScramble and shIDH1 (**B**), and NSCs expressing CSII and CSII-IDH1 (**C**) ($n=7-10$; Mean \pm SEM); and the corresponding Kaplan-Meier survival curves (**B**, **D**, **F**) ($n=9-10$). * $p<0.005$; ** $p<0.0005$; *** $p<0.01$; **** $p<0.05$; # $p<0.001$; ## $p<0.0001$. Animals studies done with help from Alexandra Chalastanis and Lisa Hurley.

Immunohistochemical analysis of sections from resected mouse brains revealed increased apoptosis (aCasp3) and decreased proliferation (Ki67) of tumor cells modified for reduced IDH1 expression in comparison to controls and decreased apoptosis and increased proliferation of NSC tumors with overexpression of IDH1 compared to vector controls (Figure 12). These data support tumor-promoting activities of IDH1 in physiologically relevant gain- and loss-of-function GBM mouse models *in vivo*.

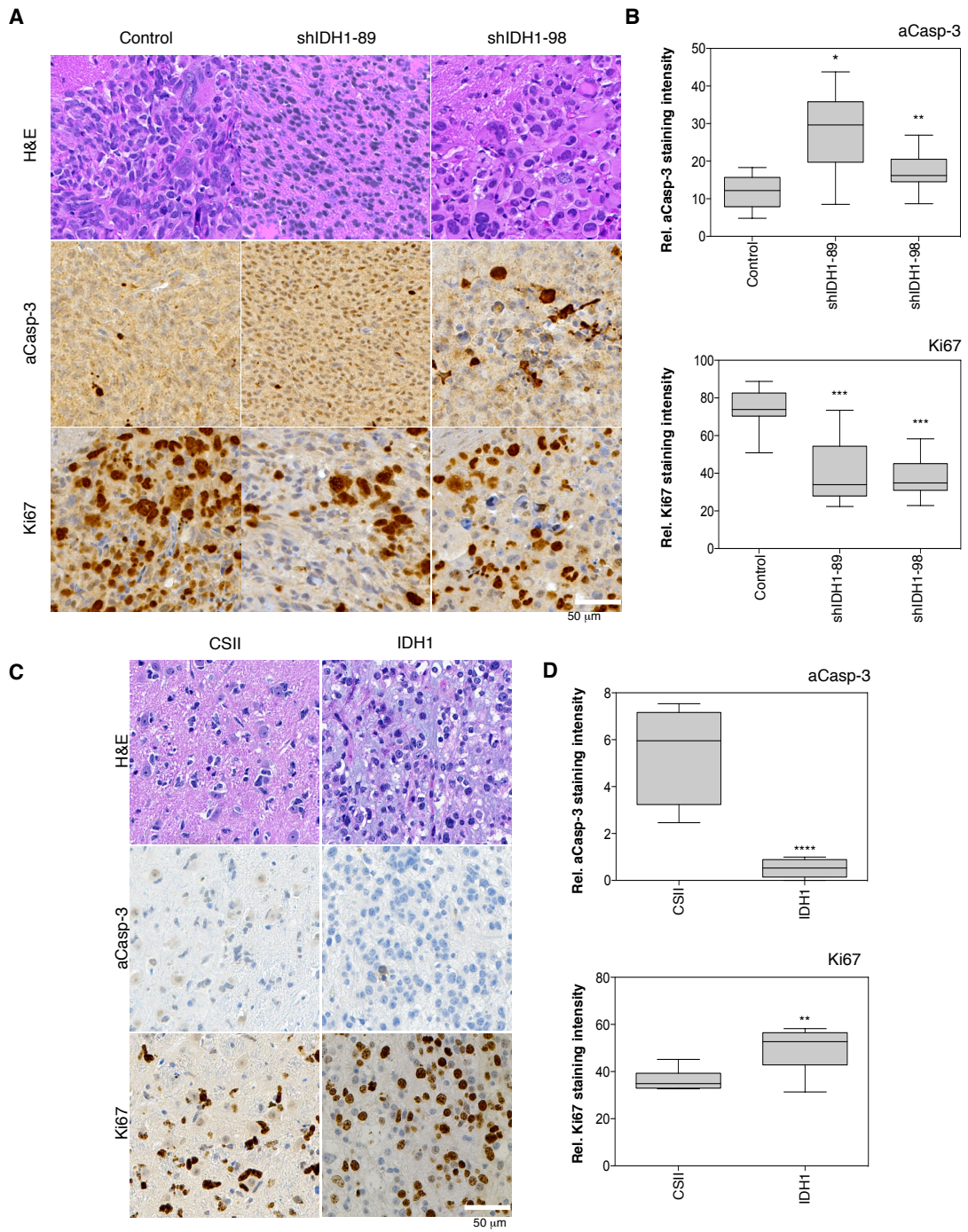


Figure 12. Knockdown of IDH1 results in increased apoptosis and decreased cell proliferation while overexpression of IDH1 results in decreased apoptosis and increased cell proliferation *in vivo*

(A) Histopathological analysis of GIC-20 pLKO and shIDH1 tumors by H&E staining, IHC for aCasp-3 (apoptosis) and Ki67 (proliferation). Bar, 50 μ m. (B) Quantification of aCasp-3 and Ki67 staining intensities by LSC (5 independent areas in 3 independent tumors per group were counted; Mean \pm SD). (C) Histopathological analysis of NSC tumors by H&E staining, IHC for aCasp-3 (apoptosis) and Ki67 (proliferation). Bar, 50 μ m. (D) Quantification of aCasp-3 and Ki67 staining intensities by LSC (6 independent areas in 1 tumor per group were counted; Mean \pm SD). * $p < 0.0005$; ** $p < 0.05$; *** $p < 0.0001$; **** $p < 0.005$. Histology staining done by Lin Li in the mouse phenotyping and histology core.

3.3 Suppression of IDH1 reduces α KG and NADPH levels, and diminishes lipid biosynthesis

Recent metabolomic flux studies in GBM cells, derivative orthotopic explant models and GBM patients revealed that simultaneous to aerobic glycolysis, glucose or acetate-derived carbons are oxidized in the TCA to produce both energy and macromolecular precursors (Marin-Valencia et al., 2012; Mashimo et al., 2014). Studies in liver and adipose cells and tissue revealed that wild-type IDH1 controls lipid metabolism due to its ability to produce lipid carbon precursors and non-mitochondrial NADPH, which is a rate-limiting factor for the synthesis of fatty acids and lipids (Koh et al., 2004; Shechter et al., 2003). Thus, we explored the effect of IDH1 on anaplerotic flux, in particular lipid biosynthesis by performing targeted metabolomic studies using gas chromatography-mass spectrometry (GC-MS). Glioma cells and GICs modified for stable IDH1 knockdown (Figure 13A) had reduced α KG (Figure 13B) and NADPH/NADP⁺ levels (Figure 13C), as expected as the products of the IDH1 enzymatic reaction.

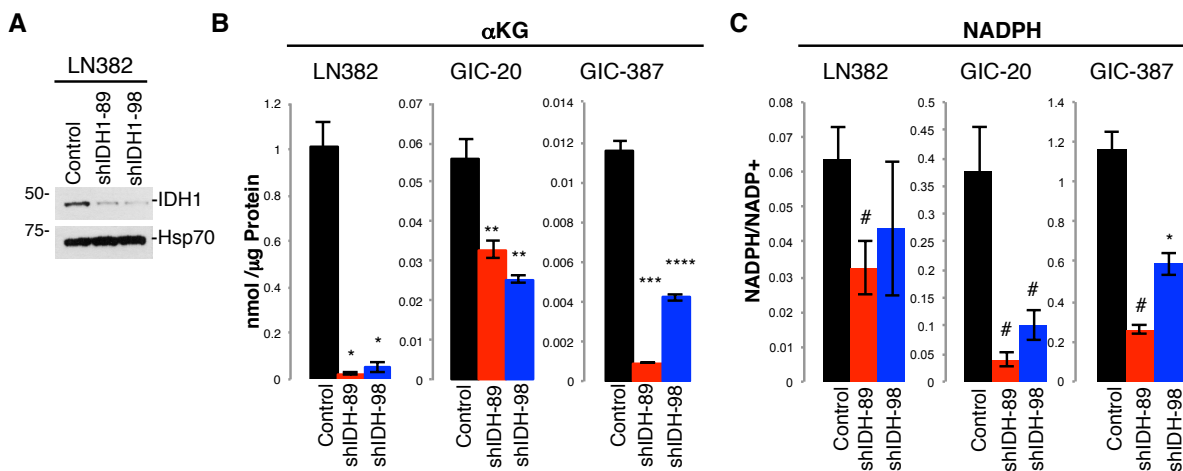


Figure 13. Knockdown of IDH1 decreases α KG and NADPH levels

(A) Western blot of IDH1 in LN382 expressing pLKO or shIDH1. Levels of α KG (B) and NADPH/NADP⁺ ratio (C) in cells infected with pLKO/shScramble, or shIDH1 ($n=2$ in triplicates; Mean \pm SD). * $p < 0.005$; ** $p < 0.01$; *** $p < 0.00005$; **** $p < 0.0005$; # $p < 0.05$.

Using uniformly ^{13}C -labeled glucose and acetate tracers, we found the reduction in the NADPH/NADP⁺ ratio to be associated with diminished saturated and unsaturated *de novo* fatty acid synthesis (Figure 14A, 14B).

Under conditions of hypoxia (Wise et al., 2011; Metallo et al., 2012) and anchorage-independent tumor spheroid growth (Jiang et al., 2016), IDH1 can promote reductive formation of citrate from glutamine by catalyzing the conversion of α KG to ICT (the ‘reverse’ reaction). Citrate can subsequently be converted to acetyl-CoA and then malonyl-CoA, which are the carbon precursors for *de novo* lipid biosynthesis. To determine whether IDH1, under normoxic conditions examined here, can promote anaplerotic replacement of acetyl-CoA by stimulating α KG production (via ‘forward reaction’), we analyzed ^{13}C label incorporation into acetyl-CoA. Using uniformly ^{13}C -labeled acetate tracer, we found that GICs expressing shIDH1 exhibited

elevated levels of ^{13}C -labeled acetyl-CoA (Figure 14C). These data suggest that acetyl-CoA accumulates in IDH1 compromised cells, as it cannot be used for *de novo* fatty acid synthesis due to limited cytoplasmic NADPH availability. Collectively, these targeted metabolic studies together with published literature suggest a critical role of cytoplasmic NADPH for mediating IDH1 metabolic effects.

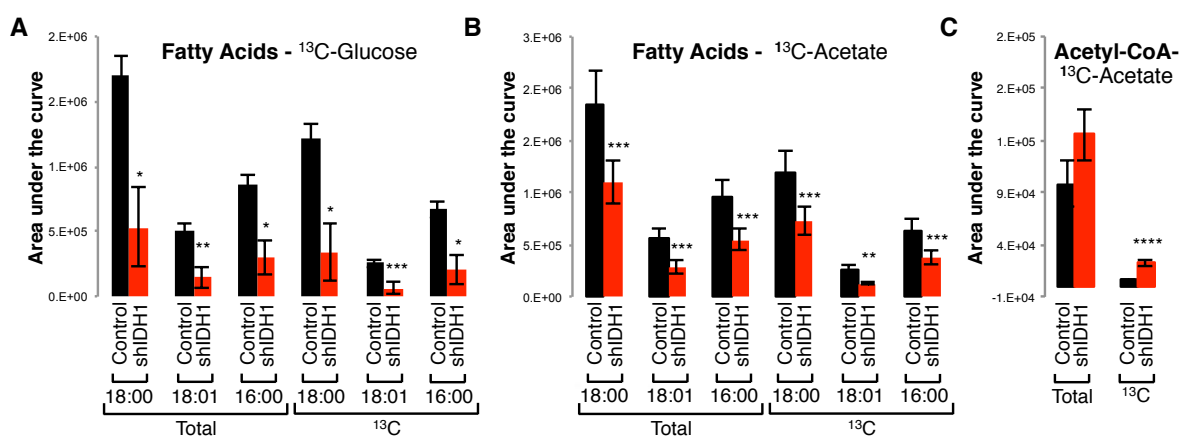


Figure 14. Knockdown of IDH1 reduces carbon flux from glucose or acetate into fatty acids

Levels of total and ^{13}C -labeled fatty acids labeled with ^{13}C -glucose (A) or -acetate (B) in GIC-20 expressing pLKO or shIDH1-89 ($n=5$; Mean \pm SD). (C) Levels of acetyl-CoA in GIC-20 (pLKO vs. shIDH1-89) labeled with ^{13}C acetate tracer ($n=3$; Mean \pm SD). * $p, 0.0005$; ** $p, 0.001$; *** $p < 0.005$; **** $p < 0.05$. ^{13}C labeling analysis done with help from Maureen Kachman and Charles Burant of the University of Michigan Metabolomics Core.

3.4 IDH1 regulates histone methylation and GIC differentiation

As αKG impacts cellular differentiation processes by regulating multiple dioxygenases, including Jumonji C (JmjC)-domain-containing histone lysine residue demethylases, we examined histone lysine methylation in GICs modified for decreased IDH1 expression. shIDH1-expressing GICs showed increases in trimethylation on H3K4, H3K9, H3K27, and H3K36

similar to hypoxic conditions (1.5% O₂; Kaelin and McKnight, 2013) (Figure 15).

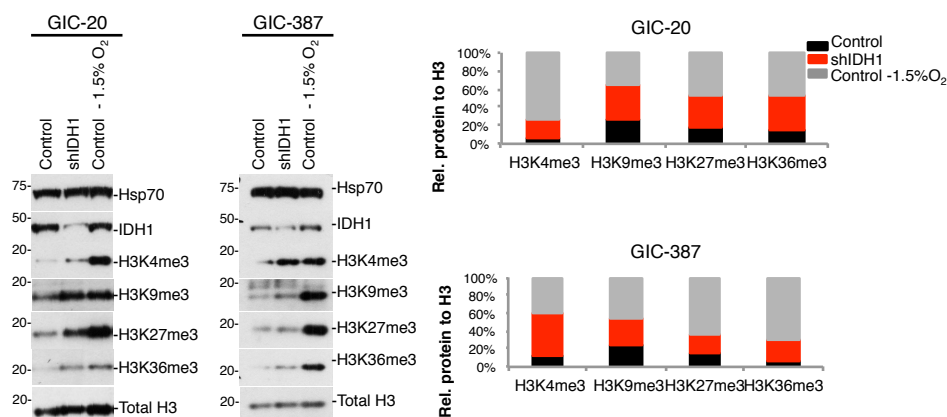


Figure 15. Knockdown of IDH1 increases histone methylation

Western blot of methylated histone species in GICs with pLKO, shIDH1-89 (GIC-20), or shIDH1-98 (GIC-387) (*representative of 3 independent experiments*). Histograms represent densitometry of each methylated histone species.

Using Extreme Limiting Dilution Assays (ELDAs), we show that reduced IDH1 expression diminished (Figure 16A), while increased IDH1 expression in NSCs enhanced stem cell frequency (Figure 16B).

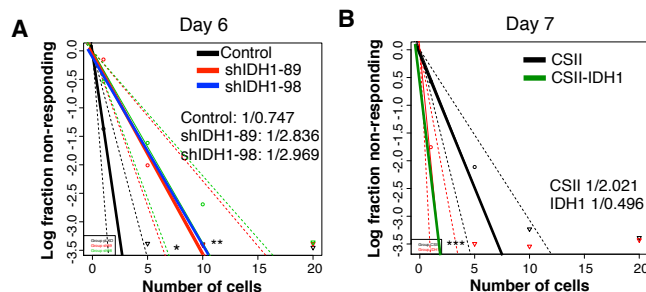


Figure 16. Decreased IDH1 expression is associated with diminished stem cell frequency ELDA of GIC-20s expressing shScramble or shIDH1 (A), and NSCs harboring empty vector control or CSII-IDH1 (B) ($n=15$ per group). Stem Cell Frequency is stated on each graph. * $p<0.0001$; ** $p<0.0005$; *** $p<0.01$.

When exposed to a poly-D-lysine/laminin matrix, GICs with stable IDH1 knockdown more readily differentiated when compared to control-infected cultures, as indicated by augmented MAP2 and GFAP protein expression, markers for neuronal and glial differentiation, respectively (Figure 17A, 17B). Pro-differentiation effect was confirmed by RT-qPCR, which revealed increased levels of *GFAP* transcripts, and decreased mRNA levels of the well-defined neural stem cell marker *Nestin* (Figure 17C). Further supporting a role for IDH1 in regulating glioma cell multipotency, our RT-qPCR analysis of endogenous *IDH1* mRNA in cell populations separated on the basis of CD133 expression, showed increased *IDH1* transcript levels in the glioma stem cell marker enriched versus non-selected populations (Figure 17D).

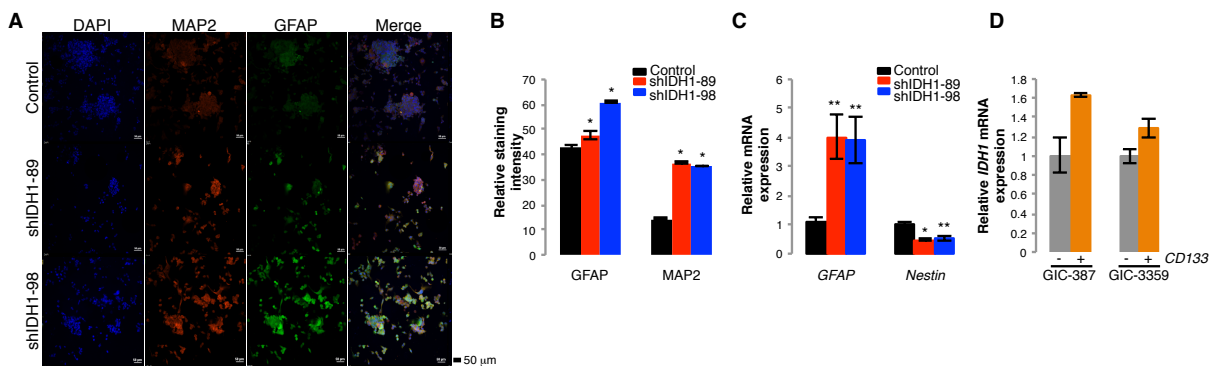
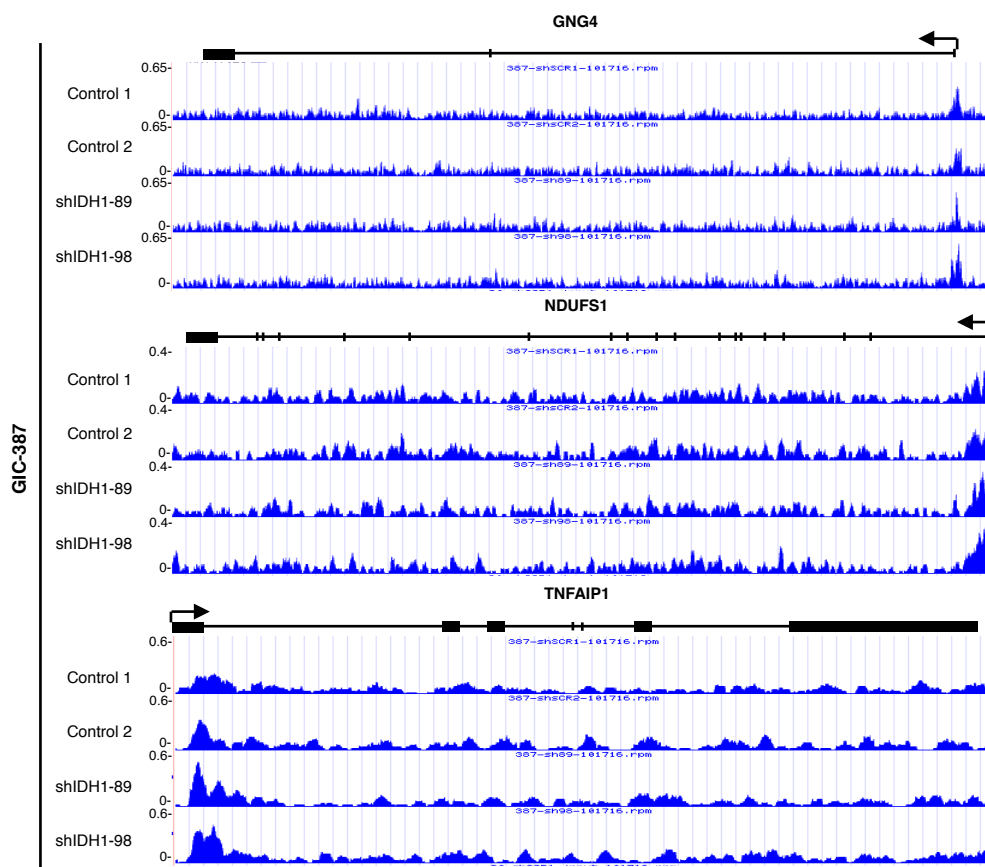


Figure 17. IDH1 knockdown induces a more differentiated GIC state

(A, B) Immunocytochemistry ($n=3$) and quantification for MAP2 and GFAP in GIC-20 expressing shScramble or shIDH1. Bar, 50 μm . ($n=25,000$; Mean \pm SD). (C) RT-qPCR for *GFAP* and *Nestin* in GIC-20 expressing shScramble or shIDH1 ($n=6-7$ per group). (D) RT-qPCR to quantify IDH1 mRNA levels in CD133+ versus CD133- populations. * $p<0.001$; ** $p<0.05$. Differentiation experiment done with help from Fotini Kouri.

To begin to understand how IDH1 impacts gene expression through modification of histone methylation, we performed ChIP-Seq experiments in two independent control and shIDH1 GIC-20 or GIC-387 infectants, using antibodies recognizing tri-methylated H3K27, K36 and K4 proteins. The most significant changes were seen with H3K4me3. Upon ChIP-Seq dataset analysis using SICER to delineate ChIP-enriched regions, to assess their statistical significance, and to identify regions of differential enrichment in shIDH1 versus control GICs, we subsequently performed Ingenuity Pathway Analysis (IPA), to prioritize genes based upon enrichment in signaling pathways associated with cancer and development. mRNA expression of the top 30 genes with most significantly altered H3K4me3 binding in GIC-387 cells was subsequently assessed by RT-qPCR. Through this integrated analysis, we identified a tumor suppresser gene signature induced by IDH1 knockdown that contained *NADH: ubiquinone oxidoreductase core subunit S1 (NDUFS1)*, *Guanine Nucleotide Binding Protein Gamma 4 (GNG4)*, and *TNF Alpha Induced Protein 1 (TNFAIP1)*, and that have been reported to suppress cancer progression through effects on ROS, chemokine receptor biology, and NFκB signaling, respectively (see Discussion). These genes showed increased binding of activating H3K4me3 (Figure 18 for full gene track; Figure 19A for zoomed in on promoter region), increased transcript levels in IDH1 KD versus control GICs as determined by RT-qPCR (Figure 19B), and correspondingly, reduced mRNA expression in TCGA GBM tumors compared to normal brain (Figure 19C).

A



B

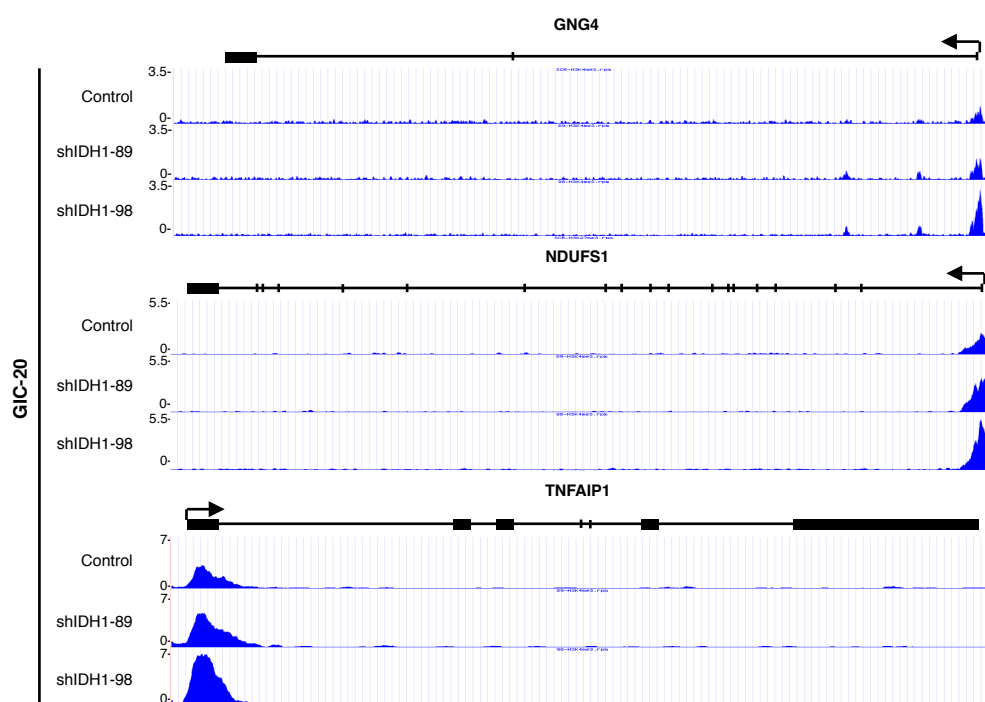


Figure 18. Increased H3K4me3 binding at promoter regions of tumor suppressor genes
Genome tracks of tumor suppressor genes *GNG4*, *NDUFS1*, and *TNFAIP1* in GIC-387 (A) and GIC-20 (B) shScramble or shIDH1 infectants. ChIP-Seq experiments done with help from Andrea Piunti and analysis done with help from Elizabeth Bartom.

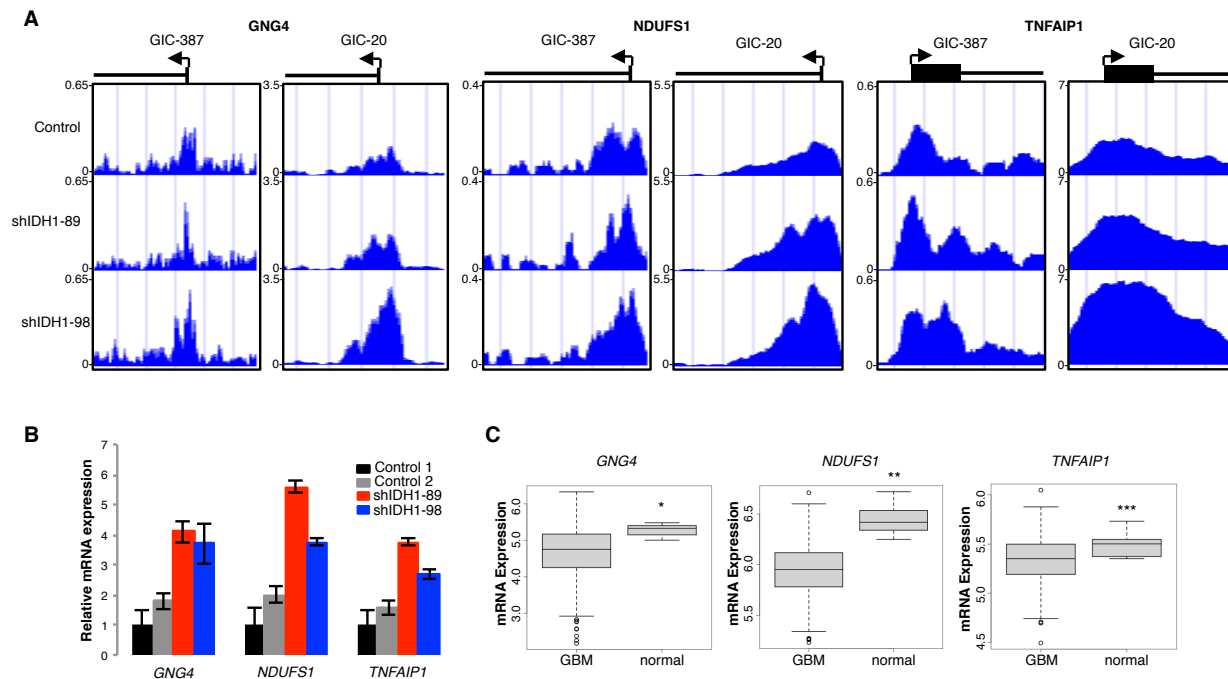


Figure 19. Increased binding of H3K4me3 leads to increased transcript levels of *GNG4*, *NDUFS1*, and *TNFAIP1*

(A) H3K4me3 occupancy of *GNG4*, *NDUFS1*, and *TNFAIP1* promoters as determined by ChIP-Seq in GICs expressing shScramble or shIDH1. (B) RT-qPCR of *GNG4*, *NDUFS1*, and *TNFAIP1* in GIC-387 expressing shScramble or shIDH1. (C) *GNG4*, *NDUFS1*, and *TNFAIP1* mRNA expression in the TCGA dataset ($n=419$). * $p < 5 \times 10^{-9}$, ** $p < 1 \times 10^{-6}$, *** $p < 0.005$. ChIP-Seq experiments done with help from Andrea Piunti and analysis with Elizabeth Bartom. TCGA analysis done by Yingtao Bi.

Two additional tumor suppressor genes, *ETS variant 6 (ETV6)* and *tumor suppressor candidate 2 (TUSC2)* in the top 30 gene list with highly differential binding between shIDH1 and shScramble cells, failed to significantly exhibit transcriptional upregulation upon IDH1 knockdown (Figure

20). This data suggest that increased binding of H3K4me3 is not indicative of active gene transcription only, demonstrating that IDH1 inhibition and associated decrease in α KG production can lead to an increase of histone methylation independently of transcription at different gene loci. Collectively, these data suggest that IDH1 inactivation reduces stem cell frequency, enhances susceptibility to differentiation cues, and regulates (tumor suppressor) gene expression by modulating histone trimethylation.

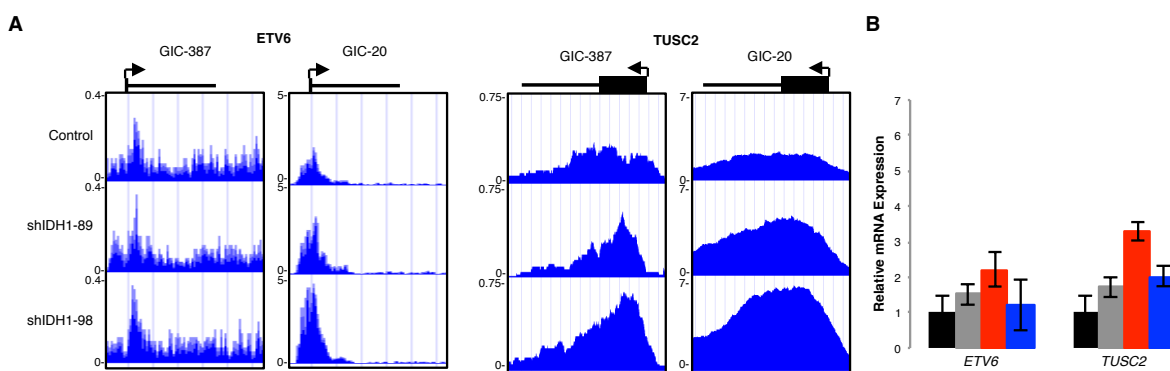


Figure 20. Increased binding of H3K4me3 leads to unchanged transcript levels of *ETV6* and *TUSC2*

(A) H3K4me3 occupancy of *ETV6* and *TUSC2* promoters as determined by ChIP-Seq using GICs with shScramble or shIDH1. (B) RT-qPCR of *ETV6* and *TUSC2* in GIC-387s with shScramble or shIDH1. ChIP-Seq experiments done with help from Andrea Piunti and analysis from Elizabeth Bartom.

3.5 IDH1 ablation increases RTKi-induced apoptosis through decreased lipid biosynthesis and increased ROS in GBM

Unabated tumor growth requires elevated lipogenesis for membrane biogenesis (Menendez and Lupu, 2007). A plethora of studies indicate that GBM tumors activate lipid biosynthesis through oncogenic EGFR/PI3K/Akt pathway activation as a survival mechanism. Consequently, blockage of *de novo* fatty acid biosynthesis (e.g., via treatment of cells with fatty acid synthase (FASN) inhibitors or siRNA targeted to the master transcription factor SREBP1) sensitizes glioma cells to EGFR inhibition (Guo et al., 2009a; Guo et al., 2009b; Guo et al., 2011). Inhibition of RTKs is also known to cooperate with ROS scavengers to reduce GIC survival (Monticone et al., 2014).

To address whether IDH1 modulates cell responses toward RTKi through its impact on lipid biosynthesis and redox balance, we examined the apoptotic response of GICs with and without amplified *EGFR* (Figure 21A, 21B), to RNAi knockdown of IDH1. Erlotinib treatment increased Annexin V positivity in shIDH1 GICs with amplified *EGFR* (GIC-387; *EGFR* amplification, *PTEN*^{+/+}), but not in GICs lacking *EGFR* amplification (GIC-20; *EGFR* non-amplified, *PTEN*^{-/-}; Figure 21C). Correspondingly, NSCs ectopically expressing IDH1 exhibited reduced apoptosis in response to Erlotinib, as evidenced by diminished effector caspase-3 and -7 activation compared to vector controls (Figure 21D).

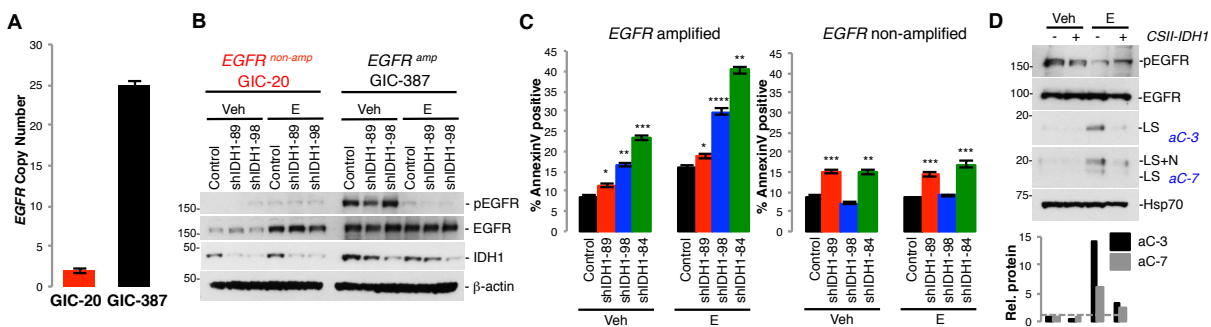


Figure 21. Knockdown of IDH1 sensitizes cells toward Erlotinib-induced apoptosis
 (A) EGFR copy number in GIC-20 and GIC-387. (B) Western blot of pEGFR and IDH1 in GICs expressing shScramble or shIDH1 (representative of 3 independent experiments). (C) Annexin V positivity of GICs expressing pLKO or shIDH1 +/- E ($n=3$; Mean \pm SD). (D) Western blot of cleaved effector caspases in NSCs overexpressing IDH1 +/- E (representative of 3 independent experiments). * $p<0.05$; ** $p<0.001$; *** $p<0.005$; **** $p<0.0005$. E, Erlotinib; LS, large subunit; LS+N, large subunit plus N-peptide.

Treatment of Erlotinib-primed cells with cell-permeable α KG (Figure 22A), or the fatty acid palmitate plus the cholesterol precursor mevalonate (Figure 22B) protected cells from the pro-apoptotic effects of IDH1 knockdown, suggesting that reduced fatty acid and cholesterol biosynthesis contributes to the pro-apoptotic effect of IDH1 knockdown.

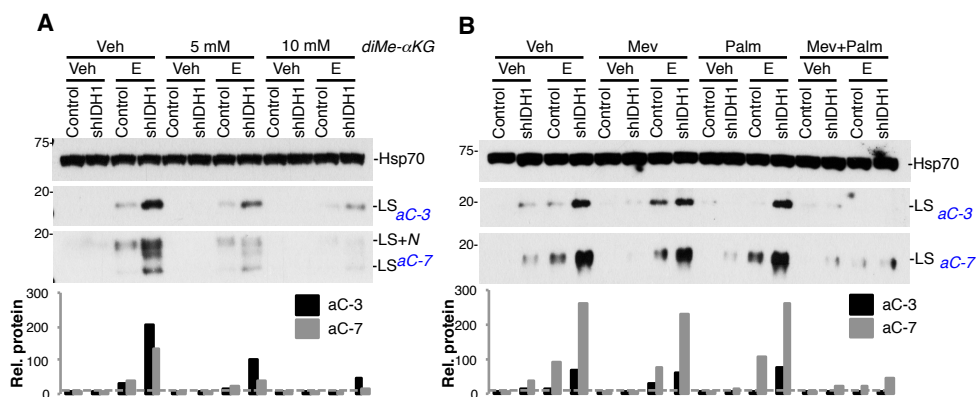


Figure 22. Knockdown of IDH1 sensitizes cells toward Erlotinib-induced apoptosis by decreasing lipid production

Western blot of cleaved effector caspases in GIC-387 expressing pLKO or shIDH1 +/- E and co-treated with diMe- α KG (A), or Mev and Palm (B) (each representative of 2 independent experiments). Histograms represent densitometry done for effector cleaved caspase-3 and -7. E, Erlotinib; diMe- α KG, diMe- α -ketoglutarate; Mev, mevalonate; Palm, palmitate; LS, large subunit; LS+N, large subunit plus N-peptide.

In addition to promoting Erlotinib treatment-associated apoptosis by limiting lipid synthesis, IDH1 knockdown in GICs augmented cellular ROS levels (Figure 23A) as a consequence of decreased reduced glutathione (GSH; Figure 23B) and NADPH (Figure 23C). Treatment of IDH1 knockdown cells with the ROS scavenger EUK-134 (Figure 23D) or *N*-acetyl cysteine (NAC) (Figure 23E) reduced effector caspase activation in response to Erlotinib treatment, suggesting that elevated ROS in shIDH1 GICs contributes to the pro-apoptotic effects of EGFR inhibition. To further confirm a role of diminished NADPH production for the pro-apoptotic effect of IDH1 knockdown, we tested whether α KG add-back impacts the NADPH/NADP⁺ ratio, and whether overexpression of cytoplasmic NADPH-generating malic enzyme 1 (ME1) can rescue pro-apoptotic effect of IDH1 KD. As shown in Figure 23F, diMe- α KG add-back

increases the NADPH/NADP⁺ ratio, and overexpression of cytoplasmic NADPH-producing ME1 antagonizes the pro-apoptotic effect of IDH1 knockdown, similar to α KG add-back (Figure 23G, 23H).

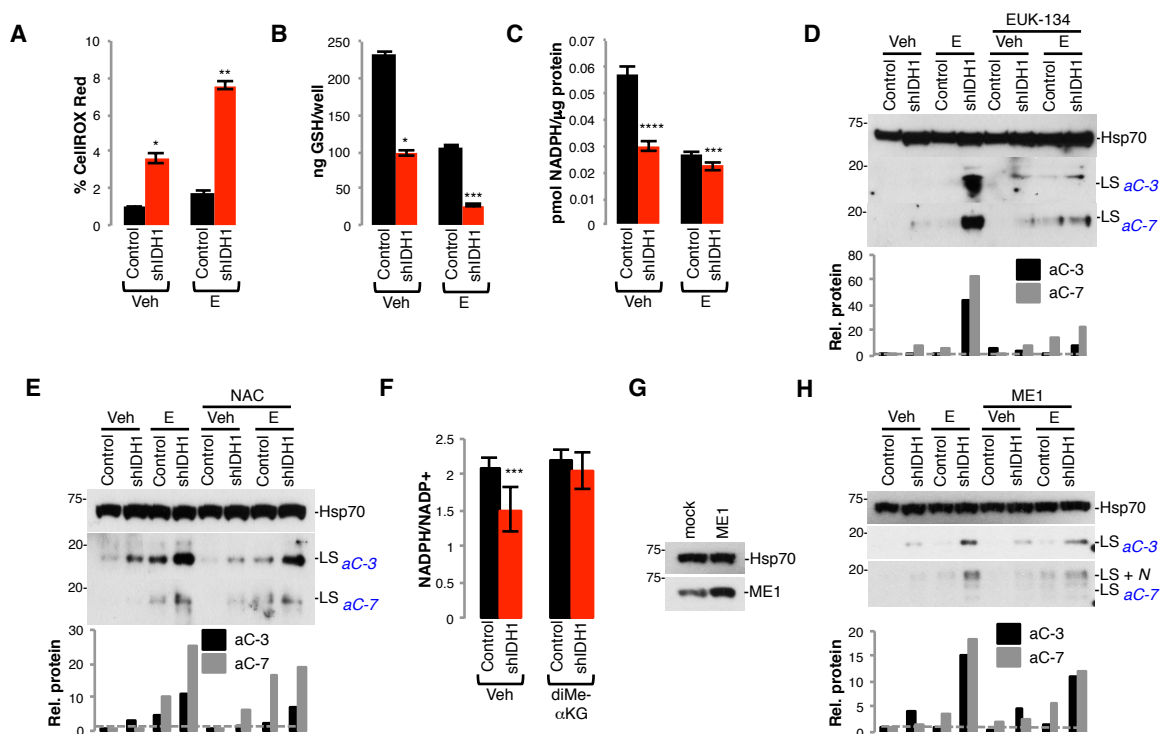


Figure 23. Knockdown of IDH1 sensitizes cells toward Erlotinib-induced apoptosis by increasing ROS production

Levels of ROS (A) ($n=3$; Mean \pm SD), reduced glutathione (GSH) (B) ($n=2$; Mean \pm SD), and NADPH (C) ($n=2$; Mean \pm SD) in pLKO or shIDH1-89-expressing GIC-387 +/- E. (D, E) Western blot of effector caspase activation in GIC-387 treated with EUK-134 or NAC, +/- E (representative of 2 independent experiments). (F) NADPH/NADP⁺ quantification in shScramble and shIDH1-expressing GIC-387 cells +/- diMe- α KG ($n=5$; Mean \pm SD). (G) Western Blot of ME1 in GIC-387 overexpressing ME1. (H) Western blot of cleaved effector caspases in GIC-387 expressing shScramble and shIDH1 +/- E (representative of 3 independent experiments). Histograms throughout represent densitometry done for effector cleaved caspase-3 and -7. * $p < 0.005$; ** $p < 0.0005$; *** $p < 0.05$; **** $p < 0.01$. E, Erlotinib; diMe- α KG, diMe- α -ketoglutarate; NAC, N-Acetyl-Cysteine; ME1, malic enzyme 1; LS, large subunit; LS+N, large subunit plus N-peptide.

Importantly, IDH1 knockdown in transformed glioma cells harboring co-activation of multiple RTKs, including EGFR, the HGFR family member MSPR and PDGFRs as seen by phospho-RTK array (Figure 24A), had similar effects as observed in patient-derived cultures with activation of EGFR only. IDH1 ablation diminished NADPH levels in the transformed cells (Figure 24B), and when combined with an RTK inhibitor cocktail caused a reduction in cellular GSH (Figure 24C) as well as increases in ROS (Figure 24D), Annexin V positivity (Figure 24E), and effector caspase activation (Figure 24F, 24G). Apoptosis sensitization by IDH1 knockdown occurs upstream of mitochondrial outer membrane permeabilization, as overexpression of Bcl-2 blocked effector caspase activation in response to IDH1 inhibition in Erlotinib-primed cells (Figure 24H, 24I). In total, these results demonstrate that IDH1 knockdown, through inhibition of NADPH and associated effects on lipid synthesis and ROS production, promotes apoptosis of tyrosine kinase inhibitor treated cancer cells.

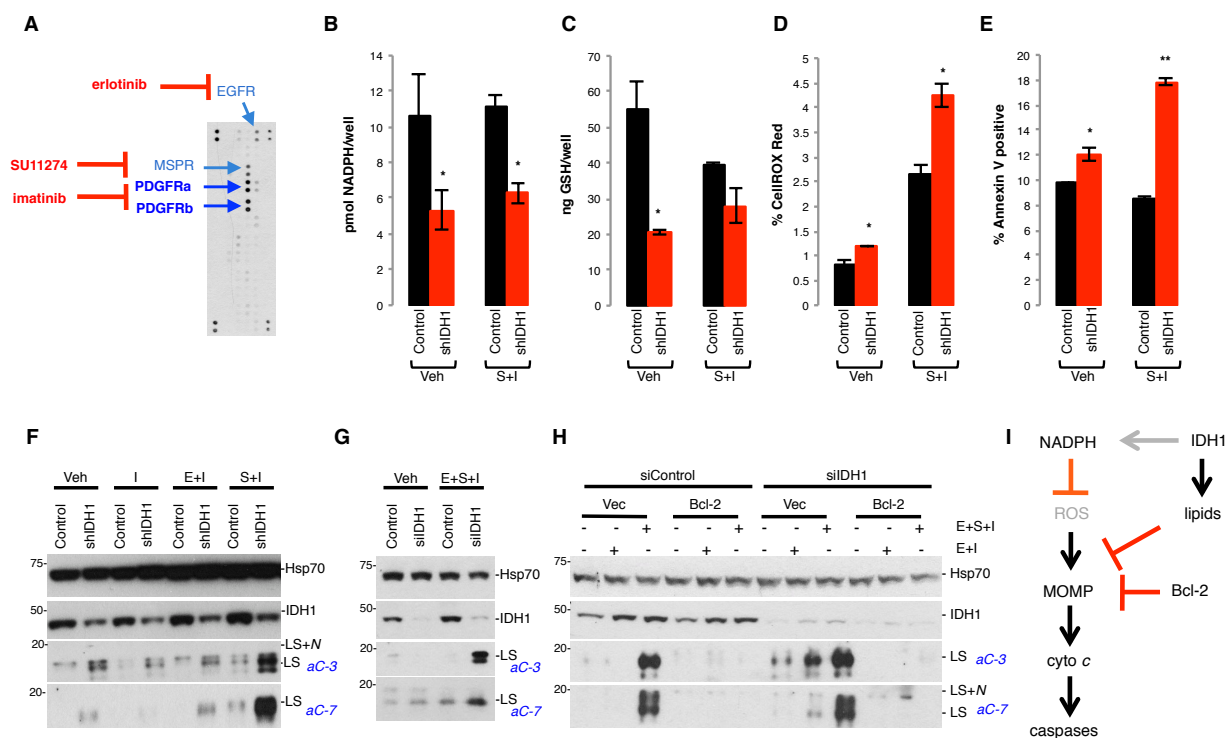


Figure 24. Knockdown of IDH1 sensitizes transformed glioma cells harboring co-activation of multiple RTKs toward RTKi

(A) Phospho-tyrosine RTK antibody array in LN382 cells (representative of 4 independent experiments). (B) NADPH (representative of 4 cultures; Mean \pm SD), (C) GSH (representative of 5 cultures; Mean \pm SD), and (D) ROS levels (3 cultures per group; Mean \pm SD) were quantified in vehicle (Veh)- and RTKi-treated control (pLKO or shScramble), or shIDH1-89-infected LN382 cells. (E) FACS-based quantification of Annexin V positivity of RTKi-treated versus vehicle-treated LN382 cells expressing shScramble and shIDH1 cultures (3 cultures per group; Mean \pm SD). Effector caspase activation as determined by western blotting of LN382 expressing shScramble or shIDH1 (F) (representative of 7 independent experiments) or siScramble or siIDH1 (G) (representative of 4 independent experiments) treated with RTKi. (H) Western blot for active effector caspases in LN382 overexpressing Bcl-2, transiently transfected with siRNA targeted to IDH1, and treated with an RTKi cocktail (representative of 2 independent experiments). (I) IDH1 pro-apoptotic effects are upstream of mitochondrial dysfunction. * $p < 0.05$; ** $p < 0.005$. MOMP, mitochondrial outer membrane permeabilization; cyto *c*, cytochrome *c*; E, Erlotinib; S, SU11274; I, Imatinib; LS, large subunit; LS+N, large subunit plus *N*-peptide. Panels G and H done by Yongfei Wu.

3.6 IDH1 protects cancer cells derived from non-glioma tumors from apoptosis

To determine if IDH1 is not only important in GBM pathogenesis, we looked at TCGA database for other solid cancer types as well as published gene expression array data from various systemic malignancies. We found that *IDH1* mRNA is also upregulated in other solid and systemic malignancies, including lung adeno- and squamous cell carcinoma (Figure 25A), as well as various types of lymphoma, including angioimmunoblastic, anaplastic large cell, peripheral T cell, and diffuse large B cell (DLBCL) subtypes (Figure 25B). Stable knockdown of IDH1 in DLBCL cells (Figure 25C) enhanced apoptotic susceptibility toward the Bruton's tyrosine kinase (BTK) inhibitor Ibrutinib, as indicated by increased Annexin V positivity of treated cells (Figure 25D), which was paralleled by attenuated α KG production (Figure 25E), reduced GSH (Figure 25F), increased ROS (Figure 25G), and decreased tumor size in a subcutaneous xenograft model (Figure 25H, 25I). These results demonstrate that IDH1 plays a role not only in glioma pathogenesis, but also other solid and systemic malignancies.

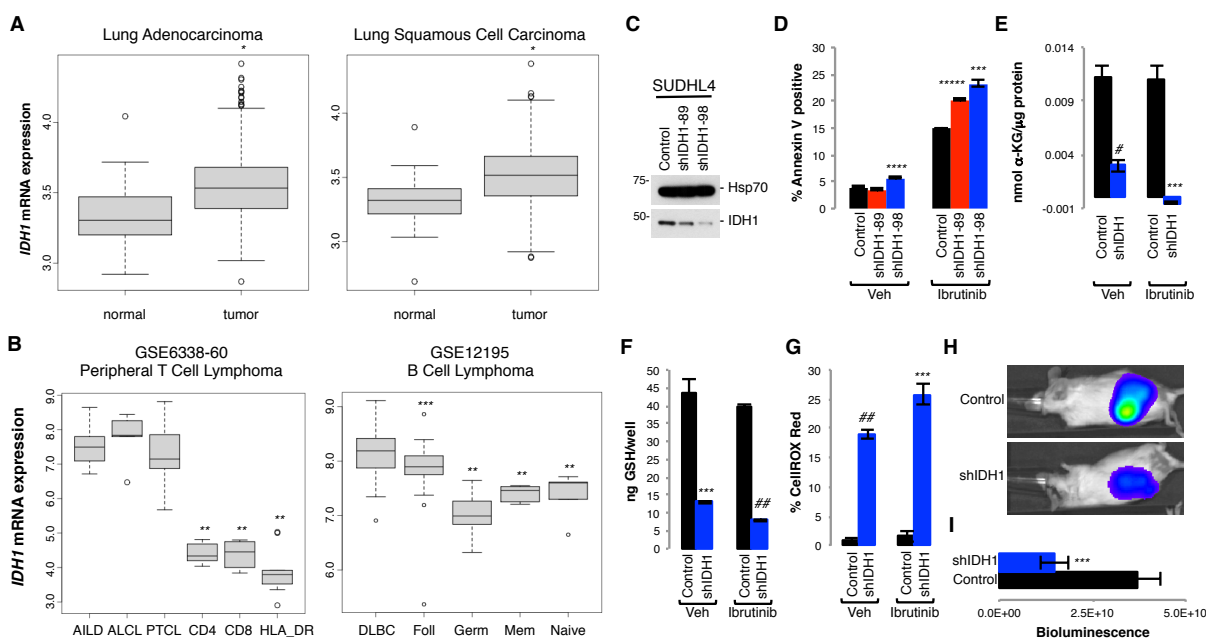


Figure 25. IDH1 protects cancer cells derived from non-glioma tumors from apoptosis

(A) TCGA dataset analysis of *IDH1* mRNA in lung adenocarcinoma ($n=488$) and lung squamous cell carcinoma ($n=489$) compared to normal lung tissue ($n=50$). (B) *IDH1* mRNA expression in AILD ($n=6$), ALCL ($n=6$), and PTCL ($n=28$) in comparison to CD4 ($n=5$), CD8 ($n=5$) or HLA-DR-positive T cells ($n=10$), and in DLBCL ($n=73$) in comparison to Foll ($n=38$), Germ ($n=10$), Mem ($n=5$) or naive B cells ($n=5$). (C) The diffuse large B cell lymphoma cell line SUDHL4 was lentivirally transduced with pLKO or shRNAs targeted to IDH1, and IDH1 protein levels were assessed by western blotting. (D) Annexin V positivity (3 cultures per group; Mean \pm SD), (E) α -KG (1 culture per group; Mean \pm SD), (F) GSH (1 culture per group; Mean \pm SD), and (G) ROS levels (3 cultures per group; Mean \pm SD) were quantified in vehicle (Veh)- or Ibrutinib-treated pLKO and shIDH1-98 cultures. (H, I) Bioluminescence of SUDHL4 pLKO and shIDH1-98 cells 14 days after flank implantation in SCID mice ($n=5$ animals per group; Mean \pm SEM). * $p < 5 \times 10^{-10}$, ** $p < 1 \times 10^{-5}$, *** $p < 0.005$, **** $p < 0.05$, ***** $p < 0.001$, # $p < 0.01$, ## $p < 0.0005$. AILD, angioimmunoblastic lymphadenopathy; ALCL, anaplastic large cell lymphoma; PTCL, peripheral T-cell lymphoma; DLBCL, diffuse large B cell lymphoma; Foll, follicular; Germ, germinal; Mem, memory. TCGA and GSE analysis done by Yingtao Bi. Animal experiment done with help from Lisa Hurley.

3.7 FoxO6 transcriptionally induces IDH1 expression in response to RTK inhibition

Results in recent studies have implicated Forkhead box O (FoxO) transcription factors as positive regulators of IDH1 expression (Charitou et al., 2015). As Akt-mediated phosphorylation inhibits FoxO transcriptional functions (Lam et al., 2013), we examined whether RTK inhibition, and its downstream effect of suppressing Akt activity, increased IDH1 transcript and protein levels through FoxO activation. Erlotinib induced IDH1 transcript and protein levels in *EGFR* amplified, but not in non-amplified GICs (Figure 26A, 26B). Similarly, a combination of RTKi, but not TMZ, a standard of care alkylating agent, promoted IDH1 expression in transformed glioma cell cultures (Figure 26C), confirming that IDH1 induction is dependent on RTK-PI3K-Akt activation. IDH1 induction was preceded by the binding of various FoxO transcription factors, including FoxO1, FoxO3, and FoxO6, to an *IDH1* intronic consensus-binding site (Figure 26D), as determined by chromatin immunoprecipitation and qPCR (Figure 26E). FoxO6 showed preferential binding to the *IDH1* consensus sequence (Figure 26E). Knockdown of FoxO6 by siRNA attenuated the RTKi-induced increase in IDH1 expression, as well as increased apoptosis as seen by cleaved caspase activation (Figure 26F). These results are consistent with IDH1 upregulation, through FoxO6 activation, as a glioma cell adaptive response to growth factor receptor inhibition.

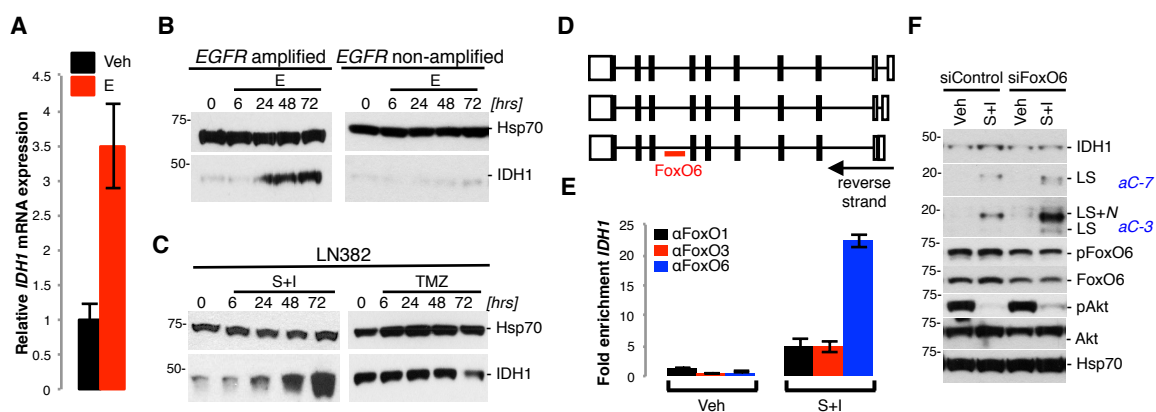


Figure 26. RTKi induce IDH1 expression through FoxO6

(A) RT-qPCR of IDH1 in GIC-387 +/- E. (B, C) Western blot of IDH1 in GIC-387, GIC-20, and LN382 cells +/- TMZ or RTKi (*representative of 2 independent experiments*). (D) Gene organization of the 3 IDH1 isoforms with the position of an intronic FoxO6 binding site. (E) ChIP using FoxO6 antibody, followed by RT-qPCR of IDH1 (*representative of 3 independent experiments*). (F) Western blot for IDH1, effector caspases, FoxO6, and total and phosphorylated Akt in LN382 cells treated with siFoxO6, +/- RTKi (*representative of 3 independent experiments*). E, Erlotinib; LS, large subunit; LS+N, large subunit plus N-peptide; S+I, SU11274 + Imatinib; TMZ, temozolomide. Panel A done by Alexandra Chalastanis. ChIP done by Fotini Kouri.

This interpretation is further supported by the results from whole genome mRNA expression profiling by microarray of vehicle- and RTKi-treated glioma cells (Figure 27A). Ingenuity Pathway analysis (www.ingenuity.com) of the 614 differentially expressed genes, identified IDH1 and lipid metabolism as the top priority signaling pathway induced upon RTKi treatment (Figure 27B, 27C). Besides *IDH1*, RTKi-induced genes included *lanosterol synthase (LSS)*, and *isopentyl-diphosphate delta isomerase 1 (IDII)*, two important genes involved in cholesterol biosynthesis (Figure 27B, 27C). We confirmed that *IDII* and *LSS* transcript levels are indeed increased upon treatment with RTKi by RT-qPCR (Figure 27D).

The importance of lipid metabolism gene induction as a modifier of RTKi responses was further supported by the results of IDH1 or LSS lentiviral knockdown in GBM transformed cells (Figure 28A), which sensitized glioma cells to RTKi-mediated apoptosis, as shown by enhanced tumor cell effector caspase activation (Figure 28B) and Annexin V positivity (Figure 28C). Thus, glioma cells adapt to growth factor inhibition by transcriptionally inducing cell death inhibitory IDH1 and attendant lipid biosynthesis via an RTK-PI3K-Akt-FoxO6 signaling axis. Such adaptation suggests that RTKi-primed glioma cells rely on IDH1-driven lipid biosynthesis for proliferation and survival, and points to co-extinction strategies that targets both aberrant RTK signaling and IDH1 activation to effectively halt unabated glioma growth.

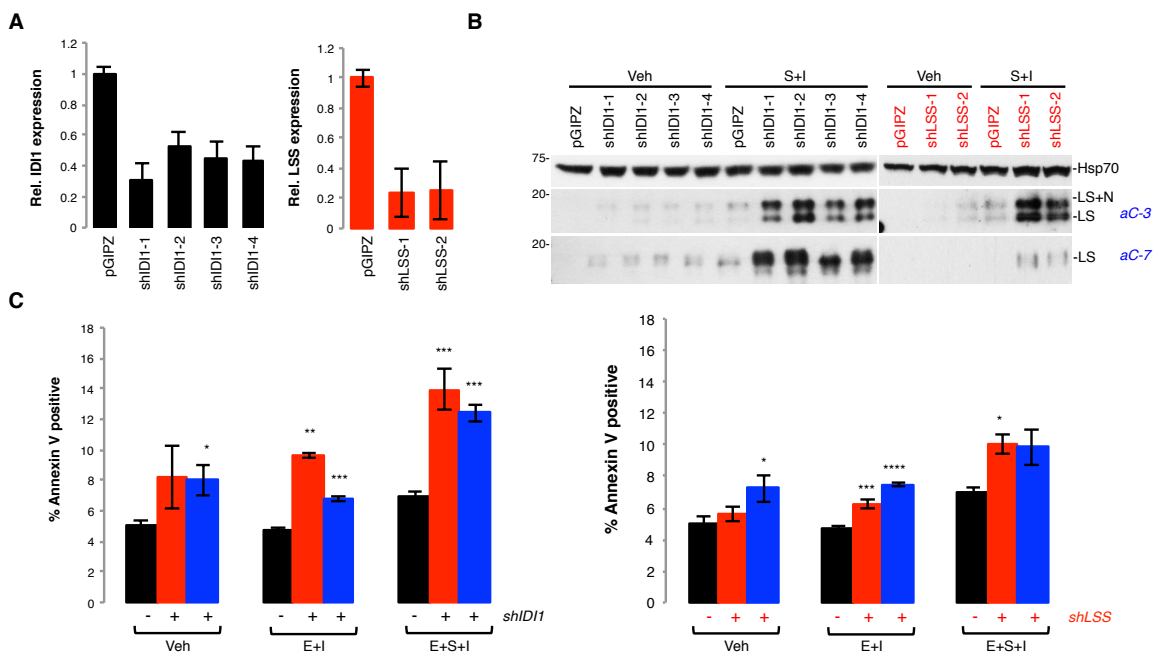


Figure 28. Knockdown of IDI1 or LSS increases RTKi-induced apoptosis

(A) *IDI1* and *LSS* mRNA expression was assessed by RT-qPCR using total RNA isolated from LN382 cells infected with shRNAs targeting either *IDI1* or *LSS* (representative of 2 independent experiments). (B) LN382 cells modified for reduced *IDI1* or *LSS* expression were treated with vehicle (Veh) or RTKi, and effector caspase activation was assessed by western blot analysis (representative of 2 independent experiments). (C) LN382 stably expressing shRNAs targeted to *IDI1* and *LSS* were treated with the indicated combinations of RTKi, and Annexin V positivity was quantified by FACS (3 cultures per group; Mean \pm SD). * $p < 0.05$; ** $p < 0.001$; *** $p < 0.01$; **** $p < 0.005$. E, Erlotinib; S, SU11274; I, Imatinib; LS, large subunit; LS+N, large subunit plus N-peptide. Done with help from Jasmine May.

3.8 Pharmacological inhibition of IDH1 reduces growth, augments RTKi susceptibility, reduces stem cell frequency, and decreases GBM progression

To address whether wild-type IDH1 is an actionable therapeutic target, we treated non-transformed cortical astrocytes, glioma cells and patient-derived GICs with GSK864. Similar to the first generation compound GSK321, compound GSK864 was initially identified as a potent

inhibitor against R132H point mutated IDH1 [IC₅₀: 15.2nM; (Okoye-Okafor et al., 2015)]. In IDH1 mutant AML cells and derivative xenografts, GSK864 was shown to decrease D-2HG levels, decrease percentage of blast cells, and increase myeloid differentiation (Okoye-Okafor et al., 2015). GSK321 has been validated as an inhibitor of wild-type IDH1 (Jiang et al., 2016), demonstrating that pharmacological inhibition of IDH1 activity blunts reductive glutamine metabolism, and in so doing enhances mitochondrial ROS, and reduces tumor spheroid growth. Importantly, at higher doses, GSK864 also inhibited wild-type IDH1 [IC₅₀: 466.5nM; (Okoye-Okafor et al., 2015)], and thus, represents a valuable tool to assess whether pharmacological inhibition of non-mutated IDH1 recapitulates cellular and tumor biological effects observed with genetic inactivation, and whether overexpression of IDH1 is an actionable genetic aberration for the treatment of intracranial GBM.

GICs infected with shScramble, but not shIDH1 expressing cells, showed a dose-dependent reduction of the NADPH/NADP⁺ ratio, when treated with GSK864 (Figure 29A). Similarly, non-transformed cortical astrocytes, expressing low levels of IDH1 protein compared to transformed glioma cells and GICs (Figure 29B) failed to respond to GSK864 treatment, as evidenced by similar NADPH/NADP⁺ ratios in vehicle vs. GSK864-treated cells (Figure 29C).

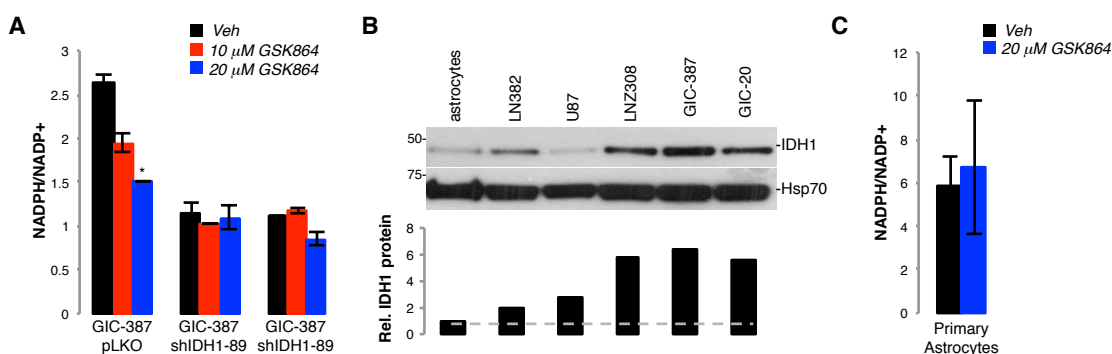


Figure 29. GSK864, an inhibitor of mutant IDH1, has activity against wild-type IDH1
 (A) NADPH/NADP⁺ levels in GIC-387 expressing shScramble or shIDH1 +/- GSK864 (representative of one experiment, done in triplicate; Mean \pm SD). (B) IDH1 western blot of transformed glioma cell lines, GICs, and primary human astrocytes (representative of 2 independent experiments). Histograms show relative levels of IDH1 protein as determined by densitometry. (C) NADPH/NADP⁺ levels in primary astrocytes +/- GSK864 ($n=2-3$, Mean \pm SD). * $p < 0.05$. Panel B done by Jasmine May.

When used in combination with RTKi in glioma cells showing hyperactivation of cMET and PDGFRs (Figure 30A, 30C, 30D), or in *EGFR*-amplified patient-derived GIC-387 cultures (Figure 30B, 30E, 30F), GSK864 reduced cell viability, and induced tumor cell apoptosis (Figure 30A-30F), as evidenced by MTT, Annexin V and western blotting for active effector caspases, respectively. Mirroring the effect of IDH1 knockdown on GIC differentiation (see Figure 16), GSK864 reduced stem cell frequency in GIC-387 cells (ELDA, Figure 30G). The pro-apoptotic effect of GSK864, similar to pro-death activity of RNAi-mediated KD of IDH1 (Figure 22A), can be abrogated by reconstituting cells with cell permeable α KG (Figure 30H), further validating compound specificity.

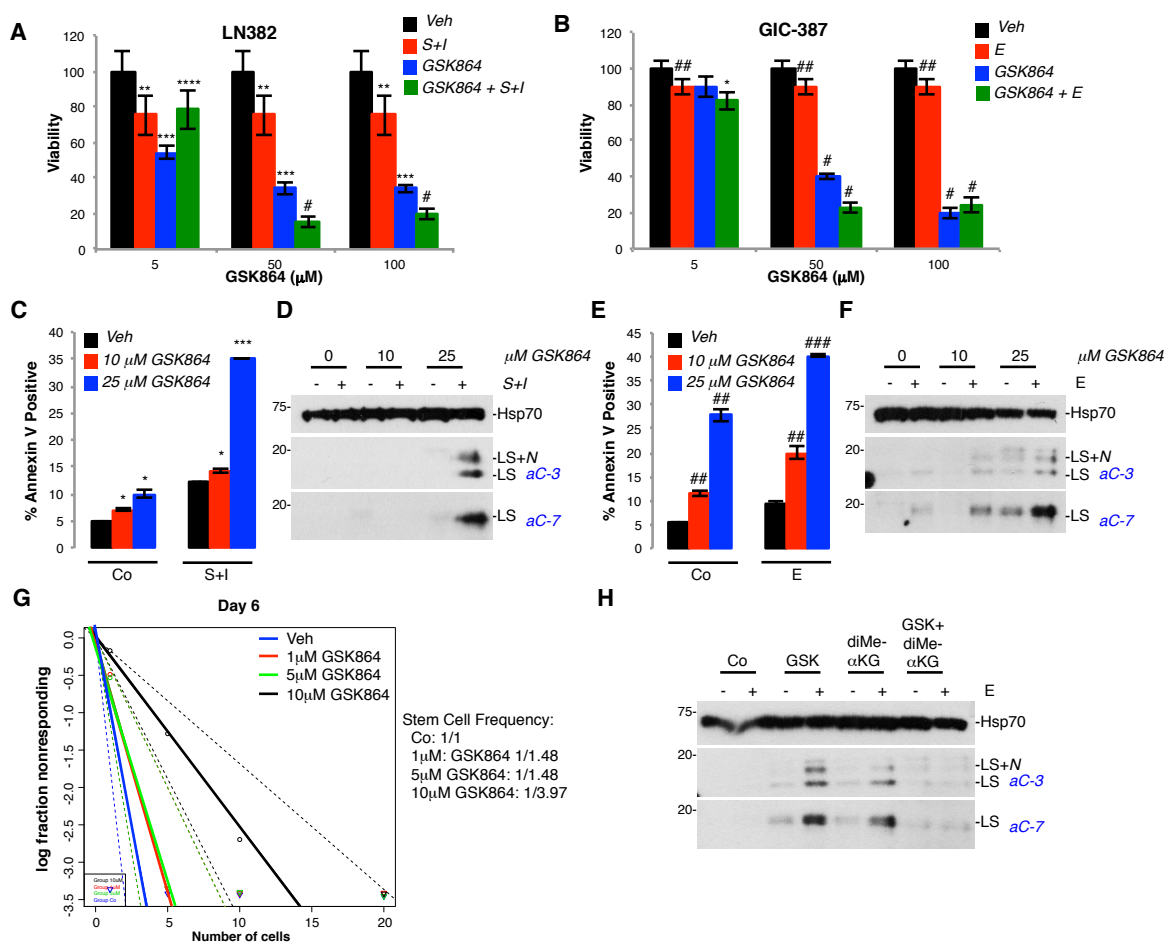


Figure 30. GSK864 inhibits GBM cell growth and increases RTKi-induced apoptosis *in vitro*

(A, B) MTT assay of LN382 and GIC-387 treated with GSK864 +/- RTKi ($n=6$; Mean \pm SD). Quantification of apoptosis in LN382 and GIC-387 treated with GSK864 +/- RTKi, by Annexin V positivity (C, E) ($n=3$; Mean \pm SD), and western blotting of effector caspase activation (D, F) (representative of 3 independent experiments). (G) ELDA of GIC-387 cells treated with GSK864. p-values between Vehicle and the following: 1 μ M, $p=1.06 \times 10^{-4}$; 5 μ M, $p=1.06 \times 10^{-4}$; 10 μ M, 9.43×10^{-11} ($n=15$). (H) Western blot of effector caspases in GIC-387 +/- GSK864, diMe- α KG, and/or E. (representative of 2 independent experiments). * $p < 0.05$; ** $p < 0.01$; *** $p < 0.00005$; **** $p < 0.001$; # $p < 0.00001$; ## $p < 0.005$; ### $p < 0.0001$. E, Erlotinib, S+I, SU11274 + Imatinib; LS, large subunit; LS+N, large subunit plus N-peptide; diMe- α KG, dimethyl- α -ketoglutarate.

To determine the effects of GSK864 *in vivo*, luciferase-modified GIC-20 cultures were intracranially injected into immunocompromised mice. Upon establishment of progressive tumor growth by non-invasive bioluminescence imaging, mice were treated with 150 mg/kg GSK864 or vehicle 13 days post cell inoculation. GBM progression was significantly impaired in mice treated with GSK864 in comparison to vehicle-treated subjects, as evidenced by reduced bioluminescence (Figure 31A, 31B), and accordingly, mice administered with compound GSK864 showed increased survival (Figure 31C). These results provide initial proof-of-concept that IDH1 is a targetable oncogenic activity.

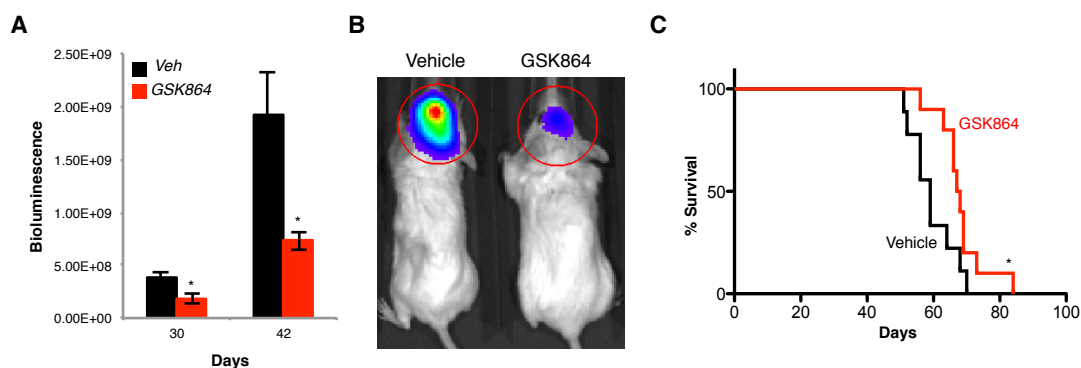


Figure 31. GSK864 decreases tumor burden and prolongs subject survival *in vivo*

Bioluminescence imaging of luciferase-expressing explants derived from GIC-20 cultures, treated with vehicle or GSK864 (**A, B**) ($n=9-10$; $Mean \pm SEM$). (**C**) Kaplan-Meier survival curves of GIC-20 engrafted mice +/- GSK864 ($n=9-10$). * $p<0.05$. Animal experiment done with help from Lisa Hurley.

CHAPTER 4: DISCUSSION

4.1 Discussion

We have demonstrated that several cancers, in particular primary GBM, show significant upregulation of wild-type IDH1 to support tumor progression. Using pharmacologic and RNAi-based loss-of-function together with cDNA complementation gain-of-function studies, we further show that upregulation of IDH1 is a novel mechanism of metabolic reprogramming, which enhances cellular anaplerosis, in particular lipid biosynthesis, alters the cellular redox state, promotes a more dedifferentiated cell state, and causes resistance toward RTK-targeted therapies (Figure 32).

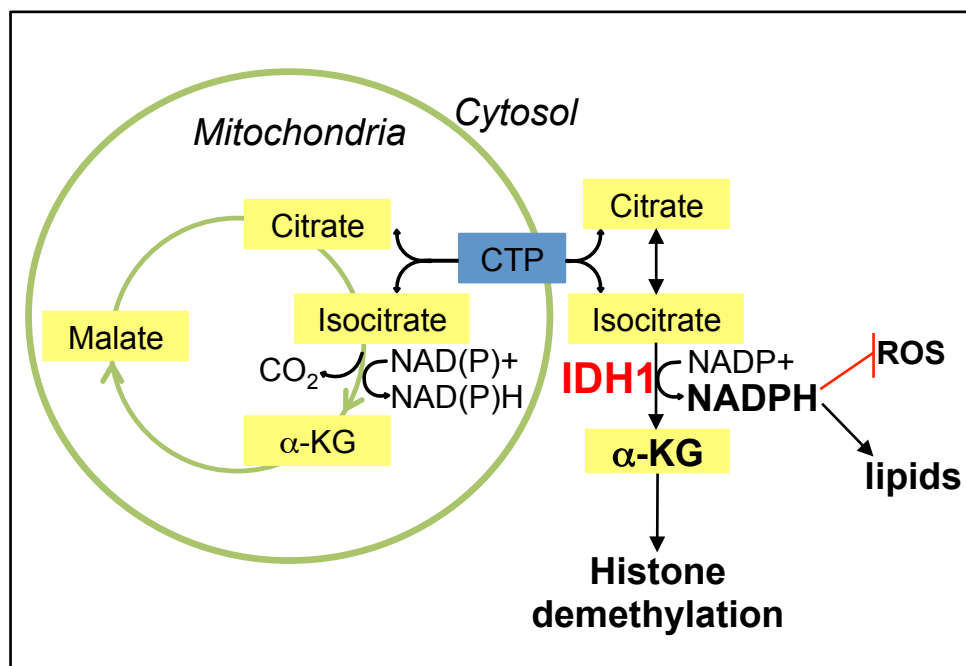


Figure 32. IDH1 promotes tumor progression

IDH1 produces NADPH and α KG necessary for maintaining redox homeostasis and *de novo* lipogenesis, and histone demethylation, respectively.

Additionally, we have shown that except for moderate upregulation of *ACOI*, *IDH1* is the only TCA-associated enzyme that is robustly overexpressed in GBM tumors. Thus, our oncogenomic analysis revealed that GBM tumors are not characterized by global induction of TCA-associated anabolic enzymes. This finding supports our central hypothesis that IDH1 induction represents a selective oncogenic mechanism contributing to tumor progression, rather than a passive non-specific adaptation to increase proliferative rates. Our TCGA-based oncogenomic analyses rely on comparisons between normal and tumor tissue and, in order to determine potential involvement of a gene aberration in disease progression, between low and high-grade disease. It is possible that differential mRNA expression in *IDH1* can reflect unselective tumor cell adaptation to meet the demands of rapid tumor cell proliferation. Despite this well-acknowledged shortcoming of genomic analyses, such approaches represents an important first step in identifying cancer-associated genetic mechanisms that contribute to or drive tumor progression. Importantly, we have confirmed initial TCGA results in independent specimen sets by quantifying IDH1 transcript as well as protein levels. Such initial oncogenomic analyses when combined with deep biological experiments as presented here are critical for the identification of novel cancer-associated mechanisms.

To support our IDH1 expression analyses, IDH1 levels were altered in mouse models of GBM. When IDH1 expression is altered in either patient derived GICs or in murine neural stem cells (NSCs), cell proliferation *in vitro* and *in vivo* as well as survival is distorted. GICs are a better model to use than transformed glioma cells as they grow in serum-free conditions and better maintain the genetic alterations that the patient had that they were derived from, whereas transformed cells grown on plastic quickly change their genetic background (Lee et al., 2006a).

NSCs were derived from *hGFAP-Cre⁺;p53^{lox/lox};Pten^{lox/+}* mice, in which 73% developed either Grade III or GBM with acute onset of neurological symptoms. These tumors resembled primary GBM with both astrocytic and oligodendroglial histopathology. In addition, these tumors had increased PI3K signaling, increased *VEGF* expression, and co-activation of multiple RTKs, including PDGFRA and EGFR, consistent with genomic features of primary GBM (Zheng et al., 2008). GICs with stable knockdown of IDH1 show reduced proliferation *in vitro* and *in vivo* by bioluminescence imaging of orthotopic xenograft mouse models. This leads to an increase in overall survival, as well as increased apoptosis and decreased proliferation in these tumors. In contrast, murine NSCs null for both *TP53* and *PTEN* were made to stably overexpress IDH1. These cells had increased proliferation and decreased overall survival in an orthotopic mouse model. These studies combined point to IDH1 as a crucial metabolic enzyme necessary for GBM growth and as a potential therapeutic target.

Recent studies suggest that dampened TCA cycle/OXPHOS activity and the associated increase in ROS and oxidative DNA damage promotes genomic instability of gliomas, in particular deletion or mutation of *TP53*, and reduces cell proliferation as a result of reduced ATP production. This loss of p53 function can trigger transformation of neural progenitor cells and initiate gliomagenesis (Bartesaghi et al., 2015) as well as jump-start glycolysis, providing ATP and cellular building blocks in the absence of normal mitochondrial OXPHOS (Berkers et al., 2013). While p53 inactivation and the reliance on glycolysis for ATP production may be sufficient to promote growth of less proliferative, lower grade tumors, highly aggressive cancers, such as GBM, depend on more efficient ways to produce ATP and macromolecules, in particular lipids, to support unabated growth (Marin-Valencia et al., 2012; Mashimo et al., 2014). Recent

studies have challenged the notion that GBM tumor metabolism is confined to aerobic glycolysis, i.e., Warburg effect. The difference between metabolism of GBM tumors grown as PDX *in vivo* and glioma cell lines grown on plastic *in vitro* likely reflect adaptation to long-term culture, and/or loss of microenvironmental factors that influence metabolism (DeBerardinis et al., 2008). As demonstrated by a recent study (Marin-Valencia et al., 2012), simultaneous to aerobic glycolysis, GBM tumors grown as PDX oxidize glucose via pyruvate dehydrogenase and the TCA cycle, and use glucose to supply anaplerosis and other biosynthetic activities. While effective to drive proliferation of cancer cells grown on plastic, these studies demonstrate that aerobic glycolysis appears to be insufficient to drive anaplerosis and support tumor cell growth *in vivo*. We therefore propose that GBM selectively induces IDH1 mRNA, protein and enzymatic activity, in order to support high-grade glioma cells with macromolecules for rapid expansion. This in turn creates a unique IDH1-dependent metabolic vulnerability of GBM that we have described and therapeutically exploited.

IDH1 upregulation and its associated increase in cytoplasmic NADPH promotes lipid biosynthesis, ROS scavenging and unabated tumor growth and survival. Several studies have implicated IDH1 in the control of lipid metabolism in non-cancerous tissues. Transgenic IDH1 expression in liver and adipose tissues promoted hyperlipidemia and obesity, paralleled by increased triglyceride and cholesterol content (Koh et al., 2004). Conversely, *in vivo* IDH1 ablation via expression of shIDH1-specific shRNA (Nam et al., 2012) or by transgenic expression of IDH1-targeting miR-181a (Chu et al., 2015) resulted in weight loss associated with reduced fat mass and circulating triglyceride levels.

NADPH is a critical and possibly rate-limiting factor required for cell proliferation, and a

reducing agent necessary for lipid biosynthesis (Lunt and Vander Heiden, 2011). Several studies point to IDH1 as a critical source of cytoplasmic NADPH. Studies by the DeBerardinis group suggested that glutamine when oxidatively metabolized to malate and then converted to pyruvate by malic enzyme can be a significant source of NADPH in human glioma cells cultivated *in vitro* (DeBerardinis et al., 2007). More than half of the glutamine taken up is excreted as lactate, which suggests that this pathway may be a significant source of NADPH production in glioma cells grown on plastic (DeBerardinis et al., 2007). Recent studies by the Bachoo group, however, revealed that in PDX models using patient-derived cells propagated solely through intracranial implantation, tumor-associated glutamine pools are high as a result of high glycolytic carbon flux and pyruvate carboxylase-dependent anaplerosis (Marin-Valencia et al., 2012; Mashimo et al., 2014). Glutamine, however, was inefficiently metabolized, and glucose represented the primary carbon source for oxidative metabolism in GBM PDX tumors. These findings were consistent with elevated pyruvate carboxylase activity in GBM tumors compared to normal brain, but lower expression levels of glutaminase (converting glutamine to glutamate in cells that use glutamine catabolism for anaplerosis). Thus, conversion of glutamine to malate to pyruvate via the pyruvate/malate cycle, or the conversion of glutamine to glutamate to α KG are unlikely to provide patient-derived glioma cells and derivative tumors with NADPH or acetyl-CoA. Furthermore, carbon flux studies in a variety of cancer cell lines using ^{13}C labeled glucose suggest that the pentose phosphate shunt cannot meet NADPH requirements for tumor cell growth (Boros et al., 1998; Boros et al., 2002). In addition, a recent study by the DePinho group suggested that mutant KRas-driven tumors, in particular pancreatic adenocarcinomas, utilize the non-oxidative instead of the oxidative, NADPH-producing pentose phosphate pathway, and thus

decouple anaplerosis from NADPH production and NADPH-mediated redox control (Ying et al., 2012). Lastly, IDH1 has a higher maximal enzymatic activity compared to other NADPH-producing enzymes in patient-derived GBM tissue (Bleeker et al., 2010), and is the most differentially expressed NADPH producing enzyme in GBM compared to normal brain tissue (Wahl et al., 2016). These studies, together with our observation that acetyl-CoA is increased in GICs after IDH1 knockdown, suggest that IDH1-generated cytoplasmic NADPH is critical and likely rate-limiting for maintaining lipid and ROS homeostasis to promote tumor cell growth and survival.

IDH1-driven metabolic reprogramming might be particularly important for maintaining the glioma stem cell compartment. α KG is necessary to maintain α KG-dependent dioxygenases involved in embryonic stem cell pluripotency as well as involved in promoting the self-renewal capacity of embryonic stem cells in vitro (Carey et al., 2015). While epigenetic changes are known to be increased and play a role in the pathogenesis of mutant IDH1 tumors, altered histone methylation is a common feature of both wild-type and mutant gliomas (Losman and Kaelin, 2013). Cortical astrocytes overexpressing wild-type IDH1 had an altered methylome compared to parental cells, although these changes were different from those in mutant-IDH1 overexpressing astrocytes (Turcan et al., 2012). GIC cultures modified for reduced IDH1 expression showed diminished stem cell frequency and increased differentiation capacity. Robust neuronal and astrocytic differentiation marker expression in shIDH1-expressing GICs exposed to a poly-D-lysine/laminin matrix may suggest that compromised IDH1 activity may selectively drive differentiation into astrocytic and/or neuronal lineages. In addition, IDH1 expression was enhanced in CD133⁺, glioma stem cell-enriched cultures in comparison to CD133⁻ non-stem

cells. CHIP-Seq and mRNA expression analysis of control versus IDH1 knockdown GICs identified a tumor suppressor gene signature modulated by IDH1 through its impact on histone methylation. Specifically, IDH1 knockdown increased the binding of trimethylated histone H3K4 to the promoter regions of *NDUFS1*, *GNG4* and *TNFAIP1*, leading to increased transcription of these tumor suppressors. In addition, each of these genes showed diminished mRNA in TCGA GBM tumors. *NDUFS1* is the largest subunit of mitochondria complex I and is responsible for oxidizing NADH, reducing ubiquinone, and moving protons across the mitochondrial inner membrane (Hirst et al., 2013). It is also a major contributor to mitochondrial ROS, and mutations within *NDUFS1* lead to a 70% reduction of complex I activity (Hoefs et al., 2010). Two recent studies showed that low expression of *NDUFS1* is an independent predictor of shorter overall survival in clear-cell renal cell carcinoma (RCC) and NSCLC (Su et al., 2016; Ellinger et al., 2016). *GNG4* is a member of the gamma subunit of the G protein family, regulates the interaction between the muscarinic receptor and voltage-sensitive calcium channels (Kalyanaraman et al., 1998), and is a putative tumor suppressor in RCC and GBM. In RCC, *GNG4* is a target gene of the von Hippel-Lindau (VHL) gene and is implicated in the tumor suppressive function of VHL (Maina et al., 2005). In GBM, *GNG4* is one of the most hypermethylated and down regulated genes and has tumor suppressive functions through regulation of the CXCR4/SDF1a signaling axis (Pal et al., 2016). *TNFAIP1* is induced by TNF α and IL6 and has roles in DNA synthesis, DNA repair, and apoptosis (Wolf et al., 1992). *TNFAIP1* has tumor suppressive functions in several cancer types, including gastric cancer, NSCLC, pancreatic cancer, and uterine cancer, by supporting tumor growth through NF κ B signaling (Cui et al., 2015; Tan et al., 2016; Zhang et al., 2013; Zhang et al., 2015; Zhou et al.,

2013). We propose that reduced NADPH levels upon genetic and pharmacological inhibition of IDH1 cooperates with increased NDUFS1, GNG4 and TNFAIP1 levels to inhibit proliferation and promote ROS-induced apoptosis. Furthermore, increased H3K4me3 binding was evident in additional tumor suppressor genes, *ETV6* and *TUSC2*, but neither showed increased transcript levels with IDH1 knockdown. This excludes the possibility that increased binding of H3K4me3 is only indicative of active gene transcription, suggesting that IDH1 inhibition and associated decrease in α KG production leads to an increase of histone methylation independent of transcription at various gene loci.

Clinical trials testing Erlotinib as a monotherapy against EGFR-amplified GBMs elicited only transient responses, with rapid tumor adaptation (Furnari et al., 2015). Our targeted expression and global transcriptomic studies point to RTKi-mediated and FoxO6-dependent induction of IDH1 as a common adaptive response to RTKi treatment. Such metabolic adaptation allows glioma cells to sustain lipid biosynthesis and to limit ROS toxicity in the absence of growth factor signaling. Furthermore, the connection between RTK signaling and lipid metabolism has been extensively studied, linking RTKs, including ERBB4, EGFR, and FGFR3, to enhanced fatty acid and cholesterol biosynthesis (Haskins et al., 2015; Bian et al., 2015; Irwin et al., 2011; Du et al., 2012). In particular, as concerns EGFR signaling, the EGFR/PI3K/Akt axis promotes GBM tumor growth through AMPK-mediated activation of fatty acid and cholesterol biosynthesis (Guo et al., 2009b). Furthermore, inhibition of SREBP1/ACC/FASN sensitizes glioma cells to EGFR inhibition (Guo et al., 2009a). Finally, EGFR/PI3K/SREBP1 signaling upregulates LDLR to promote cholesterol metabolism and the LXR agonist, GW3965 decreases GBM cell proliferation *in vitro* and *in vivo* (Guo et al., 2011). Because of this well-established

signaling mechanism, we determined whether pharmacological and genetic inactivation of IDH1, similar to *e.g.*, to the inhibition of fatty acid biosynthesis through FASN inhibitors, enhances glioma cell sensitivity to EGFR inhibitors. Similar to targeted therapies of SREBP1/ACC/FASN, which lead to increased apoptosis in cells addicted to EGFR signaling (Guo et al., 2009a), we found that inhibition of IDH1 increased Erlotinib-induced apoptosis only in cells with amplified EGFR. This increase in apoptosis could be rescued by both cell-permeable α KG or addition of both fatty acid and cholesterol precursors. Both mevalonate and palmitate, precursors for cholesterol and fatty acid synthesis respectively, had to be added together to diminish the IDH1 and EGFR targeted therapies concomitant increase in apoptosis, pointing to lipid and cholesterol synthesis both as important downstream mediators of the IDH1 protective effect.

While fatty acid biosynthesis plays a significant role in the IDH1-mediated protective effect of GBM, we also wanted to determine if NADPH from IDH1 was necessary for maintaining redox homeostasis. Knockdown of IDH1 led to decreased NADPH levels and associated decrease in GSH levels and increase in ROS levels in response to Erlotinib. This led to increased apoptosis and two different antioxidants, EUK-134 and NAC, both rescued this phenotype. Furthermore, addition of cell-permeable α KG increased NADPH/NADP⁺ levels demonstrating α KG from IDH1 reaction can further increase NADPH levels in GBM tumor cells. NADPH is the key product of this reaction as addition of malic enzyme 1 (ME1), a cytosolic enzyme that also produces NADPH, can also rescue the Erlotinib-induced apoptosis in shIDH1 expressing cells. Furthermore, these results hold true in a transformed glioma cell line with multiple-RTKs hyperactivated. As fatty acid synthesis is downstream of RTK-PI3K signaling, IDH1 inactivation and concurrent reduction in NADPH, α KG, and lipid biosynthesis sensitizes glioma cells

irrespective of their RTK activation profile and PTEN status, suggesting that IDH1 targeted therapies may represent a universal modality against GBM.

In addition to IDH1 overexpression in GBM, we also found that *IDH1* mRNA expression is increased in lung adeno- and squamous cell carcinomas compared to normal lung tissue as well as in angioimmunoblastic (AITL), anaplastic large cell (ALCL), peripheral T-cell (PTCL), and diffuse large B cell (DLBCL) lymphomas. Lung adeno- and squamous cell carcinomas are NSCLCs and mutations in IDH1/2 have not been reported in these cancers. However, increased wild-type IDH1 has been reported in NSCLC tumors and in the blood plasma of these patients, which is negatively correlated with patient survival (Tan et al., 2011; Sun et al., 2013). IDH2 mutations have been reported in 20-45% of AITL, but IDH1/2 mutations have not been found in ALCL, PTCL, and DLBCL (Cairns et al., 2012). While these cancer types are not associated with IDH mutations, but have overexpression of IDH1, this points to IDH1 overexpression as a possible therapeutic target independent of IDH1 mutation status. Furthermore, we show that knockdown of IDH1 increases Ibrutinib-induced apoptosis, decreasing α KG, and GSH levels, and increases intracellular ROS. IDH1 KD also leads to smaller tumors in a DLBCL subcutaneous xenograft model. Ibrutinib is a Bruton's tyrosine kinase (BTK) inhibitor which binds to the ATP-binding site within the tyrosine kinase domain of BTK. Ibrutinib is currently approved for mantle cell lymphoma (MCL) and chronic lymphocytic leukemia (CLL) patients who have undergone previous treatment, CLL patients with 17p deletion, and Waldenstrom's macroglobulinemia (WM) patients. It is in ongoing clinical trials that show promise for other forms of non-Hodgkin's lymphoma (NHL), including DLBCL, and follicular lymphoma (FL) (Wang et al., 2015). Many B-cell malignancies depend on B-cell receptor (BCR) signaling and

have increased activation of this pathway, pointing to members of this pathway as being potential therapeutic targets. BTK is downstream of BCR signaling and activates NF κ B transcription factor to inhibit apoptosis and promote proliferation. While Ibrutinib has shown efficacy and is approved for certain types of NHL, it is currently being used in combination with other therapeutics to further increase the efficacy (Wang et al., 2015). We show that inhibition of IDH1 in combination with Ibrutinib increases the efficacy of Ibrutinib in a DLBCL preclinical model. Therefore, co-extinction strategies targeting both IDH1 in combination with already approved tyrosine kinase inhibitors, such as BTK inhibitors, may enhance their efficacy.

Moreover, IDH1 may represent a resistance mechanism to RTK-targeted therapies. We found that IDH1 levels are increased in response to RTKi-treatment, but not to other standard therapies, including TMZ. Recent studies have implicated FoxOs as transcription factors that promote IDH1 expression and lead to increases in cytosolic α KG and NADPH levels (Charitou et al., 2015). FoxOs are also known to be activated by RTKis, including FoxO6 specifically being activated by Erlotinib (Lam et al., 2013; Rothenberg et al., 2015). To determine if IDH1 upregulation in response to RTKis is dependent of FoxOs, we performed a ChIP experiment using antibodies against three different FoxO transcription factors, FoxO1, FoxO3, and FoxO6. While all three had increased binding to a forkhead response element consensus sequence in response to RTKi treatment, FoxO6 had a more significant response. FoxO6 is the least well defined of the FoxO transcription factors, which may be due to the fact that it was once considered only present in the brain, but it is now known to have a much wider distribution throughout various tissues (Lee and Dong, 2017). FoxO6 has the least amount of homology with the other FoxOs, at only around 30% and does not include a nuclear export signal as the others

do. FoxO6 remains in the nucleus and its function is not inhibited by exportation to the cytoplasm, but rather through direct phosphorylation at Thr26 and Ser184 by Akt/PKB, disrupting FoxO6 from binding to DNA (Lee and Dong, 2017). FoxO6 has several key functions, including glucose and lipid metabolism, as well as regulation of oxidative stress (Lee and Dong, 2017). In particular, a global FoxO6 knockout mouse develops normally, however these mice have decreased hepatic gluconeogenesis and decreased fasting glycemia. When these mice are fed a high fat diet, they have decreased oil red O staining, consistent with decreased hepatic fat deposition (Calabuig-Navarro et al., 2015). Similar to IDH1 transgenic mice, liver-specific FoxO6 transgenic mice had increased plasma triglyceride levels, nonesterified fatty acid levels, triglyceride very low density lipoprotein levels, and impaired fat tolerance. While there was no difference in body weight between FoxO6 transgenic mice and wild-type controls, transgenic mice had increased fat content in the liver as well as increased expression in lipogenesis genes, SREBP1, FASN, and ACC (Kim et al., 2014). Furthermore, hepatocellular carcinoma patients had increased FoxO6 expression, which correlated with decreased survival, and increase in oxidative stress markers (Chen et al., 2016). These studies point to FoxO6 playing a significant role in lipid biosynthesis as well as redox homeostasis. As we have demonstrated that IDH1 is important in these functions, the role FoxO6 plays may be in part be due through its upregulation of IDH1.

To further implicate increased IDH1 expression as a resistance mechanism to targeted therapies, we performed a genome-wide microarray assay comparing GBM cells treated with or without RTKis. Ingenuity pathway analysis pointed to the superpathway of cholesterol biosynthesis as the most upregulated pathway in cells treated with RTKi compared to vehicle-treated cells. Not

only did this pathway include *IDH1* as being upregulated, but also *IDH1* and *LSS*. *IDH1* catalyzes the conversion of isopentenyl diphosphate (IPP) to dimethylallyl diphosphate (DMAPP) ultimately leading to cholesterol synthesis. *IDH1* is negatively regulated by STAT6 through a miR-197/FOXJ2 pathway in lung cancer cells (Dubey et al., 2011; Dubey and Saini, 2015). *LSS* catalyzes the conversion of oxidosqualene to lanosterol in the first step of cholesterol, steroid hormones, and vitamin D synthesis. Inhibition of *LSS* has been used as an anti-cancer therapeutic in pre-clinical studies of GBM, pancreatic, and colon cancers (Staedler et al., 2012; Maione et al., 2015). To support the implication of *LSS* and *IDH1* in cancer progression, we showed that knockdown of either *IDH1* or *LSS* enhanced RTKi-induced apoptosis, further implicating lipid and cholesterol biosynthesis as key resistance mechanisms toward RTKis.

In addition to showing the effects of genetic manipulation of *IDH1* on GBM progression, we also wanted to confirm that pharmacological *IDH1* inhibition has similar effects. We used GSK864, originally an inhibitor of mutant *IDH1*, but also with inhibitory effects on wild-type *IDH1*. The selectivity of GSK864 and first generation GSK321 for *IDH1* was determined by chemoproteomics experiments, using a closely related and inactive derivative (GSK990) as a negative control. While GSK321 was first characterized with IC_{50} values of 4.6, 46, and 496 nM for R132H *IDH1* mutant, wild-type *IDH1*, and wild-type *IDH2*, respectively, its derivative, GSK864 was found to have enhanced pharmacokinetic properties (Okoye-Okafor et al., 2015). GSK864 has potent effect against mutant *IDH1*, and to a lesser degree against wild-type *IDH1* with IC_{50} values of 15.2, 466.5, and 1,360 nM for R132H mutant *IDH1*, wild-type *IDH1*, and wild-type *IDH2*, respectively (Okoye-Okafor et al., 2015). Besides detailed evaluation of these GSK drugs reported in Okoye-Okafor et al., it is important to stress that GSK321 has been

validated as an inhibitor of wild-type IDH1. In a model of anchorage-independent growth of lung cancer cells, carbon from glutamine was reductively carboxylated through IDH1 to maintain redox homeostasis within these cells (Jiang et al., 2016). In addition, inhibition of IDH1 with GSK321, similar to IDH1 genetic ablation, resulted in blunted reductive glutamine metabolism, and in so doing, enhances mitochondrial ROS and reduces tumor spheroid growth (Jiang et al., 2016). This study points to this class of GSK inhibitors as important pharmacological tools not only for mutant IDH1, but also wild-type IDH1. We have shown that GSK864 is also specific for wild-type IDH1, as it reduces NADPH levels in GICs, but not in IDH1 low-expressing cortical human astrocytes, or in GICs modified for IDH1 knockdown. In addition, GSK864 also enhances the RTKi-induced decreased proliferation, and enhanced apoptosis, as well as decreases stem-cell frequency, similar to genetic knockdown of IDH1. Furthermore, we demonstrate that the pro-apoptotic effect of GSK864, similar to the pro-death activity of RNAi-mediated knockdown of IDH1, can be abrogated by reconstituting cells with cell permeable α KG, suggesting that GSK864 is targeting wild-type IDH1. In addition, it is conceivable that different thresholds for IDH1 inactivation exists to trigger apoptosis, promote differentiation, and inhibit growth, as RTKi treatment leads to upregulation of IDH1 levels, suggesting that higher IDH1 expression may require higher drug concentrations to observe biological effects. However, in our PDX mouse model studies, we used a standard concentration (150 mg/kg) of GSK864, the same used to suppress AML xenograft progression (Okoye-Okafor et al., 2015), to show that pharmacologic inhibition also decreases tumor size and prolongs survival, pointing to IDH1 as a therapeutically targetable enzyme.

Oncogenic mutations in IDH1 and IDH2 have been identified in acute myelogenous leukemia, low-grade gliomas, and secondary GBM, but are rare in primary GBM specimens (Losman and Kaelin, 2013; Horbinski, 2013). Remarkably, patients with wild-type GBM tumors have a mean survival of 15 months compared to 31 months for patients with mutant IDH1 GBM tumors and ectopic expression studies point to tumor suppressive effects of mutant IDH1. Expression of Arg132 point-mutated IDH1 in established IDH1-wild-type glioma cell lines reduced proliferation *in vitro* and extended the survival of mice bearing derived orthotopic xenografts (Bralten et al., 2011). Similarly, RCAS-driven expression of mutant IDH1 in NSCs derived from *p53*-deficient Nestin-*tv-a* mice reduces progenitor cell growth *in vitro* and glioma formation *in vivo* despite elevated D-2HG production in IDH1 mutant compared to wild-type cells. This growth-inhibitory effect of mutant IDH1 is associated with diversion of α KG from wild-type IDH1 and reduced carbon flux from glucose or glutamine into lipids (Chen et al., 2014). Murine NSCs lack glutamate dehydrogenase 2 (GLUD2) and expression of GLUD2 or administration of glutamate, a neocortical neurotransmitter and substrate for GLUD2, compensates for growth and flux deficiencies elicited by mutant IDH1 by replenishing α KG via increased glutaminolysis. These observations suggest that *IDH1* mutant tumors require a specialized metabolic niche characterized by elevated glutamate flux for growth and expansion. Recent studies suggest that *IDH1* mutant gliomas arise from a neural precursor population that is spatially and temporally restricted in the brain, possibly coinciding with remodeling of the prefrontal cortex (Lai et al., 2011). Primary GBM, on the other hand, inefficiently metabolize glutamine and most likely are unable to sustain high glutamine flux to support α KG and lipid biogenesis. To support anaplerosis, in particular lipid biogenesis flux via enhanced α KG and NADPH, we propose that

the upregulation of non-mutated IDH1 is important for primary GBM progression. Our data suggest a novel treatment paradigm for wild-type IDH1 (representing 90% of all high-grade gliomas), not IDH1 mutant GBM tumors.

Cancer up-regulates a variety of metabolic genes that conspire to reprogram tumor cell metabolism and support unabated growth and therapy resistance. Consequently, drug development efforts focus on inhibiting a plethora of metabolic enzymes with overexpression in various cancers, many of which are being tested in combination with targeted and conventional chemo- and radiation therapies (Cantor and Sabatini, 2012; Granchi, et al., 2014; Tarrado-Castellarnau, et al., 2016; Vander Heiden et al., 2011; Zhao et al., 2013). In light of the low expression of IDH1 in normal brain, robust upregulation of IDH1 in GBM tumors, and the absence of developmental and fertility-related abnormalities in global *IDH1* knockout mice (Itsumi et al., 2015), our data suggest that small molecule inhibitors of IDH1, such as GSK864, warrant further preclinical testing, especially when used in combination with inhibitors of RTK-PI3K signaling.

4.2 Summary and Future Directions

As we have shown here, IDH1 is a critical enzyme overexpressed in primary GBM, and other solid and systemic malignancies. This increase in IDH1, enhances NADPH and α KG production necessary for lipid biosynthesis, maintaining redox balance, and maintaining a dedifferentiated state. Additionally, IDH1 levels can be further increased by treatment with RTKis, pointing to an adaptive response of GBM tumor cells, that can be exploited to further promote the apoptotic

effects of RTKis. Both genetic and pharmacologic studies point to IDH1 as an actionable therapeutic target that should be exploited in GBM.

While this work points to IDH1 as an actionable therapeutic target, there are additional studies that would build on our work. First and foremost, the identification of the mechanism underlying *IDH1* mRNA upregulation in GBM tumors would be interesting and important, as it would further our understanding of IDH1 biology as well as support our finding that upregulation of IDH1 is specific. As pointed out in the introduction, other metabolic enzymes, including *TKTL1*, *ACC*, *FASN*, and *HK2*, have also been shown to be upregulated in GBM and may be therapeutic targets. While the mechanism of how these genes are upregulated has not been fully elucidated, it will be important to determine if IDH1 and these other enzymes share common regulatory mechanisms.

While our studies represent an initial proof-of-concept that cancer-associated IDH1 through α KG production can regulate gene expression in glioma-initiating cells, these studies can and should be further expanded. It is important to identify the specific demethylases that are impacted by IDH1-driven α KG production, to confirm that the changes in methylation status are not due to indirect effect on the transcriptional activation. Furthermore, the implication of *GNG4*, *NDUFS1*, and *TNFAIP1* as tumor suppressive genes that play a role in IDH1 tumor-promoting activities, needs in depth characterization as these genes contribute to IDH1 dedifferentiation and oncogenic effects.

While we provide a detailed overview of IDH1 biology in GBM, we also show that IDH1 plays a role in other solid and systemic malignancies, pointing to IDH1 as a potential therapeutic target

in multiple cancer types. Further analysis of IDH1 within lymphomas as well as in lung cancers should be determined as these tumors have increased *IDH1* mRNA expression compared to normal tissue.

As we have shown that IDH1 is an actionable therapeutic target, it is important to find more potent and specific wild-type IDH1 inhibitors. In on-going studies, we are working with Milan Mrksich and SAMDI Tech to discover and characterize novel wild-type IDH1 inhibitors. Novel inhibitors specific for wild-type IDH1 will be important tools to further elucidate the mechanisms behind IDH1 upregulation in GBM, as well as be important to confirm our studies done with the mutant IDH1 inhibitor GSK864, to show more specifically that it is wild-type IDH1 inhibition leading to decreased NADPH and α KG, necessary for stem cell maintenance, *de novo* lipogenesis, and redox homeostasis, and not off-target effects of the high concentrations of GSK864 that we had to use.

In addition to discovering novel small molecule inhibitors of IDH1, work has been ongoing in collaboration with Dr. Chad Mirkin's group to functionalize IDH1 siRNA to spherical nucleic acids (SNAs). SNA technology was discovered by Dr. Mirkin and have many advantages over traditional therapeutics. In GBM mouse models, our groups have been able to show that SNAs cross the BBB when given systemically, accumulate within and disseminate throughout an orthotopic glioma explant, and robustly downregulate gene expression within intracerebral tumors (Jensen et al., 2013). In on-going work, siRNA targeted to IDH1 have been made and initial *in vitro* studies have shown positive results. These IDH1-SNAs need to be further characterized and studied *in vivo*.

Our work is the first to show the potential of wild-type IDH1 as a therapeutic actionable target to treat primary GBM tumors, which have had very little therapeutic advances over the years.

REFERENCES

Amary, M.F., Bacsi, K., Maggiani, F., Damato, S., Halai, D., Berisha, F., Pollock, R., O'Donnell, P., Grigoriadis, A., Diss, T., Eskandarpour, M., Presneau, N., Hogendoorn, P.C., Futreal, A., Tirabosco, R., Flanagan, A.M. (2011). IDH1 and IDH2 mutations are frequent events in central chondrosarcoma and central periosteal chondromas but not in other mesenchymal tumours. *J. Pathol.* *224*, 334-343.

Barkovich, K.J., Hariono, S., Garske, A.L., Zhang, J., Blair, J.A., Fan, Q.W., Shokat, K.M., Nicolaides, T., Weiss, W.A. (2012). Kinetics of inhibitor cycling underlie therapeutic disparities between EGFR-driven lung and brain cancers. *Cancer Discov.* *2*, 450-457.

Bartesaghi, S., Graziano, V., Galavotti, S., Henriquez, N.V., Betts, J., Saxena, J., Minieri, V.A.D., Karlsson, A., Martins, L.M., Capasso, M., Nicotera, P., Brandner, S., De Laurenzi, V., Salomoni, P. (2015). Inhibition of oxidative metabolism leads to p53 genetic inactivation and transformation in neural stem cells. *Proc. Natl. Acad. Sci. U. S. A.* *112*, 1059-1064.

Berkers, C.R., Maddocks, O.D., Cheung, E.C., Mor, I., Vousden, K.H. (2013). Metabolic regulation by p53 family members. *Cell Metab.* *18*, 617-633.

Bian, Y., Yu, Y., Wang, S., Li, L. (2015). Up-regulation of fatty acid synthase induced by EGFR/ERK activation promotes tumor growth in pancreatic cancer. *Biochem. Biophys. Res. Commun.* *463*, 612-617.

Bleeker, F.E., Atai, N.A., Lamba, S., Jonker, A., Rijikeboer, D., Bosch, K.S., Tigchelaar, W., Troost, D., Vandertop, W.P., Bardelli, A., Van Noorden, C.J. (2010). The prognostic IDH1(R132H) mutation is associated with reduced NADP⁺-dependent IDH activity in glioblastoma. *Acta Neuropathol.* *119*, 487-494.

Borger, D.R., Tanabe, K.K., Fan, K.C., Lopez, H.U., Fantin, V.R., Straley, K.S., Schenkein, D.P., Hezel, A.F., Ancukiewicz, M., Liebman, H.M., Kwak, E.L., Clark, J.W., Ryan, D.P., Deshpande, V., Dias-Santagata, D., Ellisen, L.W., Zhu, A.X., Iafrate, A.J. (2012). Frequent mutation of isocitrate dehydrogenase (IDH) 1 and IDH2 in cholangiocarcinoma identified through broad-based tumor genotyping. *Oncologist* 17, 72-79.

Boros, L.G., Lee, P.W., Brandes, J.L., Cascante, M., Muscarella, P., Schirmer, W.J., Melvin, W.S., Ellison, E.C. (1998). Nonoxidative pentose phosphate pathways and their direct role in ribose synthesis in tumors: is cancer a disease of cellular glucose metabolism? *Med. Hypotheses* 50, 55-59.

Boros, L.G., Torday, J.S., Paul Lee, W.N., Rehan, V.K. (2002). Oxygen-induced metabolic changes and transdifferentiation in immature fetal rat lung lipofibroblasts. *Mol. Genet. Metab.* 77, 230-236.

Bralten, L.B., Kloosterhof, N.K., Balvers, R., Sacchetti, A., Lapre, L., Lamfers, M., Leenstra, S., de Jonge, H., Kros, J.M., Jansen, E.E., Struys, E.A., Jakobs, C., Salomons, G.S., Diks, S.H., Peppelenbosch, M., Kremer, A., Hoogenraad, C.C., Smitt, P.A., French, P.J. (2011). IDH1 R132H decreases proliferation of glioma cell lines in vitro and in vivo. *Ann. Neurol.* 69, 455-463.

Brennan, C.W., Verhaak, R.G., McKenna, A., Campos, B., Noushmehr, H., Salama, S.R., Zheng, S., Chakravarty, D., Sanborn, J.Z., Berman, S.H., Beroukhi, R., Bernard, B., Wu, C.J., Genovese, G., Shmulevich, I., Barnholtz-Sloan, J., Zou, L., Vegesna, R., Shukla, S.A., Ciriello, G., Yung, W.K., Zhang, W., Sougnez, C., Mikkelsen, T., Aldape, K., Bigner, D.D., Van Meir,

E.G., Prados, M., Sloan, A., Black, K.L., Eschbacher, J., Finocchiaro, G., Friedman, W., Andrews, D.W., Guha, A., Iacocca, M., O'Neill, B.P., Foltz, G., Myers, J., Weisenberger, D.J., Penny, R., Kucherlapati, R., Perou, C.M., Hayes, D.N., Gibbs, R., Marra, M., Mills, G.B., Lander, E., Spellman, P., Wilson, R., Sander, C., Weinstein, J., Meyerson, M., Gabriel, S., Laird, P.W., Haussler, D., Getz, G., Chin, L; TCGA Research Network. (2013). The somatic genomic landscape of glioblastoma. *Cell* *155*, 462-477.

Cairns, R.A., Harris, I.S., Mak, T.W. (2011). Regulation of cancer cell metabolism. *Nat. Rev. Cancer* *11*, 85-95.

Cairns, R.A., Iqbal, J., Lemonnier, F., Kucuk, C., de Leval, L., Jais, J., Parrens, M., Martin, A., Xerri, L., Brousset, P., Chan, L.C., Chan, W., Gaulard, P., Mak, T.W. (2012). IDH2 mutations are frequent in angioimmunoblastic T-cell lymphoma. *Blood* *119*, 1901-1903.

Calabuig-Navarro, V., Yamauchi, J., Lee, S., Zhang, T., Liu, Y.Z., Sadelek, K., Coudriet, G.M., Piganelli, J.D., Jiang, C.L., Miller, R., Lowe, M., Harashima, H., Dong, H.H. (2015). Forkhead Box O6 (FoxO6) depletion attenuates hepatic gluconeogenesis and protects against fat-induced glucose disorder in mice. *J. Biol. Chem.* *290*, 15581-15594.

Cancer Genome Atlas Research Network. (2008). Comprehensive genomic characterization defines human glioblastoma genes and core pathways. *Nature* *455*, 1061-1068.

Cancer Genome Atlas Research Network, Brat, D.J., Verhaak, R.G., Aldape, K.D., Yung, W.K., Salama, S.R. Cooper, L.A., Rheinbay, E., Miller, C.R., Vitucci, M., Morozova, O., Roberson, A.G., Noushmehr, H., Laird, P.W., Cherniack, A.D., Akbani, R., Huse, J.T., Ciriello, G., Poisson, L.M., Barnholtz-Sloan, J.S., Berger, M.S., Brennan, C., Colen, R.R., Colman, H.,

Flander, A.E., Giannini, C., Grifford, M., Iavarone, A., Jain, R., Joseph, I., Kim, J., Kasaian, K., Mikkelsen, T., Murray, B.A., O'Neill, B.P., Pachter, L., Parsons, D.W., Sougnez, C., Sulman, E.P., Vandenberg, S.R., Van Meir, E.G., von Deimling, A., Zhang, H., Crain, D., Lau, K., Mallery, D., Morris, S., Paulauskis, J., Penny, R., Shelton, T., Sherman, M., Yena, P., Black, A., Bowen, J., Dicostanzo, K., Gastier-Foster, J., Leraas, K.M., Lichtenberg, T.M., Pierson, C.R., Ramirez, N.C., Taylor, C., Weaver, S., Wise, L., Zmuda, E., Davidsen, T., Demchok, J.A., Eley, G., Ferguson, M.L., Hutter, C.M., Mills Shaw, K.R., Ozenberger, B.A., Sheth, M., Sofia, H.J., Tarnuzzer, R., Wang, Z., Yang, L., Zenklusen, J.C., Ayala, B., Baboud, J., Chudamani, S., Jensen, M.A., Liu, J., Pihl, T., Raman, R., Wan, Y., Wu, Y., Ally, A., Auman, J.T., Balasundaram, M., Balu, S., Baylin, S.B., Beroukhim, R., Bootwalla, M.S., Bowlby, R., Bristow, C.A., Brooks, D., Butterfield, Y., Carlsen, R., Carter, S., Chin, L., Chu, A., Chuah, E., Cibulskis, K., Clarke, A., Coetzee, S.G., Dhalla, N., Fennell, T., Fisher, S., Gabriel, S., Getz, G., Gibbs, R., Guin, R., Hadjipanayis, A., Hayes, D.N., Hinoue, T., Hoadley, K., Holt, R.A., Hoyle, A.P., Jefferys, S.R., Jones, S., Jones, C.D., Kucherlapati, R., Lai, P.H., Lander, E., Lee, S., Lichtenstein, L., Ma, Y., Maglinte, D.T., Mahadeshwar, H.S., Marra, M.A., Mayo, M., Meng, S., Meyerson, M.L., Mieczkowski, P.A., Moore, R.A., Mose, L.E., Mungall, A.J., Pantazi, A., Parfenov, M., Park, P.J., Parker, J.S., Perou, C.M., Protopopov, A., Ren, X., Roach, J., Sabedot, T.S., Schein, J., Schumacher, S.E., Seidman, J.G., Seth, S., Shen, H., Simons, J.V., Sipahimalani, P., Soloway, M.G., Song, X., Sun, H., Tabak, B., Tam, A., Tan, D., Tang, J., Thiessen, N., Triche, T.Jr., Van Den Berg, D.J., Veluvolu, U., Waring, S., Weisenberger, D.J., Wilkerson, M.D., Wong, T., Wu, J., Xi, L., Xu, A.W., Yang, L., Zack, T.I., Zhang, J., Aksoy, B.A., Arachchi, H., Benz, C., Bernard, B., Carlin, D., Cho, J., DiCara, D., Frazer, S., Fuller, G.N., Gao,

J., Gehlenborg, N., Haussler, D., Heiman, D.I., Iype, L., Jacobonsen, A., Ju, Z., Katzman, S., Kim, H., Knijnenburg, T., Kreisberg, R.B., Lawrence, M.S., Lee, W., Leinonen, K., Lin, P., Ling, S., Liu, W., Liu, Y., Liu, Y., Lu, Y., Mills, G., Ng, S., Noble, M.S., Paull, E., Rao, A., Reynolds, S., Saksena, G., Sanborn, Z., Sander, C., Schultz, N., Senbabaoglu, Y., Shen, R., Shmulevich, I., Sinha, R., Stuart, J., Sumer, S.O., Sun, Y., Tasmanm, N., Taylor, B.S., Voet, D., Weinhold, N., Weistein, J.N., Yang, D., Yoshihara, K., Zheng, S., Zhang, W., Zou, L., Abel, T., Sadeghi, S., Cohen, M.L., Eschbacher, J., Hattab, E.M., Raghunathan, A., Schniederjan, M.J., Aziz, D., Barnett, G., Barrett, W., Bigner, D.D., Boice, L., Brewer, C., Calatozzolo, C., Campos, B., Carlotti, C.G. Jr., Chan, T.A., Cuppini, L., Curley, E., Cuzzubbo, S., Devine, K., DiMeco, F., Duell, R., Elder, J.B., Fehrenbach, A., Finocchiaro, G., Friedman, W., Fulop, J., Gardner, J., Hermes, B., Herold-Mende, C., Jungk, C., Kendler, A., Lehman, N.L., Lipp, E., Liu, O., Mandt, R., McGraw, M., Mclendon, R., McPherson, C., Neder, L., Nguyen, P., Noss, A., Nunziata, R., Ostrom, Q.T., Palmer, C., Perin, A., Pollo, B., Potapov, A., Potapova, O., Rathmell, W.K., Rotin, D., Scarpace, L., Schilero, C., Senecal, K., Shimmerl, K., Shurkhay, V., Sifri, S., Singh, R., Sloan, A.E., Smolenski, K., Staugaitis, S.M., Steele, R., Thorne, L., Tirapelli, D.P., Unterberg, A., Vallurupalli, M., Wang, Y., Warnick, R., Williams, F., Wolinsky, Y., Bell, S., Rosenberg, M., Stewart, C., Huang, F., Grimsby, J.L., Radenbaugh, A.J., Zhang, J. (2015). Comprehensive, integrative genomic analysis of diffuse lower-grade gliomas. *N. Engl. J. Med.* 372, 2481-2498.

Cantor, J.R., and Sabatini, D.M. (2012). Cancer cell metabolism: one hallmark, many faces. *Cancer Discov.* 2, 881-898.

Carey, B.W., Finley, L.W., Cross, J.R., Allis, C.D., Thompson, C.B. (2015). Intracellular α -

ketoglutarate maintains the pluripotency of embryonic stem cells. *Nature* 518, 413-416.

Chakrabarti, G., Gerber, D.E., Boothman, D.A. (2015). Expanding antitumor therapeutic windows by targeting cancer-specific nicotinamide adenine dinucleotide phosphate-biogenesis pathways. *Clin. Pharmacol.* 7, 57-68.

Charitou, P., Rodriguez-Colman, M., Gerrits, J., van Triest, M., Groot Koerkamp, M., Hornsveld, M., Holstege, F., Verhoeven-Duif, N.M., and Burgering, B.M. (2015). FOXOs support the metabolic requirements of normal and tumor cells by promoting IDH1 expression. *EMBO Rep.* 16, 456-466.

Chen, F.X., Woodfin, A.R., Gardini, A., Rickels, R.A., Marshall, S.A., Smith, E.R., Shiekhattar, R., and Shilatifard, A. (2015a). PAF1, a molecular regulator of promoter-proximal pausing by RNA Polymerase II. *Cell* 162, 1003-1015.

Chen, F., Gao, X., and Shilatifard, A. (2015b). Stably paused genes revealed through inhibition of transcription initiation by the TFIIH inhibitor triptolide. *Genes Dev.* 29, 39-47.

Chen, H.Y., Chen, Y.M., Wu, J., Yang, F.C., Lv, Z., Xu, X.F., Zheng, S.S. (2016). Expression of FOXO6 is associated with oxidative stress level and predicts the prognosis in hepatocellular cancer: a comparative study. *Medicine (Baltimore)* 95, e3708.

Chen, R., Nishimura, M.C., Kharbanda, S., Peale, F., Deng, Y., Daemen, A., Forrest, W.F., Kwong, M., Hedehus, M., Hatzivassiliou, G., Friedman, L.S., Phillips, H.S. (2014). Hominoid-specific enzyme GLUD2 promotes growth of IDH1R132H glioma. *Proc. Natl. Acad. Sci. U. S. A.* 111, 14217-14222.

- Chu, B., Wu, T., Miao, L., Mei, Y., and Wu, M. (2015). MiR-181a regulates lipid metabolism via IDH1. *Sci. Rep.* 5, 8801.
- Cloos, P.A., Christensen, J., Agger, K., Helin, K. (2008). Erasing the methyl mark: histone demethylases at the center of cellular differentiation and disease. *Genes Dev.* 22, 1115-1140.
- Cloughesy, T.F., Cavenee, W.K., and Mischel, P.S. (2014). Glioblastoma: from molecular pathology to targeted treatment. *Annu. Rev. Pathol.* 9, 1-25.
- Compagno, M., Lim, W.K., Grunn, A., Nandula, S.V., Brahmachary, M., Shen, Q., Bertoni, F., Ponzoni, M., Scandurra, M., Califano, A., Bhagat, G., Chadburn, A., Dalla-Favera, R., Pasqualucci, L. (2009). Mutations of multiple genes cause deregulation of NF-kappaB in diffuse large B-cell lymphoma. *Nature* 459, 717-721.
- Cui, R., Meng, W., Sun, H.L., Kim, T., Ye, Z., Fassan, M., Jeon, Y.J., Li, B., Vicentini, C., Peng, Y., Lee, T.J., Luo, Z., Liu, L., Xu, D., Tili, E., Jin, V., Middleton, J., Chakravarti, A., Lautenschlaeger, T., Croce, C.M. (2015). MicroRNA-224 promotes tumor progression in nonsmall cell lung cancer. *Proc. Natl. Acad. Sci. U. S. A.* 112, E4288-4297.
- Dalziel, K. (1980). Isocitrate dehydrogenase and related oxidative decarboxylases. *FEBS Lett.* 117, 11-19.
- DeBerardinis, R.J., Mancuso, A., Daikhin, E., Nissim, I., Yudkoff, M., Wehrli, S., and Thompson, C.B. (2007). Beyond aerobic glycolysis: transformed cells can engage in glutamine metabolism that exceeds the requirement for protein and nucleotide synthesis. *Proc. Natl. Acad. Sci. U. S. A.* 104, 19345-19350.

- DeBerardinis, R.J., Sayed, N., Ditsworth, D., Thompson, C.B. (2008). Brick by brick: metabolism and tumor cell growth. *Curr. Opin. Genet. Dev.* *18*, 54-61.
- Du, X., Wang, Q.R., Chan, E., Merchant, M., Liu, J., French, D., Ashkenazi, A., Qing, J. (2012). FGFR3 stimulates stearyl CoA desaturase 1 activity to promote bladder tumor growth. *Cancer Res.* *72*, 5843-5855.
- Dubey, R., Chhabra, R., Saini, N. (2011). Small interfering RNA against transcription factor STAT6 leads to increased cholesterol synthesis in lung cancer cell lines. *PLoS One* *6*, e28509.
- Dubey, R. and Saini, N. (2015). STAT6 silencing up-regulates cholesterol synthesis via miR-197/FOXJ2 axis and induces ER stress-mediated apoptosis in lung cancer cells. *Biochim. Biophys. Acta.* *1849*, 32-43.
- Dunn, G.P., Rinne, M.L., Wykosky, J., Genovese, G., Quayle, S.N., Dunn, I.F., Agarwalla, P.K., Chheda, M.G., Campos, B., Wang, A., Brennan, C., Ligon, K.L., Furnari, F., Cavenee, W.K., Depinho, R.A., Chin, L., Hahn, W.C. (2012). Emerging insights into the molecular and cellular basis of glioblastoma. *Genes Dev.* *26*, 756-784.
- Ellinger, I., Poss, M., Bruggemann, M., Gromes, A., Schmidt, D., Ellinger, N., Tolkach, Y., Dietrich, D., Kristiansen, G., Muller, S.C. (2016). Systematic expression analysis of mitochondria complex I identifies NDUFS1 as a biomarker in clear-cell renal-cell carcinoma. *Clin. Genitourin Cancer Epub ahead of print.*
- Fernandez, C.A., Des Rosiers, C., Previs, S.F., David, F., and Brunengraber, H. (1996). Correction of ¹³C mass isotopomer distributions for natural stable isotope abundance. *J. Mass Spectrom.* *31*, 255-262.

Friedmann-Morvinski, D., Bushong, E.A., Ke, E., Soda, Y., Marumoto, T., Singer, O., Ellisman, M.H., Verma, I.M. (2012). Dedifferentiation of neurons and astrocytes by oncogenes can induce gliomas in mice. *Science* 338, 1080-1084.

Furnari, F.B., Cloughesy, F.F., Cavenee, W.K., and Mischel, P.S. (2015). Heterogeneity of epidermal growth factor receptor signaling networks in glioblastoma. *Nature Rev. Cancer* 15, 302-310.

Gotz, M., and Huttner, W.B. (2005). The cell biology of neurogenesis. *Nat. Rev. Mol. Cell Biol.* 6, 777-788.

Granchi, D., Fancelli, D., Minutolo, F. (2014). An update on therapeutic opportunities offered by cancer glycolytic metabolism. *Bioorg. Med. Chem. Lett.* 24, 4915-4925.

Graubert, T.A., and Mardis, E.R. (2011). Genomics of acute myeloid leukemia. *Cancer J.* 17, 487-491.

Guo, D., Bell, E.H., Chakravarti, A. (2013). Lipid metabolism emerges as a promising target for malignant glioma therapy. *CNS Oncol.* 2, 289-299.

Guo, D., Hildebrandt, I.J., Prins, R.M., Soto, H., Mazzotta, M.M., Dang, J., Shyy, J.Y., Watson, A.D., Phelps, M., Radu, C.G., Cloughesy, T.F., Mischel, P.S. (2009a). The AMPK agonist AICAR inhibits the growth of EGFRvIII-expressing glioblastomas by inhibiting lipogenesis. *Proc. Natl. Acad. Sci. U.S.A.* 106, 12932-12937.

Guo, D., Prins, R.M., Dang, J., Kuga, D., Iwanami, A., Soto, H., Lin, K.Y., Huang, T.T., Akhavan, D., Hock, M.B., Zhu, S., Kofman, A.A., Bensinger, S.J., Yong, W.H., Vinters, H.V., Horvath, S., Watson, A.D., Kuhn, J.G., Robins, H.I., Mehta, M.P., Wen, P.Y., DeAngelis, L.M.,

Prados, M.D., Mellinghoff, I.K., Cloughesy, T.F., Mischel, P.S. (2009b). EGFR signaling through an Akt-SREBP-1-dependent, rapamycin-resistant pathway sensitizes glioblastomas to antilipogenic therapy. *Sci. Signal.* 2, ra82.

Guo, D., Reinitz, F., Youssef, M., Hong, C., Nathanson, D., Akhavan, D., Kuya, D., Amzajerdi, A.N., Soto, H., Zhu, S., et al. (2011). An LXR agonist promotes glioblastoma cell death through inhibition of an EGFR/AKT/SREBP-1/LDLR-dependent pathway. *Cancer Discov.* 1, 442-456.

Haskins, J.W., Zhang, S., Means, R.E., Kelleher, J.K., Cline, G.W., Canfran-Duque, A., Suarez, Y., Stern, D.F. (2015). Neuregulin-activated ERBB4 induces SREBP-2 cholesterol biosynthetic pathway and increases low-density lipoprotein uptake. *Sci. Signal.* 8, ra111.

Hausinger, R.P. (2004). FeII/alpha-ketoglutarate-dependent hydroxylases and related enzymes. *Crit. Rev. Biochem. Mol. Biol.* 39, 21-68.

Hirst, J. (2013). Mitochondrial complex I. *Annu. Rev. Biochem.* 82, 551-575.

Hoefs, S.J., Skjeldal, O.H., Rodenburg, R.J., Nedregard, B., van Kaauwen, E.P., Spiekorkotter, U., von Kleist-Retzow, J.C., Smeitink, J.A., Nijtmans, L.G., van den Heuvel, L.P. (2010). Novel mutations in the NDUFS1 gene cause low residual activities in human complex I deficiencies. *Mol. Genet. Metab.* 100, 251-256.

Holland, E.C. (2001). Gliomagenesis: genetic alterations and mouse models. *Nat. Rev. Genet.* 2, 120-129.

Horbinski, C. (2013). What do we know about IDH1/2 mutations so far, and how do we use it? *Acta. Neuropathol.* 125, 621-636.

Hu, D., Garruss, A.S., Gao, X., Morgan, M.A., Cook, M., Smith, E.R., Shilatifard, A. (2013). The MII2 branch of the COMPASS family regulates bivalent promoters in mouse embryonic stem cells. *Nat. Struct. Mol. Biol.* *20*, 1093-1097.

Hu, Y., and Smyth, G.K. (2009). ELDA: extreme limiting dilution analysis for comparing depleted and enriched populations in stem cell and other assays. *J. Immunol. Methods* *347*, 70-78.

Huang, P.H., Mukasa, A., Bonavia, R., Flynn, R.A., Brewer, Z.E., Cavenee, W.K., Furnari, F.B., White, F.M. (2007). Quantitative analysis of EGFRvIII cellular signaling networks reveals a combinatorial therapeutic strategy for glioblastoma. *Proc. Natl. Acad. Sci. U.S.A.* *104*, 12867-12872.

Irwin, M.E., Mueller, K.L., Bohin, N., Ge, Y., Boerner, J.L. (2011). Lipid raft localization of EGFR alters the response of cancer cells to the EGFR tyrosine kinase inhibitor gefitinib. *J. Cell Physiol.* *226*, 2316-2328.

Ito, K., and Suda, T. (2014). Metabolic requirements for the maintenance of self-renewing stem cells. *Nat. Rev. Mol. Cell Biol.* *15*, 243-256.

Itsumi, M., Inoue, S., Elia, A.J., Murakami, K., Sasaki, M., Lind, E.F., Brenner, D., Harris, I.S., Chio, I.I., Afzal, S., et al. (2015). *Idh1* protects murine hepatocytes from endotoxin-induced oxidative stress by regulating the intracellular NADP(+)/NADPH ratio. *Cell Death Differ.* *22*, 1837-1845.

Jensen, S.A., Day, E.S., Ko, C.H., Hurley, L.A., Luciano, J.P., Kouri, F.M., Merkel, T.J., Luthi,

A.J., Patel, P.C., Cutler, J.I., Daniel, W.L., Scott, A.W., Rotz, M.W., Meade, T.J., Giljohann, D.A., Mirkin, C.A., Stegh, A.H. (2013). Spherical nucleic acid nanoparticle conjugates as an RNAi-based therapy for glioblastoma. *Sci. Transl. Med.* 5, 209ra152.

Jiang, L., Shestov, A.A., Swain, P., Yang, C., Parker, S.J., Wang, Q.A., Terada, L.S., Adams, N.D., McCabe, M.T., Pietrak, B., Schmidt, S., Metallo, C.M., Dranka, B.P., Schwartz, B., DeBerardinis, R.J. (2016). Reductive carboxylation supports redox homeostasis during anchorage-independent growth. *Nature* 532, 255-258.

Jo, S.H., Lee, S.H., Chun, H.S., Lee, S.M., Koh, H.J., Lee, S.E., Chun, J.S., Park, J.W., and Huh, T.L. (2002). Cellular defense against UVB-induced phototoxicity by cytosolic NADP(+)-dependent isocitrate dehydrogenase. *Biochem. Biophys. Res. Commun.* 292, 542-549.

Jue, T.R., McDonald, K.L. (2016). The challenges associated with molecular targeted therapies for glioblastoma. *J. Neurooncol.* 127, 427-434.

Kaelin, W.G. Jr., and McKnight, S.L. (2013). Influence of metabolism on epigenetics and disease. *Cell* 153, 56-69.

Kalyanaraman, S., Copeland, N.G., Gilbert, D.G., Jenkins, N.A., Gautam, N. (1998). Structure and chromosomal localization of mouse G protein subunit gamma 4 gene. *Genomics* 49, 147-151.

Kim, D.H., Zhang, T., Lee, S., Calabuig-Navarro, V., Yamauchi, J., Piccirillo, A., Fan, Y., Uppala, R., Goetzman, E., Dong, H.H. (2014). FoxO6 integrates insulin signaling with MTP for regulating VLDL production in the liver. *Endocrinology* 155, 1255-1267.

Kim, S.Y., Lee, S.M., Tak, J.K., Choi, K.S., Kwon, T.K., and Park, J.W. (2007). Regulation of

singlet oxygen-induced apoptosis by cytosolic NADP⁺-dependent isocitrate dehydrogenase. *Mol. Cell Biochem.* 302, 27-34.

Klinger, S., Guo, B., Yao, J., Yan, H., Zhang, L., Vaseva, A.V., Chen, S., Canoll, P., Horner, J.W., Wang, Y.A., Paik, J.H., Ying, H., Zheng, H. (2015). Development of resistance to EGFR-targeted therapy in malignant glioma can occur through EGFR-dependent and -independent mechanisms. *Cancer Res.* 75, 2109-2119.

Koh, H.J., Lee, S.M., Son, B.G., Lee, S.H., Ryoo, Z.Y., Chang, K.T., Park, J.W., Park, D.C., Song, B.J., Veech, R.L., Song, H., Huh, T.L. (2004). Cytosolic NADP⁺-dependent isocitrate dehydrogenase plays a key role in lipid metabolism. *J. Biol. Chem.* 279, 39968-39974.

Kouri, F.M., Hurley, L.A., Daniel, W.L., Day, E.S., Hua, Y., Hao, L., Peng, C.Y., Merkel, T.J., Queisser, M.A., Ritner, C., et al. (2015). miR-182 integrates apoptosis, growth, and differentiation programs in glioblastoma. *Genes Dev.* 29, 732-745.

Lai, A., Kharbanda, S., Pope, W.B., Tran, A., Solis, O.E., Peale, F., Forrest, W.F., Pujara, K., Carrillo, J.A., Pandita, A., Ellingson, B.M., Bowers, C.W., Soriano, R.H., Schmidt, N.O., Mohan, S., Yong, W.H., Seshagiri, S., Modrusan, Z., Jiang, Z., Aldape, K.D., Mischel, P.S., Liao, L.M., Escovedo, C.J., Chen, W., Nghiemphu, P.L., James, C.D., Prados, M.D., Westphal, M., Lamszus, K., Cloughesy, T., Phillips, H.S. (2011). Evidence for sequenced molecular evolution of IDH1 mutant glioblastoma from a distinct cell of origin. *J. Clin. Oncol.* 29, 4482-4490.

Lam, E.W., Brosens, J.J., Gomes, A.R., and Koo, C.Y. (2013). Forkhead box proteins: tuning forks for transcriptional harmony. *Nature Rev. Cancer* 13, 482-495.

Langbein, S., Zerilli, M., Zur Hausen, A., Staiger, W., Rensch-Boschert, K., Lukan, N., Popa, J., Ternullo, M.P., Steidler, A., Weiss, C., Grobholz, R., Willeke, F., Alken, P., Stassi, G., Schubert, P., Coy, J.F. (2006). Expression of transketolase TKTL1 predicts colon and urothelial cancer patient survival: Warburg effect reinterpreted. *Br. J. Cancer* 94, 578-585.

Lathia, J.D., Mack, S.C., Mulkearns-Hubert, E.E., Valentim, C.L., Rich, J.N. (2015). Cancer stem cells in glioblastoma. *Genes Dev.* 29, 1203-1217.

Lee, J., Kotliarova, S., Kotliarov, Y., Li, A., Su, Q., Donin, N.M., Pastorino, S., Purow, B.W., Christopher, N., Zhang, W., Park, J.K., Fine, H.A. (2006). Tumor stem cells derived from glioblastomas cultured in bFGF and EGF more closely mirror the phenotype and genotype of primary tumors than do serum-cultured cell lines. *Cancer Cell* 9, 391-403.

Lee, J.C., Vivanco, I., Beroukhi, R., Huang, J.H., Feng, W.L., DeBiasi, R.M., Yoshimoto, K., King, J.C., Nghiemphu, P., Yuza, Y., Xu, Q., Greulich, H., Thomas, R.K., Paez, J.G., Peck, T.C., Linhart, D.J., Glatt, K.A., Getz, G., Onofrio, R., Ziaugra, L., Levine, R.L., Gabriel, S., Kawaguchi, T., O'Neill, K., Khan, H., Liau, L.M., Nelson, S.F., Rao, P.N., Mischel, P., Pieper, R.O., Cloughesy, T., Leahy, D.J., Sellers, W.R., Sawyers, C.L., Meyerson, M., Mellinghoff, I.K. (2006). Epidermal growth factor receptor activation in glioblastoma through novel missense mutations in the extracellular domain. *PLoS Med.* 3, e485.

Lee, S., and Dong, H.H. (2017). FoxO integration of insulin signaling with glucose and lipid metabolism. *J. Endocrinol.* 233, R67-R79.

Lee, S.M., Koh, H.J., Park, D.C., Song, B.J., Huh, T.L., Park, J.W. (2002). Cytosolic NADP(+)-dependent isocitrate dehydrogenase status modulates oxidative damage to cells. *Free Radic. Biol.*

Med. 32, 1185-1196.

Li, B., and Dewey, C.N. (2011). RSEM: accurate transcript quantification from RNA-Seq data with or without a reference genome. *BMC Bioinformatics* 12, 323.

Li, X., Wu, C., Chen, N., Gu, H., Yen, A., Cao, L., Wang, E., Wang, L. (2016). PI3K/Akt/mTOR signaling pathway and targeted therapy for glioblastoma. *Oncotarget* 7, 33440-33450.

Lin, A.P., Abbas, S., Kim, S.W., Ortega, M., Bouamar, H., Escobedo, Y., Varadarajan, P., Qin, Y., Sudderth, J., Schulz, E., Deutsch, A., Mohan, S., Ulz, P., Neumeister, P., Rakheja, D., Gao, X., Hinck, A., Weintraub, S.T., DeBerardinis, R.J., Sill, H., Dahia, P.L., Aguiar, R.C. (2015). D2HGDH regulates alpha-ketoglutarate levels and dioxygenase function by modulating IDH2. *Nat. Commun.* 6, 7768.

Losman, J.A., and Kaelin Jr., W.G. (2013). What a difference a hydroxyl makes: mutant IDH1, (R)-2-hydroxyglutarate, and cancer. *Genes Dev.* 27, 836-852.

Lu, C., Ward, P.S., Kapoor, G.S., Rohle, D., Turcan, S., Abdel-Wahab, O., Edwards, C.R., Khanin, R., Figueroa, M.E., Melnick, A., Wellen, K.E., O'Rourke, D.M., Berger, S.L., Chan, T.A., Levine, R.L., Mellinghoff, I.K., Thompson, C.B. (2012). IDH mutation impairs histone demethylation and results in a block to cell differentiation. *Nature* 483, 474-478.

Lunt, S.Y., and Vander Heiden, M.G. (2011). Aerobic glycolysis: meeting the metabolic requirements of cell proliferation. *Annu. Rev. Cell Dev. Biol.* 27, 441-464.

Mahipal, A., Kothari, N., Gupta, S. (2014). Epidermal growth factor receptor inhibitors: coming of age. *Cancer Control* 21, 74-79.

Mailloux, R.J., Beriault, R., Lemire, J., Singh, R., Chenier, D.R., Hamel, R.D., and Appanna,

V.D. (2007). The tricarboxylic acid cycle, an ancient metabolic network with a novel twist. *PLoS One* 2, e690.

Maina, E.N., Morris, M.R., Zatyka, M., Raval, R.R., Banks, R.E., Richards, F.M., Johnson, C.M., Maher, E.R. (2005). Identification of novel VHL target genes and relationship to hypoxic response pathways. *Oncogene* 24, 4549-4558.

Maione, F., Oliaro-Bosso, S., Meda, C., Di Nicolantonio, F., Bussolino, F., Balliano, G., Viola, F., Giraudo, E. (2015). The cholesterol biosynthesis enzyme oxidosqualene cyclase is a new target to impair tumour angiogenesis and metastasis dissemination. *Sci. Rep.* 5, 9054.

Mardis, E.R., Ding, L., Dooling, D.J., Larson, D.E., McLellan, M.D., Chen, K., Koboldt, D.C., Fulton, R.S., Delehaunty, K.D., McGrath, S.D., Fulton, L.A., Locke, D.P., Magrini, V.J., Abbott, R.M., Vickery, T.L., Reed, J.S., Robinson, J.S., Wylie, T., Smith, S.M., Carmichael, L., Eldred, J.M., Harris, C.C., Walker, J., Peck, J.B., Du, F., Dukes, A.F., Sanderson, G.E., Brummett, A.M., Clark, E., McMichael, J.F., Meyer, R.J., Schindler, J.K., Pohl, C.S., Wallis, J.W., Shi, X., Lin, L., Schmidt, H., Tang, Y., Haipek, C., Wiechert, M.E., Ivy, J.V., Kalicki, J., Elliott, G., Ries, R.E., Payton, J.E., Westervelt, P., Tomasson, M.H., Watson, M.A., Baty, J., Heath, S., Shannon, W.D., Nagarajan, R., Link, D.C., Walter, M.J., Graubert, T.A., DiPersio, J.F., Wilson, R.K., Ley, T.J. (2009). Recurring mutations found by sequencing an acute myeloid leukemia genome. *N. Engl. J. Med.* 361, 1058-1066.

Marin-Valencia, I., Yang, C., Mashimo, T., Cho, S., Baek, H., Yang, X.L., Rajagopalan, K.N., Maddie, M., Vemireddy, V., Zhao, Z., Cai, L., Good, L., Tu, B.P., Hatanpaa, K.J., Mickey, B.E., Mates, J.M., Pascual, J.M., Maher, E.A., Malloy, C.R., Deberardinis, R.J., Bachoo, R.M. (2012).

Analysis of tumor metabolism reveals mitochondrial glucose oxidation in genetically diverse human glioblastomas in the mouse brain in vivo. *Cell Metab.* 15, 827-837.

Mashimo, T., Pichumani, K., Vemireddy, V., Hatanpaa, K.J., Singh, D.K., Sirasanagandla, S., Nannepaga, S., Piccirillo, S.G., Kovacs, Z., Foong, C., Huang, Z., Barnett, S., Mickey, B.E., DeBerardinis, R.J., Tu, B.P., Maher, E.A., Bachoo, R.M. (2014). Acetate is a bioenergetics substrate for human glioblastoma and brain metastases. *Cell* 159, 1603-1614.

Masui, K., Cavenee, W.K., Mischel, P.S. (2016). Cancer metabolism as a central driving force of glioma pathogenesis. *Brain Tumor Pathol.* 33, 161-168.

Medes, G., Thomas, A., Weinhouse, S. (1953). Metabolism of neoplastic tissue. IV. A study of lipid synthesis in neoplastic tissue slices in vitro. *Cancer Res.* 13, 27-29.

Menendez, J.A., and Lupu, R. (2007). Fatty acid synthase and the lipogenic phenotype in cancer pathogenesis. *Nature Rev. Cancer* 7, 763-777.

Metallo, C.M., Gameiro, P.A., Bell, E.L., Mattaini, K.R., Yang, J., Hiller, K., Jewell, C.M., Johnson, Z.R., Irvine, D.J., Guarente, L., Kelleher, J.K., Vander Heiden, M.G., Iliopoulos, O., Stephanopoulos, G. (2011). Reductive glutamine metabolism by IDH1 mediates lipogenesis under hypoxia. *Nature* 481, 380-384.

Molenaar, R.J., Botman, D., Smits, M.A., Hira, V.V., van Lith, S.A., Stap, J., Henneman, P., Khurshed, M., Lenting, K., Mul, A.N., Dimitrakopoulou, D., van Drunen, C.M., Hoebe, R.A., Radivoyevitch, T., Wilmink, J.W., Maciejewski, J.P., Vandertop, W.P., Leenders, W.P., Bleeker, F.E., van Noorden, C.J. (2015). Radioprotection of IDH1-mutated cancer cells by the IDH1-mutant inhibitor AGI-5198. *Cancer Res.* 75, 4790-4802.

Monticone, M., Taherian, R., Stigliani, S., Carra, E., Monteghirfo, S., Longo, L., Daga, A., Dono, M., Zupo, S., Giaretti, W., Castagnola, P. (2014). NAC, tiron and trolox impair survival of cell cultures containing glioblastoma tumorigenic initiating cells by inhibition of cell cycle progression. *PLoS One* 9, e90085.

Morgenstern, J.P. and Land, H. (1990). Advanced mammalian gene transfer: high titre retroviral vectors with multiple drug selection markers and a complementary helper-free packaging cell line. *Nucleic Acids Res.* 18, 3587-3596.

Mullen, A.R., Wheaton, W.W., Jin, E.S., Chen, P.H., Sullivan, L.B., Cheng, T., Yang, Y., Linehan, W.M., Chandel, N.S., DeBerardinis, R.J. (2011). Reductive carboxylation supports growth in tumour cells with defective mitochondria. *Nature* 481, 385-388.

Nam, W.S., Park, K.M., and Park, J.W. (2012). RNA interference targeting cytosolic NADP(+)-dependent isocitrate dehydrogenase exerts anti-obesity effect in vitro and in vivo. *Biochim. Biophys. Acta.* 1822, 1181-1188.

Nathanson, D.A., Gini, B., Mottahedeh, J., Visnyei, K., Koga, T., Gomez, G., Eskin, A., Hwang, K., Wang, J., Masui, K., Paucar, A., Yang, H., Ohashi, M., Zhu, S., Wykosky, J., Reed, R., Nelson, S.F., Cloughesy, T.F., James, C.D., Rao, P.N., Kornblum, H.I., Heath, J.R., Cavenee, W.K., Furnari, F.B., Mischel, P.S. (2014). Targeted therapy resistance mediated by dynamic regulation of extrachromosomal mutant EGFR DNA. *Science* 343, 72-76.

Ohgaki, H., and Kleihues, P. (2005). Population-based studies on incidence, survival rates, and genetic alterations in astrocytic and oligodendroglial gliomas. *J. Neuropathol. Exp. Neurol.* 64, 479-489.

Okoye-Okafor, U.C., Bartholdy, B., Cartier, J., Gao, E.N., Pietrak, B., Rendina, A.R., Rominger, C., Quinn, C., Smallwood, A., Wiggall, K.J., et al. (2015). New IDH1 mutant inhibitors for treatment of acute myeloid leukemia. *Nat. Chem. Biol.* *11*, 878-886.

Pal, I., Patil, V., Mondal, B., Shukla, S., Hegde, A.S., Arivazhagan, A., Santosh, V., and Somasundaram, K. (2016). Epigenetically silenced GNG4 inhibits SDF1a/CXCR4 signaling in mesenchymal glioblastoma. *Genes Cancer* *7*, 136-147.

Pal, S., Bi, Y., Macyszyn, L., Showe, L.C., O'Rourke, D.M., and Davuluri, R.V. (2014). Isoform-level gene signature improves prognostic stratification and accurately classifies glioblastoma subtypes. *Nucleic Acids Res.* *42*, e64.

Parsons, D.W., Jones, S., Zhang, X, Lin, J.C., Leary, R.J., Angenendt, P., Mankoo, P., Carter, H., Siu, I.M., Gallia, G.L., et al. (2008). An integrated genomic analysis of human glioblastoma multiforme. *Science* *321*, 1807-1812.

Paschka, P., Schlenk, R.F., Gaidzik, V.I., Habdank, M., Kronke, J., Bullinger, L., Spath, D., Kayser, S., Zucknick, M., Gotze, K., Horst, H.A., Germing, U., Dohner, H., Dohner, K. (2010). IDH1 and IDH2 mutations are frequent genetic alterations in acute myeloid leukemia and confer adverse prognosis in cytogenetically normal acute myeloid leukemia with NPM1 mutation without FLT3 internal tandem duplication. *J. Clin. Oncol.* *28*, 3636-3643.

Pavlova, N.N., and Thompson, C.B. (2016). The emerging hallmarks of cancer metabolism. *Cell Metab.* *23*, 27-47.

Piccaluga, P.P., Agostinelli, C., Califano, A., Rossi, M., Basso, K., Zupo, S., Went, P., Klein, U.,

Zinzani, P.L., Baccarani, M., Dalla Favera, R., Pileri, S.A. (2007). Gene expression analysis of peripheral T cell lymphoma, unspecified, reveals distinct profiles and new therapeutic targets. *J. Clin. Invest.* *117*, 823-834.

Raizer, J.J., Giglio, P., Hu, J., Groves, M., Merrell, R., Conrad, C., Phuphanich, S., Puduvalli, V.K., Loghin, M., Paleologos, N., Yuan, Y., Liu, D., Rademaker, A., Yung, W.K., Vaillant, B., Rudnick, J., Chamberlain, M., Vick, N., Grimm, S., Tremont-Lukats, I.W., De Groot, J., Aldape, K., Gilbert, M.R., Brain Tumor Trials Collaborative. (2016). A phase II study of bevacizumab and erlotinib after radiation and temozolomide in MGMT unmethylated GBM patients. *J. Neurooncol.* *126*, 185-192.

Reardon, D.A., Desjardins, A., Vredenburgh, J.J., Gururangan, S., Friedman, A.H., Herndon, J.E.2nd, Marcello, J., Norfleet, J.A., McLendon, R.E., Sampson, J.H., Friedman, H.S. (2010). Phase 2 trial of erlotinib plus sirolimus in adults with recurrent glioblastoma. *J. Neurooncol.* *96*, 219-230.

Reitman, Z.J., Jin, G., Karoly, E.D., Spasojevic, I., Yang, J., Kinzler, K.W., He, Y., Bigner, D.D., Vogelstein, B., Yan, H. (2011). Profiling the effects of isocitrate dehydrogenase 1 and 2 mutations on the cellular metabolome. *Proc. Natl. Acad. Sci. U.S.A.* *108*, 3270-3275.

Reitman, Z.J., and Yan, H. (2010). Isocitrate dehydrogenase 1 and 2 mutations in cancer: alterations at a crossroads of cellular metabolism. *J. Natl. Cancer Inst.* *102*, 932-941.

Robinson, M.D., McCarthy, D.J., and Smyth, G.K. (2010). edgeR: a bioconductor package for differential expression analysis of digital gene expression data. *Bioinformatics* *26*, 139-140.

Rohle, D., Popovici-Muller, J., Palaskas, N., Turcan, S., Grommes, C., Campos, C., Tsoi, J.,

Clark, O., Oldrini, B., Komisopoulou, E., Kunii, K., Pedraza, A., Schalm, S., Silverman, L., Miller, A., Wang, F., Yang, H., Chen, Y., Kernytsky, A., Rosenblum, M.K., Liu, W., Biller, S.A., Su, S.M., Brennan, C.W., Chan, T.A., Graeber, T.G., Yen, K.E., Mellinghoff, I.K. (2013). An inhibitor of mutant IDH1 delays growth and promotes differentiation of glioma cells. *Science* 340, 626-630.

Rothenberg, S.M., Concannon, K., Cullen, S., Boulay, G., Turke, A.B., Faber, A.C., Lockerman, E.L., Rivera, M.N., Engelman, J.A., Maheswaran, S., Haber, D.A. (2015). Inhibition of mutant EGFR in lung cancer cells triggers SOX2-FOXO6-dependent survival pathways. *Elife* 4.

Salazar-Ramiro, A., Ramirez-Ortega, D., Perez de la Cruz, V., Hernandez-Pedro, N.Y., Gonzalez-Esquivel, D.F., Sotelo, J., Pineda, B. (2016). Role of redox status in development of glioblastoma. *Front. Immunol.* 7, 156.

Sanzey, M., Abdul Rahim, S.A., Oudin, A., Dirkse, A., Kaoma, T., Vallar, L., Herold-Mende, C., Bjerkvig, R., Golebiewska, A., Noclou, S.P. (2015). Comprehensive analysis of glycolytic enzymes as therapeutic targets in the treatment of glioblastoma. *PLoS One* 10, e0123544.

Sasaki, M., Knobbe, C.B., Munger, J.C., Lind, E.F., Brenner, D., Brustle, A., Harris, I.S., Holmes, R., Wakeham, A., Haight, J., You-Ten, A., Schalm, S., Su, S.M., Virtanen, C., Reifenberger, G., Ohashi, P.S., Barber, D.L., Figueroa, M.E., Melnick, A., Zuniga-Pflucker, J.C., Mak, T.W. (2012a). IDH1(R132H) mutation increases murine haematopoietic progenitors and alters epigenetics. *Nature* 488, 656-659.

Sasaki, M., Knobbe, C.B., Itsumi, M., Elia, A.J., Harris, I.S., Chio, I.I., Cairns, R.A., McCracken, S., Wakeham, A., Haight, J., Ten, A.Y., Snow, B., Ueda, T., Inoue, S., Yamamoto,

K., Ko, M., Rao, A., Yen, K.E., Su, S.M., Mak, T.K. (2012b). D-2-hydroxyglutarate produced by mutant IDH1 perturbs collagen maturation and basement membrane function. *Genes Dev.* 26, 2038-2049.

Shechter, I., Dai, P., Huo, L., and Guan, G. (2003). IDH1 gene transcription is sterol regulated and activated by SREBP-1a and SREBP-2 in human hepatoma HepG2 cells: evidence that IDH1 may regulate lipogenesis in hepatic cells. *J. Lipid Res.* 44, 2169-2180.

Snuderl, M., Fazlollahi, L., Le, L.P., Nitta, M., Zhelyazkova, B.H., Davidson, C.J., Akhavanfard, S., Cahill, D.P., Aldape, K.D., Betensky, R.A., Louis, D.N., Iafrate, A.J. (2011). Mosaic amplification of multiple receptor tyrosine kinase genes in glioblastoma. *Cancer Cell* 20, 810-817.

Staedler, D., Chapuis-Bernasconi, C., Dehmlow, H., Fischer, H., Juillerat-Jeanneret, L., Aebi, J.D. (2012). Cytotoxic effects of combination of oxidosqualene cyclase inhibitors with atorvastatin in human cancer cells. *J. Med. Chem.* 55, 4990-5002.

Stommel, J.M., Kimmelman, A.C., Ying, H., Nabioullin, R., Ponugoti, A.H., Wiedemeyer, R., Stegh, A.H., Bradner, J.E., Ligon, K.L., Brennan, C., Chin, L., DePinho, R.A. (2007). Coactivation of receptor tyrosine kinases affects the response of tumor cells to targeted therapies. *Science* 318, 287-290.

Stupp, R., Mason, W.P., van den Bent, M.J., Weller, M., Fisher, B., Taphoorn, M.J., Belanger, K., Brandes, A.A., Marosi, C., Bogdahn, U., Curschmann, J., Janzer, R.C., Ludwin, S.K., Gorlia, T., Allgeier, A., Lacombe, D., Cairncross, J.G., Eisenhauer, E., Mirimanoff, R.O.; European Organisation for Research and Treatment of Cancer Brain Tumor and Radiotherapy Groups;

National Cancer Institute of Canada Clinical Trials Group. (2005). Radiotherapy plus concomitant and adjuvant temozolomide for glioblastoma. *N. Engl. J. Med.* 352, 987-996.

Su, C.Y., Chang, Y.C., Yang, C.J., Huang, M.S., Hsiao, M. (2016). The opposite prognostic effect of NDUFS1 and NDUFS8 in lung cancer reflects the oncojanus role of mitochondrial complex I. *Sci. Rep.* 12, 31357.

Sun, N., Chen, Z., Tan, F., Zhang, B., Yao, R., Zhou, C., Li, J., Gao, Y., Liu, Z., Tan, X., Zhou, F., He, M.Y., Shao, K., Li, N., Qiu, B., Sun, J., Yu, Y., Wang, S., Zhao, Y., Shi, X., He, J. (2013). Isocitrate dehydrogenase 1 is a novel plasma biomarker for diagnosis of non-small cell lung cancer. *Clin. Cancer Res.* 19, 5136-5145.

Suva, M.L., Rheinbay, E., Gillespie, S.M., Patel, A.P., Wakimoto, H., Rabkin, S.D., Riggi, N., Chi, A.S., Cahill, D.P., Nahed, B.V., Curry, W.T., Martuza, R.L., Rivera, M.N., Rossetti, N., Kasif, S., Beik, S., Kadri, S., Tirosh, I., Wortman, I., Shalek, A.K., Rozenblatt-Rosen, O., Regev, A., Louis, D.N., Bernstein, B.E. (2014). Reconstructing and reprogramming the tumor-propagating potential of glioblastoma stem-like cells. *Cell* 157, 580-594.

Szerlip, N.J., Pedraza, A., Chakravarty, D., Azim, M., McGuire, J., Fang, Y., Ozawa, T., Holland, E.C., Huse, J.T., Jhanwar, S., Leversha, M.A., Mikkelsen, T., Brennan, C.W. (2012). Intratumoral heterogeneity of receptor tyrosine kinases EGFR and PDGFRA amplification in glioblastoma defines subpopulations with distinct growth factor response. *Proc. Natl. Acad. Sci. U.S.A.* 109, 3041-3046.

Tan, F., Jiang, Y., Sun, N., Chen, Z., Lv, Y., Shao, K., Li, N., Qiu, B., Gao, Y., Li, B., Tan, X., Zhou, F., Wang, Z., Ding, D., Wang, J., Sun, J., Hang, J., Shi, S., Feng, X., He, F., He, J. (2012).

Identification of isocitrate dehydrogenase 1 as a potential diagnostic and prognostic biomarker for non-small cell lung cancer by proteomic analysis. *Mol. Cell Proteomics* 11, M111.008821.

Tan, Z.W., Xie, S., Hu, S.Y., Liao, T., Liu, P., Peng, K.H., Yang, X.Z., He, Z.L., Tang, H.Y., Cui, Y., Peng, X.N., Zhang, J., Zhou, C. (2016). Caudatin targets TNFAIP1/NFkB and cytochrome c/caspase signaling to suppress tumor progression in human uterine cancer. *Int. J. Oncol.* 49, 1638-1650.

Tarrado-Castellarnau, M., de Atauri, P., Cascante, M. (2016). Oncogenic regulation of tumor metabolism reprogramming. *Oncotarget* 7, 62726-62753.

Turcan, S., Rohle, D., Goenka, A., Walsh, L.A., Fang, F., Yilmaz, E., Campos, C., Fabius, A.W., Lu, C., Ward, P.S., Thompson, C.B., Kaufman, A., Guryanova, O., Levine, R., Heguy, A., Viale, A., Morris, L.G., Huse, J.T., Mellinghoff, I.K., Chan, T.A. (2012). IDH1 mutation is sufficient to establish the glioma hypermethylator phenotype. *Nature* 483, 479-483.

Vander Heiden, M.G., Lunt, S.Y., Dayton, T.L., Fiske, B.P., Israelsen, W.J., Mattaini, K.R., Vokes, N.I., Stephanopoulos, G., Cantley, L.C., Metallo, C.M., Locasale, J.W. (2011). Metabolic pathway alterations that support proliferation. *Cold Spring Harb. Symp. Quant. Biol.* 76, 325-334.

Van Meir, E.G., Hadjipanayis, C.G., Norden, A.D., Shu, H.K., Wen, P.Y., Olson, J.J. (2010). Exciting new advances in neuro-oncology: the avenue to a cure for malignant glioma. *CA Cancer J. Clin.* 60, 166-193.

Vartanian, A., Agnihotri, S., Wilson, M.R., Burrell, K.E., Tonge, P.D., Alamsahebpour, A., Jalali, S., Taccone, M.S., Mansouri, S., Golbourn, B., Aldape, K.D., Zadeh, G. (2016). Targeting

hexokinase 2 enhances response to radio-chemotherapy in glioblastoma. *Oncotarget* 7, 69518-69535.

Veech, R.L., Eggleston, L.V., Krebs, H.A. (1969). The redox state of free nicotinamide-adenine dinucleotide phosphate in the cytoplasm of rat liver. *Biochem. J.* 115, 609-619.

Verhaak, R.G., Hoadley, K.A., Purdom, E., Wang, V., Qi, Y., Wilerson, M.D., Miller, C.R., Ding, L., Golub, T., Mesirov, J.P., Alexe, G., Lawrence, M., O'Kelly, M., Tamayo, P., Weir, B.A., Gabriel, S., Winckler, W., Gupta, S., Jakkula, L., Feiler, H.S., Hodgson, J.G., James, C.D., Sarkaria, J.N., Brennan, C., Kahn, A., Spellman, P.T., Wilson, R.K., Speed, T.P., Gray, J.W., Meyerson, M., Getz, G., Perou, C.M., Hayes, D.N.; Cancer Genome Atlas Research Network. (2010). Integrated genomic analysis identifies clinically relevant subtypes of glioblastoma characterized by abnormalities in PDGFRA, IDH1, EGFR, and NF1. *Cancer Cell* 17, 98-110.

Vivanco, I., Robins, H.I., Rohle, D., Campos, C., Grommes, C., Nghiemphu, P.L., Kubek, S., Oldrini, B., Chheda, M.G., Yannuzzi, N., Tao, H., Zhu, S., Iwanami, A., Kuga, D., Dang, J., Pedraza, A., Brennan, C.W., Heguy, A., Liau, L.M., Lieberman, F., Yung, W.K., Gilbert, M.R., Reardon, D.A., Drappatz, J., Wen, P.Y., Lamborn, K.R., Chang, S.M., Prados, M.D., Fine, H.A., Horvath, S., Wu, N., Lassman, A.B., DeAngelis, L.M., Yong, W.H., Kuhn, J.G., Mischel, P.S., Mehta, M.P., Cloughesy, T.F., Mellinghoff, I.K. (2012). Differential sensitivity of glioma-versus lung cancer-specific EGFR mutations to EGFR kinase inhibitors. *Cancer Discov.* 2, 458-471.

Volker, H.U., Hagemann, C., Coy, J., Wittig, R., Sommer, S., Stojic, J., Haubitz, I., Vince, G.H., Kammerer, U., Monoranu, C.M. (2008). Expression of transketolase-like 1 and activation of Akt

in grade IV glioblastomas compared with grades II and III astrocytic gliomas. *Am. J. Clin. Pathol.* *130*, 50-57.

Wahl, D.R., Dresser, J., Wilder-Romans, K., Parsels, J.D., Zhao, S.G., Davis, M., Zhao, L., Kachman, M., Wernisch, S., Burant, C.F., Morgan, M.A., Feng, F.Y., Speers, C., Lyssiotis, C.A. (2016). Glioblastoma therapy can be augmented by targeting IDH1-mediated NADPH biosynthesis. *Cancer Res.* *77*, 960-970.

Wang, K., Singh, D., Zeng, Z., Coleman, S.J., Huang, Y., Savich, G.L., He, X., Mieczkowski, P., Grimm, S.A., Perou, C.M., MacLeod, J.N., Chiang, D.Y., Prins, J.F., Liu, J. (2010). MapSplice: accurate mapping of RNA-seq reads for splice junction discovery. *Nucleic Acids Res.* *38*, e178.

Wang, Y., Zhang, L.L., Champlin, R.E., Wang, M.L. (2015). Targeting Bruton's tyrosine kinase with ibrutinib in B-cell malignancies. *Clin. Pharmacol. Ther.* *97*, 455-468.

Warburg, O., Wind, F., Negelein, E. (1927). The metabolism of tumors in the body. *J. Gen. Physiol.* *8*, 519-530.

Wise, D.R., Ward, P.S., Shay, J.E., Cross, J.R., Gruber, J.J., Sachdeva, U.M., Platt, J.M., DeMatteo, R.G., Simon M.C., Thompson, C.B. (2011). Hypoxia promotes isocitrate dehydrogenase-dependent carboxylation of α -ketoglutarate to citrate to support cell growth and viability. *Proc. Natl. Acad. Sci. U. S. A.* *108*, 19611-19616.

Wolf, A., Agnihotri, S., Guha, A. (2010). Targeting metabolic remodeling in glioblastoma multiforme. *Oncotarget* *1*, 552-562.

Wolf, A., Agnihotri, S., Micallef, J., Mukherjee, J., Sabha, N., Cairns, R., Hawkins, C., Guha, A. (2011). Hexokinase 2 is a key mediator of aerobic glycolysis and promotes tumor growth in

human glioblastoma multiforme. *J. Exp. Med.* 208, 313-326.

Wolf, F.W., Marks, R.M., Sarma, V., Byers, M.G., Katz, R.W., Shows, T.B., Dixit, V.M. (1992). Characterization of a novel tumor necrosis factor- α -induced endothelial primary response gene. *J. Biol. Chem.* 267, 1317-1326.

Xu, S., Grullon, S., Ge, K., and Peng, W. (2014). Spatial clustering for identification of ChIP-enriched regions (SICER) to map regions of histone methylation patterns in embryonic stem cells. *Methods Mol. Biol.* 1150, 97-111.

Xu, W., Yang, H., Liu, Y., Yang, Y., Wang, P., Kim, S.H., Ito, S., Yang, C., Wang, P., Xiao, M.T., Liu, L.X., Jiang, W.Q., Liu, J., Zhang, J.Y., Wang, B., Frye, S., Zhang, Y., Xu, Y.H., Lei, Q.Y., Guan, K.L., Zhao, S.M., Xiong, Y. (2011). Oncometabolite 2-hydroxyglutarate is a competitive inhibitor of α -ketoglutarate-dependent dioxygenases. *Cancer Cell* 19, 17-30.

Yasumoto, Y., Miyazaki, H., Vaidyan, L.K., Kagawa, Y., Ebrahimi, M., Yamamoto, Y., Ogata, M., Katsuyama, Y., Sadahiro, H., Suzuki, M., Owada, Y. (2016). Inhibition of fatty acid synthase decreases expression of stemness markers in glioma stem cells. *PLoS One* 11, e0147717.

Ying, H., Kimmelman, A.C., Lyssiotis, C.A., Hua, S., Chu, G.C., Fletcher-Sananikone, E., Locasale, J.W., Son, J., Zhang, H., Coloff, J.L., Yan, H., Wang, W., Chen, S., Viale, A., Zheng, H., Paik, J.H., Lim, C., Guimaraes, A.R., Martin, E.S., Chang, J., Hezel, A.F., Perry, S.R., Hu, J., Gan, B., Xiao, Y., Asara, J.M., Weissleder, R., Wang, Y.A., Chin, L., Cantley, L.C., DePinho, R.A. (2012). Oncogenic Kras maintains pancreatic tumors through regulation of anabolic glucose metabolism. *Cell* 149, 656-670.

Zhang, J., Nuebel, E., Daley, G.Q., Koehler, C.M., Teitell, M.A. (2012). Metabolic regulation in

pluripotent stem cells during reprogramming and self-renewal. *Cell Stem Cell* 11, 589-595.

Zhang, P., Guo, Z., Hu, R., He, X., Jiao, X., Zhu, X. (2015). Interaction between microRNA-181a and TNFAIP1 regulates pancreatic cancer proliferation and migration. *Tumour Biol.* 36, 9693-9701.

Zhang, X., Li, X., Tan, Z., Liu, X., Yang, C., Ding, X., Hu, X., Zhou, J., Xiang, S., Zhou, C., Zhang, J. (2013). MicroRNA-373 is upregulated and targets TNFAIP1 in human gastric cancer, contributing to tumorigenesis. *Oncol. Lett.* 6, 1427-1434.

Zhao, S., Lin, Y., Xu, W., Jiang, W., Zha, Z., Wang, P., Yu, W., Li, Z., Gong, L., Peng, Y., Ding, J., Lei, Q., Guan, K.L., Xiong, Y. (2009). Glioma-derived mutations in IDH1 dominantly inhibit IDH1 catalytic activity and induce HIF-1alpha. *Science* 324, 261-265.

Zhao, Y., Butler, E.B., Tan, M. (2013). Targeting cellular metabolism to improve cancer therapeutics. *Cell Death Dis.* 4, e532

Zheng, H., Ying, H., Yan, H., Kimmelman, A.C., Hiller, D.J., Chen, A.J., Perry, S.R., Tonon, G., Chu, G.C., Ding, Z., Stommel, J.M., Dunn, K.L., Wiedemeyer, R., You, M.J., Brennan, C., Wang, Y.A., Ligon, K.L., Wong, W.H., Chin, L., DePinho, R.A. (2008). p53 and Pten control neural and glioma stem/progenitor cell renewal and differentiation. *Nature* 455, 1129-1133.

Zhou, C., Li, X., Zhang, X., Liu, X., Tan, Z., Yang, C., Zhang, J. (2013). microRNA-372 maintains oncogene characteristics by targeting TNFAIP1 and affects NFkB signaling in human gastric carcinoma cells. *Int. J. Oncol.* 42, 635-642.

CURRICULUM VITAE

Andrea E. Calvert

1708 W. Pearson St., Chicago, IL

(614) 580-1740

a-calvert@u.northwestern.edu

Summary

Highly motivated cancer biologist with extensive laboratory capabilities in molecular and cell biology. Great oral presentation and written proficiencies. Thrives in collaborative environments with high motivation and strong problem solving skills. Desires to help bring creative drug development solutions to treat various cancers.

Education

- 2017 **Northwestern University, Feinberg School of Medicine** Chicago, IL
 Ph.D., Driskill Graduate Program in the Life Sciences (*Cancer Biology*)
Certificate of Management: Kellogg School of Management
- Management for Scientists and Engineers, 2014
 - Managerial Challenges in the Pharmaceutical, Biotechnology, and Medical Device Industries, 2015
- 2008 **Wake Forest University** Winston-Salem, NC
 Bachelor of Arts in Chemistry, Minor in Biology, *cum laude*

Research Experience

- 2010-Present **Northwestern University, Feinberg School of Medicine** Chicago, IL
 Graduate Research Assistant, Department of Neurology
- Developed and carried out a strategy to investigate and target a novel oncogenic protein in glioblastoma in a highly collaborative project; supervised by Dr. Alexander Stegh
 - Co-Authored three other scientific projects to determine novel therapeutic targets for glioblastoma
 - Supervised, trained, and mentored three junior graduate students
 - Authored/co-authored two high-impact factor publications
 - Awarded prestigious interdepartmental NIH training grant fellowship
 - Maintained compliance with internal safety regulatory boards
- 2008-2010 **Nationwide Children's Hospital** Columbus, OH
 Research Assistant
- Investigated potential drug targets and therapeutics for neonatal pulmonary hypertension; supervised by Dr. Bernadette Chen
 - Co-authored three publications
 - Responsible for developing and executing experiments, and overall management of the lab
- 2007 **Nationwide Children's Hospital** Columbus, OH
 Research Aide

- Worked closely with post-doctoral scientist to determine potential therapeutic targets in pulmonary hypertension; supervised by Dr. Leif Nelin
- Co-authored one publication

- 2007 **Wake Forest University** Winston-Salem, NC
Undergraduate Research Assistant
- Worked in an analytical chemistry laboratory to investigate the properties of dye-protein interactions; supervised by Dr. Christa Colyer
 - Assisted in project design; ran experiments and analysis independently

Skills

Laboratory Skills:

- qRT-PCR
- Primer Design
- Sequencing
- Sub-cloning
- SDS-PAGE/Western Blot
- Gel Electrophoresis
- ELISA
- Immuno-Precipitations
- Chromatin-Immunoprecipitation
- Mammalian Cell Culture
- Immunofluorescence
- Flow Cytometry/FACS
- Transformations
- Transfections
- Recombinant DNA Techniques
- Lentiviral and Retroviral Transductions
- Solution Preparation
- Microscopy
- Mouse Work

Professional Skills:

- Microsoft Office Suite
- Google Drive
 - Docs, Sheets, Forms
- ImageJ
- Adobe Creative Suite
- GraphPad Prism
- Web-based Molecular Biology Tools
 - Primer 3, CLUSTAL, BLAST, etc.
- Scientific Writing
- Manuscript Editing
- Public Speaking
- Grant Proposals
- Peer Review
- Organized Online Notebook Keeping
- Collaborative Projects
- Experimental Design
- Data Analysis

Publications

- **Calvert AE**, Chalastanis A, Wu Y, Hurley LA, Kouri FM, Bi Y, Kachman M, May JL, Bartom E, Hua Y, Misha RK, Schiltz GE, Dubrovskiy O, Mazar AP, Peter ME, Zheng H, James CD, Burant CF, Chandel NS, Davuluri RV, Horbinski C, Stegh AH. Cancer-associated IDH1 promotes growth and resistance to targeted therapies in the absence of mutation. *Cell Reports*. 2017. In press.
- Chen B, Xue J, Meng X, Slutzky JL, **Calvert AE**, Chicoine LG. Resveratrol prevents hypoxia-induced arginase II expression and proliferation of human pulmonary artery smooth muscle cells via Akt-dependent signaling. *Am J Physiol Lung Cell Mol Physiol*. 2014 Aug 15; 307(4): L317-25.

- Jensen SA, **Calvert AE**, Volpert G, Kouri FM, Hurley LA, Luciano JP, Wu Y, Chalastanis A, Futerman AH, Stegh AH. Bcl2L13 is a ceramide synthase inhibitor in glioblastoma. *Proc Natl Acad Sci USA*. 2014 Apr 15; 111(15): 5682-7.
- Chen B, **Calvert AE**, Meng X, Nelin LD. Pharmacologic agents elevating cAMP prevent arginase II expression and proliferation of pulmonary artery smooth muscle cells. *Am J Respir Cell Mol Biol*. 2012 Aug; 47(2): 218-26.
- Chicoine LG, Stenger MR, Cui H, **Calvert AE**, Evans RJ, English BK, Liu Y, Nelin LD. Nitric oxide suppression of cellular proliferation depends on cationic amino acid transporter activity in cytokine-stimulated pulmonary endothelial cells. *Am J Physiol Lung Cell Mol Physiol*. 2011 Apr; 300(4):L596-604.
- Chen B, **Calvert AE**, Cui H, Nelin LD. Hypoxia promotes human pulmonary artery smooth muscle cell proliferation through induction of arginase. *Am J Physiol Lung Cell Mol Physiol*. 2009 Dec; 297(6): L1151-9.

Presentations

- Center of Cancer Nanotechnology Excellence Site Visit, Poster Presentation, Evanston, IL, May 2016.
- American Association of Cancer Research Meeting, Poster Presentation, New Orleans, LA, April 2016.
- Lurie Cancer Center Symposium, Oral Presentation, Chicago, IL, July 2015.
- Cancer Research Club Research in Progress, Oral Presentation, Chicago, IL, January 2014.
- NIH/NCI Carcinogenesis T32 Meeting, Oral Presentation, Chicago, IL, March 2013.
- Pediatric Academic Societies Annual Meeting, Poster Presentation, Vancouver, BC, Canada, May 2010.
- Pediatric Academic Societies Annual Meeting, Poster Presentation, Baltimore, MD, May 2009.

Leadership and Outreach

- Student Assisted Mentoring Program (STAMP), Mentor for junior graduate students, 2014-2015.
- Northwestern International Explorers, Mentor for international graduate students across all disciplines, 2013.
- Graduate School Genetics Course, Teaching Assistant, 2013.

Awards, Fellowships, and Professional Memberships

- NIH/NCI T32 Carcinogenesis Training Grant Fellowship, 2012-2014.
- American Association of Cancer Research (AACR), Member, 2016-present.
- Northwestern Cancer Research Club, Member, 2011-present.
- Northwestern Cancer Cluster, Member, 2011-present.
- Northwestern Oncology Research Journal Club, Member, 2012-2014.
- Collaborative Learning and Integrated Mentoring in the Biosciences (CLIMB), Member, 2010-2011.
- Wake Forest University Dean's List, 7 semesters, 2004-2007.

Additional InformationKellogg Certificate of Management

Management for Scientists and Engineers, 2014.

- Highly competitive program for PhD candidates in various science and engineering programs
- Covered many topics including: economics and strategy, accounting for decision making, leadership, team building, finance, operations management, risk and uncertainty, IP management, negotiations, crisis management, entrepreneurship and innovation, and marketing management.

Managerial Challenges in the Pharmaceutical, Biotechnology, and Medical Device Industries (HEMA-453), 2015.

- Topics covered included: history of pharmaceuticals, strategic management in drug discovery process, history of regulation, business development, and ethics.